Quantification of CD4+ cell Count via a Nanofibre-based Biosensor

by

Alexander M. Lloyd

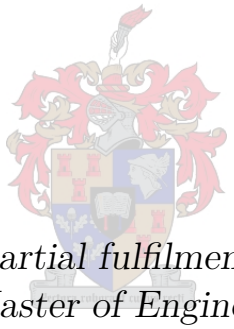

Thesis presented in partial fulfilment of the requirements for the degree of Master of Engineering in Electronic Engineering in the Faculty of Engineering at Stellenbosch University

Supervisor: Prof. W.J. Perold
Co-supervisor: Prof. P.R. Fourie

April 2019

Declaration

By submitting this thesis electronically, I declare that the entirety of the work contained therein is my own, original work, that I am the sole author thereof (save to the extent explicitly otherwise stated), that reproduction and publication thereof by Stellenbosch University will not infringe any third party rights and that I have not previously in its entirety or in part submitted it for obtaining any qualification.

Date: April 2019

Abstract

Quantification of CD4+ cell Count via a Nanofibre-based Biosensor

A.M. Lloyd

Department of Electrical and Electronic Engineering,
University of Stellenbosch,
Private Bag X1, Matieland 7602, South Africa.

Thesis: MEng (Electronic)

April 2019

Antigen-substrate binding has been found to cause a change in the resistance of conductive nanofibre substrates. This thesis endeavoured to exploit this phenomenon to produce sensors capable of quantifying CD4+ cell count. Producing nanofibre substrates with appropriate robustness and reproducibility cheaply remains challenging. Previous methods coated non-conductive nanofibres with a non-uniform conductive coating or used carbon nanofibre mats that were very susceptible to mechanical stress. To address these factors that negatively affect reproducibility, intrinsically conductive nanofibres were electrospun from an organic semiconducting polymer through an adaptation of an existing method that decreased the overall material cost. The production process was tuned so as to produce mats with appropriate electrical characteristics and the fibres were aligned in a uniform direction so as to provide directed current paths. These mats were then spun directly onto interdigitated electrodes that had been printed onto semi-hydrophobic paper with silver ink via a modified inkjet printer. By employing appropriate cross-linking chemistry, antibodies were bound to the produced nanofibres. These antibodies served as the biorecognition element for the sensor. The data were analysed and it was evident that the binding event did indeed cause a change in resistance. While this resistance could not be repeatably quantified owing to base variance between electrodes, this thesis lays the groundwork for further research.

Uittreksel

Kwantifiseering van CD4+ sel Telling deur Middel van 'n Nanovesel-gebaseerde Biosensor

A.M. Lloyd

Departement Elektriese en Elektroniese Ingenieurswese,
Universiteit van Stellenbosch,
Privaatsak X1, Matieland 7602, Suid Afrika.

Tesis: MIng (Elektronies)

April 2019

Daar is al bevind dat antigeen-substraat binding 'n verandering veroorsaak in die weerstand van geleidende nanovesel-substrate. Hierdie tesis het gepoog om hierdie verskynsel in te span met die oog op die vervaardiging van sensors wat in staat is om CD4+ seltelling te kwantifiseer. Om nanovesel-substrate met 'n gepaste vlak van robuustheid en reproduseerbaarheid op 'n goedkoop wyse te produseer, bly 'n uitdaging. Vorige metodes het behels dat nie-geleibare nanovesels bedek word met 'n nie-uniforme geleidende laag, of het gebruik gemaak van koolstof nanovesel matte wat baie vatbaar was vir meganiese stres. Dit was noodsaaklik om hierdie faktore aan te spreek weens hul negatiewe impak op reproduseerbaarheid. Gevolglik is inherent geleidende nanovesels ge-elektrospin uit 'n organiese semi-geleidende polimeer; dit is vermag deur 'n bestaande metode aan te pas op so 'n wyse dat die kostes verbonde daaraan verlaag is. Die proses is verfyn met die doel om matte met die gepaste elektriese eienskappe te produseer en vesels wat in 'n uniforme rigting le, te vervaardig; sodoende is direkte stroompaaie geskep. Hierdie nanoveselmatte is gespin op elektrodes; die elektrodes is met silwer ink gedruk op semi-hidrofobiese papier deur middel van 'n aangepaste injet drukker. Deur die gebruik van kruisbindingchemie is teenliggaampies gebind tot die geproduseerde nanovesels. Hierdie teenliggaampies het gedien as die "biorecognitionëlement. Uit die analise van die data het dit geblyk dat die bindingproses wel 'n verandering in weerstand tot gevolg gehad het. Alhoewel die weerstand nie herhaalbaar gekwantifiseer kon word nie weens basis afwyking tussen die elektrodes, lê hierdie tesis die grondslag vir verdere navorsing.

Acknowledgements

I would like to express my sincere gratitude to the following people and organisations...

Professor W.J. Perold
Professor P.R. Fourie
Daniel Retief
Marietjie Booyens
Wessel Croukamp
Werner van Eeden
Coreen Lloyd
Hendrik Scheepers de Bruin
Peter Lloyd
CAF SEM Unit
CAF Confocal Unit

Contents

List of Figures

List of Tables

Nomenclature

Compounds

PEO	Polyethylene oxide
PEDOT:PSS	Poly(3,4-ethylenedioxythiophene) polystyrene sulfonate
PVA	Polyvinyl alcohol
DMF	*N,N*-Dimethylformamide
PEI	Polyethyleneimene
BS3	Bis(sulfosuccinimidyl)suberate
ABS	Acrylonitrile butadiene styrene
GOPS/GOPTS	(3-Glycidyloxypropyl)trimethoxysilane
BSA	Bovine Serum Albumin
FITC	Fluorescein isothiocyanate
PAMAM	Poly(amidoamine)

Abbreviations

mw	Molecular Weight
wt%	Weight Percentage
IDE	Inter-digitated Electrodes
PWM	Pulse-width Modulation
DI	De-ionised
ICP	Intrinsically Conductive Polymer
DIP	Dual in-line Package
SOT	Small Outline Transistor

Chapter 1

Context and Introduction

1.1 Background to the Research Problem

The development of antimicrobial resistance (AMR) is a global problem, recognised by the World Health Organisation (WHO)[1]. AMR is when microorganisms, such as viruses, fungi and bacteria, develop a resistance to antimicrobial medication [2]. As such, ensuring the survival of patients suffering from serious infections incredibly difficult, much like in the pre-antibiotic era [3]. The origins of this development are understood, and the ramifications apparent, however, addressing the problem remains challenging. The reason for the difficulty relates to the origin of the phenomenon itself, namely that the use of these agents is exactly what lead to the resistance towards them. The literature is quite clear in its belief that the development of AMR lies largely at the feet of the abuse of antimicrobials.

Methods for addressing this development are clearly necessary. The WHO has thus implemented a number of measures in this regard, such as the Global Antimicrobial Surveillance System, the development of a methodology for monitoring antibiotic consumption at national levels and issuing a list of priority antibiotic resistant bacterial pathogens to help identify where medicines are most urgently needed [2].

The development of new antimicrobial medication was the standard for many years [3]. Unfortunately this is no longer sufficient to stem the tide. Additionally, there is little development on this front owing to financial constraints.

The prevention of infections has also been identified by the WHO as a critical step in addressing the spread of resistant organisms[2]. Barrier techniques, such as isolation, are employed to limit infection, but these methods are primarily effective against organisms from exogenous sources, that is those from outside of the body, [3]. These methods have little to no impact on organisms emerging from endogenous sources, that is those from inside of the body. Furthermore, as the size of the isolated group increases, the practicality of employing barrier methods decreases [3].

Likely the most effective means of addressing antibiotic resistance is the effective use of antibiotics. Some researchers suggest that ”amplification of resistance by antibiotic use is a major, perhaps the major factor” in terms of the selective pressure that gave rise to the development of this phenomenon[4]. J.M.T. Hamilton-Miller suggested that limiting the use of antibiotics is the only practical way to address the development of resistance[5], while Tenover and McGowen state that, ”[i]mproving antimicrobial use is a cornerstone

of dealing with multiresistant hospital organisms." [3].

Many of the methods implemented by the WHO revolve around monitoring the the use and misuse of antibiotics[2]. It stands to reason that a vital role in addressing the development of drug-resistant bacteria falls on the shoulders of accurate diagnoses. By accurately diagnosing a patient, it becomes possible to use targeted medicines, and thereby prevent the overuse of broad-spectrum antibiotics. This would decrease the rate at which resistance towards antibiotics is developed.

The WHO has placed a great deal of focus on the control of drug-resistance in Human Immunodeficiency Virus (HIV), tuberculosis and malaria[2]. Having recognised the need for a global coordinated effort to address HIV drug resistance, the WHO created a global action plan [6]. This pandemic in particular has found a particularly strong foothold in South Africa.

HIV actively attacks the immune system, making the patient increasingly vulnerable to infection. Once the individual's immune system is compromised, the individual is diagnosed with Acquired Immune Deficiency Syndrome (AIDS)[7]. To address the risk of an HIV/AIDS patient becoming ill, broad-spectrum antibiotics can be prescribed to stave off infection, however, it is exactly this type of abuse of antibiotics that results in the development of drug-resistant varieties. To address this it becomes necessary to monitor the progression of the virus closely. This is achieved through the determination of T-cell count via flow cytometry, a process requiring specialised equipment and highly trained personnel.

With a large portion of South Africans currently living in rural areas, and as such often reliant on mobile healthcare services, access to T-cell quantification is limited. The limited number of testing facilities, coupled with sample transport delays, means that it can take anywhere from a number of days, to several weeks before test results can be delivered. It is clear that there is a need for a point-of-care device that is able to provide accurate T-cell count rapidly, and cheaply. By quantifying this result, it becomes possible to gauge the degree of resistance a patient has towards contracting infection. This type of analysis is often achieved through the use of biosensors.

Biosensors are devices that combine a biological element with a physiochemical detection element or transducer. The biological component interacts with the target analyte in a manner that produces a response that is observable by the transducer[8].

Many different biosensing methods exist, such as electronic, electrochemical, optical and piezoelectric sensors. The output of the biosensor is determined by the type of transducing element chosen. The effectivity of any biosensor is largely governed by two important factors, the first of which being the biorecognition element.

The biorecognition element needs to be highly specific. The lower the specificity of the element, the greater the likelihood that the biorecognition element reacts with something other than the target analyte in one's sample. This type of specificity can be achieved through a number of means, such as the use of antibodies, enzymes and specialised binding receptors and proteins.

The second consideration is the method of binding the biorecognition element to the transducer. One of the most common methods is to functionalise the surface of the transducer. This entails treating the transducer so that it presents specific functional groups on its surface. These functional groups can then be used to bind the biorecognition element

through crosslinking chemistry. An alternative to functionalisation is the entrapment of the biorecognition elements through the use of hydrogels.

T-cell count, specifically CD4+ cell count, can vary drastically from person to person. A healthy person should have in the region of 1000 CD4+ cells per microlitre of blood, while a severely ill person's count is often at around 200 cells per microlitre[9]. This necessitates that as many cells as possible need to be bound in order to obtain accurate results. In a biosensor, the number of available binding sites is proportional to the available surface area, meaning that a transducer with a large surface area is desired. In the context of a point-of-care device, however, another parameter of interest is overall volume. Larger volumes of material can increase cost and stand the risk of the biosensor becoming cumbersome. Given both these considerations it becomes evident that the actual parameter of interest is the surface area to volume ratio. The need for a large surface area to volume ratio naturally brings nanofibres to the forefront of transducer consideration.

1.2 Introduction

1.2.1 Motivation

This research is driven by two equally important factors. The first factor is the development of antimicrobial resistance. AMR, if left unchecked, would cause countless fatalities. The WHO has recognised the importance of addressing this issue, and has implemented various policies in order to combat the development thereof. It is evident that one of the, if not the most, important steps in addressing AMR is the controlled and appropriate use of existing antibiotics. To this end, it is important to develop different types of sensing apparatus that are fast, accurate, and readily available to people from all walks of life. Rapid diagnosis coupled with consistent monitoring is the most effective way to stem the tide.

The second factor is the HIV/AIDS pandemic. Millions of people worldwide suffer from HIV/AIDS. While there is currently no cure readily available, accurate diagnosis is of great importance in the fight to curb the spread of this virus. Additionally, tracking the progress of the virus is vital in the fight to extend the patient's life expectancy. Africa and South Africa in particular have a great need for development on these fronts.

1.2.2 Research Question

Primary: Can a nanofibre-based biosensor be developed to quantify patient immunity accurately.

Secondary: Can this sensor be developed cheaply

1.2.3 Research Aims and Goals

i Produce intrinsically conductive nanofibres with a uniform diameter.

ii Produce a sensor that can produce a measurable change when exposed to CD4+ cells. This sensor should ideally be uniform in terms of its base characteristics.

iii Plot the characteristic curves and or trend lines and establish the relationship between resistance and increasing CD4+ cell concentration.

1.2.4 Research Objectives

i
- To determine the effect of a lower molecular-weight PEO on fibre production
- To investigate the effect of increasing amounts of PEO on the solution
- To investigate the effect of fibre alignment on mat conductivity

ii
- To spin fibres directly onto IDEs, thus forming resistive elements
- To produce resistive elements with low variance
- To design resistive-sensing electronics with noise mitigation

iii
- To analyse variance and establish trend lines from the obtained data sets

1.2.5 Scope

The scope of this thesis delineates what needs to be considered and what does not. The following falls within the scope:

CD4+ cells

- Quantification of CD4+ cells is the standard method for determining HIV/AIDS progression as there is a direct correlation between CD4+ cell count and HIV progression

The following falls outside the scope of this thesis:

Any other immunity markers

1.2.6 Chapter Outlines

Chapter 2: General Literature Review

Chapter 2 comprises a general literature review. The structure of this thesis is such that a number of experiments were conducted, each with its own relevant materials and typically independent of each other. Consequently, each experiment-based chapter will start with its own brief, more focussed literature review. This particular chapter comprises the following sections:

- Introduction
- Antimicrobial Resistance
- Immunity, HIV and AIDS
- Relevant Markers
- Conclusion

Chapter 3: Biosensors

This chapter discusses the history of biosensors, as well as their use today. This section elaborates on various methods currently employed in the development of biosensors, and will look at the design choices that resulted in the final design. This chapter comprises the following sections:

- Introduction
- Literature Review
- – History of Biosensors
  – Established Biorecognition Elements
  – Established Methods of Biosensing
  – ∗ Thin Films
    ∗ Nanofibres
- Theoretical Design Development
- Conclusion

Chapter 4: Nanofibres and Nanofibre Production

This chapter discusses the history of nanofibres and the different methods of nanofibre production. Different methods of nanofibre production are compared and the method most suited to this application is decided upon. This chapter also details the developmental procedure involved in producing a nanofibre-production setup, and verifies that the produced setup is capable of producing nanofibres. This chapter comprises the following sections:

- Introduction
- Literature Review
- – A history and explanation of available production methods
  – Evaluation of method applicability in the context of this thesis
- System Design
- System Verification
- Conclusion

Chapter 5: Development of Intrinsically-conductive Nanofibres

This chapter discusses the development procedure followed to make intrinsically-conductive nanofibres. This section follows documented procedure closely, substituting one component for a cheaper version with a lower molecular weight, and subsequently elaborates on the effect on the nanofibre-production process. Finally, the produced fibres are evaluated and characterised. This chapter comprises the following sections:

- Introduction
- Literature Review
- – Effect of various parameters on electrospinning
  – Function of the components in the solution

- Initial Customisation of Solution
- Primary Nanofibre Production
- Primary Fibre Characteristics (Verification)
- Secondary Nanofibre Solution Customisation and Electrode Production
- Secondary Fibre Characteristics (Verification)
- Final Fibre Solution Customisation and Electrode Production
- Final Fibre Characteristics (Verification)

Chapter 6: Developing Sensors from Polymer Nanofibres

This chapter discusses the method of sensing to be utilised in this thesis. This section details how the produced nanofibres are incorporated into a sensing circuit. The circuit itself is evaluated and explained. This chapter is comprised of the following components:

- Introduction
- Literature Review
- – Existing implementations of resistive sensing
  – Important considerations
- Design
- Conclusion

Chapter 7: Sensor Functionalisation and Crosslinking

This chapter discusses the procedures involved in converting the standard fibres into a sensitive and selective sensing element. Focus is placed on both functionalisation and the required crosslinking chemistry. This chapter comprises the following components:

- Introduction
- Literature Review
- Functionalisation Methodology
- Functionalisation Verification
- Antibody Crosslinking Chemistry
- Lysozyme Analysis: Pre and Post Antibody Addition
- CD4 Analysis: Pre and Post Antibody Addition
- Conclusion

Chapter 8: Characterisation of Nanofibre-based Biosensors

This chapter serves to evaluate the produced sensors and interpret the obtained results. This chapter comprises the following components:

- Introduction
- Lysozyme Analysis: Pre and Post Protein Addition
- CD4 Analysis: Pre and Post Protein Addition

Chapter 9: Conclusion

Chapter 10: Recommendations for further research

Chapter 2

General Literature Review

2.1 Introduction

AMR and HIV/AIDS are two pandemics currently at large, with no foreseeable solution currently available. Methods should be researched and employed to limit the development of these pandemics as far as possible. As mentioned in Chapter 1, it is believed that the development and implementation of a suitable biosensor would contribute towards this goal. This section aims to provide an overview of the literature concerning certain specific topics directly related to the development of the biosensor developed in this thesis.

2.2 Antimicrobial Resistance

An understanding of AMR requires an understanding of microbes. Microbes are defined as "…living organisms that multiply frequently and spread rapidly"[10]. Bacteria, viruses and some parasites are all examples of microbes. It is important to note that not all microbes are harmful to the human body. In fact, certain microbes are beneficial, such as the bacteria that aid in digestion.

AMR refers to the ability of microbes to live and grow while in the presence of an antimicrobial agent that would normally kill them or limit their growth [10]. Multiple sources agree that AMR is a grave problem. In 2014 the Centers for Disease Control and Prevention (CDC) listed AMR as the second-most significant health threat [11]. This prompted the CDC to launch an initiative to combat AMR, and as such they have distributed significant funds to support health departments. These investments are aimed at improving detection, response and control of resistive pathogens, prevention of the spread of resistive infections, and encouraging innovation to develop new strategies, drugs and diagnostic methods to address this problem [12]. The WHO undertook an action plan to address the development of AMR, which was revised in 2017 [2]. The objectives of this action plan or framework are to preserve current antimicrobial medicines through appropriate distribution and use, to promote research into and the development of new antimicrobial agents, as well as diagnostic tools for detecting AMR, and to promote affordable access to antimicrobial medicines and diagnostic tools [1]. Robert Gaynes points out that infectious diseases were among the most common causes of death in the pre-antimicrobial era, and that some of these diseases are re-emerging owing to AMR[4]. While it is evident that there is an emphasis on the need to address AMR, it is also clear that the proposed methods for dealing with the problem rely fundamentally on two ideas: appropriate control of

existing antimicrobials and the development of new antimicrobials. The reasoning behind this is best understood when analysing the mechanisms behind the development of AMR, as well as the history of antimicrobials and how AMR has affected their use and efficacy.

It is widely held and well-supported that the development of AMR can largely be ascribed to the effect of antimicrobial use on the natural evolutionary path of microbes [13][14]. The "Chatelier Principle" proposes that, "when a system experiences a disturbance…, it will respond to restore a new equilibrium state." This holds true for organic systems, and indeed, for micro-organisms. Hamilton-Miller writes that the introduction of antibiotics placed a great deal of stress on bacteria species in the form of selection pressure [5]. Selection pressure refers to environmental conditions that allow those members of a species with novel mutations or newly acquired characteristics to survive, while those that remain unchanged, die [3]. It is therefore apparent that the acquisition of resistance was a natural progression of events. When one couples this natural progression to the average lifecycle of many pathogenic bacteria, approximately 20 minutes, it also becomes evident that the acquisition of resistance is trivial. In fact, the capacity of microorganisms to develop resistance has been said to surpass our imagination [15]. Hamilton-Miller posits that the evolutionary relationship between bacteria from the pre-antibiotic era and present day is similar to the relationship between modern man and Dryopithecus, the common ancestor of man and apes [5].

The first antimicrobial agent to be developed was called Salvarsan and was synthesised by Paul Ehrlich in 1910. A synthetic drug, Salvarsan was used in the treatment of syphilis. In the history of antimicrobials, 1928 stands out as a notable year as Alexander Fleming discovered penicillin. He noticed that in an area surrounding a blue mold contaminant in a culture dish, the growth of *Staphylococcus aureus* (*S. aureus*) was inhibited [15]. In 1942, Florey and Chain succeeded in obtaining purified penicillin for the first time, and in 1945, Fleming, Chain and Florey were awarded a Nobel Prize. The following two decades saw the development of a number of new antimicrobial agents, such as streptomycin, chloramphenicol, tetracycline, macrolide and nalidixic acid[15]. While penicillin is still widely used today, penicillin-resistant (by means of the secretion of penicillinase) strains of *S. aureus* were not only in existence, but increasing in number in the 1950s[15]. To address this, methicillin was developed in 1960, however, a methicillin-resistant variety was discovered only a year later [15]. This development is not unique to *S. aureus*.

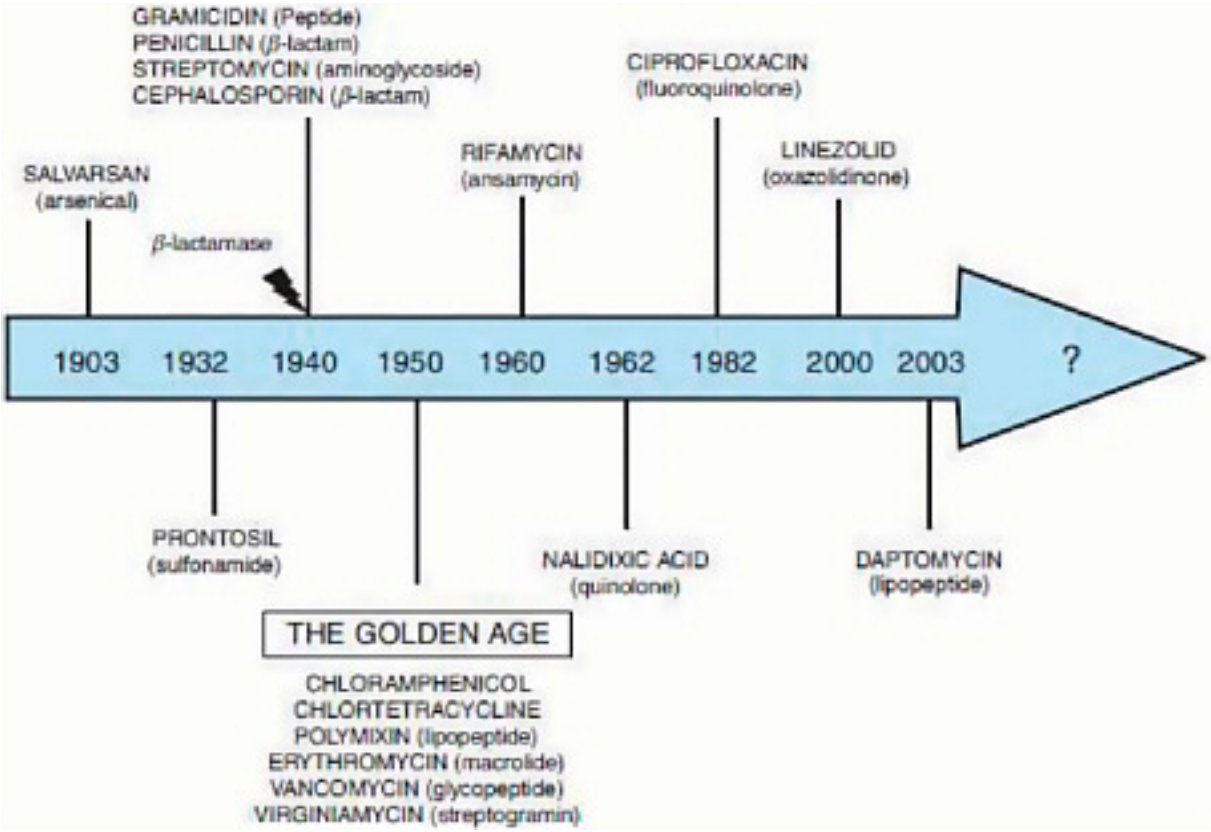

Figure 2.1: History of Antibiotics[16]

It is important to note from the above diagram that in recent years, little to no development of new antimicrobials has taken place. In fact, antibiotic drug discovery started to wane in the 1980s [4]. A WHO news release concerning an article on the clinical development pipeline of antibacterial agents highlighted the serious lack of development of new antibiotics [17]. The main reason behind this is the financial feasibility, or rather, the lack thereof. Developing a new drug is an incredibly expensive procedure consisting of multiple phases [18]. Ever-increasing health and safety regulations only add to the complexity. Naturally, newer antimicrobial agents are very often more expensive than their established counterparts [4]. The price of antibiotics may also influence which antibiotics are prescribed [14]. When one considers the costs involved in drug development, coupled with the rapidity with which drug-resistant strains develop as well as the effect of product cost on the likelihood of prescription, it stands to reason that pharmaceutical companies do not see the development of new antimicrobials as a sound investment. These companies are likely to see a greater return on investment with other products [14]. While it is clear that efforts must be made to develop new antimicrobials despite the cost, this development alone is by no means sufficient. To quote Gaynes, "[t]he problem of antibiotic resistance…cannot be solved solely by the repetitive introduction of new antibiotics. That strategy would be too costly and ultimately would fail."[4].

It is widely agreed that the best way to combat AMR is through the appropriate regulation of the use of antibiotics. This type of control has been described as "…exceedingly important." [4] and "[t]he only practical option we have at present to stem the tide…[of AMR]". This stance is corroborated by the emphasis placed on the control of antimicrobials by institutions like the WHO and the CDC. Evidence supporting the belief that

antimicrobial use acts as a form of selection pressure can be found in the agricultural industry. In agriculture, antimicrobials are used not only to treat diseases and infections, but also to prevent them proactively. A study by the Institut Pasteur found that bacteria capable of passing on the gene in *Salmonella* governing Ampicillin (an antibiotic derived from penicillin) resistance emerged in the late 1950s. This was surprising as Ampicillin was only made available to European markets in 1961, with drug-resistant strains already noted between 1962 and 1964 [19]. It is suggested that a likely cause for this was the then common practice of adding small quantities of penicillin to animal feed [19]. This study was released only weeks after the WHO called for more responsible and prudent use of antimicrobials in agriculture [1]. Bearing this in mind, it is worrying that the CDC believes that "[a]t least 30% of antibiotics prescribed in outpatient settings are unnecessary" [11].

It is clear that controlling the use and distribution of antimicrobial agents is paramount in the fight against AMR. Implementing improved control, however, is a not a trivial matter, especially in areas where resources are limited. Administering broad-spectrum antibiotics, for example, is one of the only available avenues when awaiting the results of certain diagnostic tests which only contributes to the problem of AMR for the above-mentioned reasons. It is clear that one of the avenues that requires development when it comes to addressing AMR is diagnostic tools. Obtaining accurate diagnostic information quickly enables the immediate application of targeted agents, which not only helps to address AMR, but is likely to enhance the recovery-rate of the patient.

2.3 Immunity, HIV and AIDS

Immunity is a collective term referring to a variety of mechanisms that prevent infection. Immunity consists of specific and non-specific components which are either active or passive. Active immunity refers to all of the components of immunity that are brought about by one's own body, whereas passive immunity refers to components of immunity that were developed in the body of another person. An example of passive immunity is the immunity an infant has obtained from its mother. During pregnancy, antibodies are transferred through the placenta from the mother to the child. Other examples of passive immunization include injections of immune serum globulin and injections of tetanus antitoxin [20].

The non-specific components, or innate components, of immunity protect against a wide variety of antigens. Some examples include skin, stomach acid and enzymes in tears and skin oils. The specific components are, like their name suggests, focussed on targeting specific antigens. Acquired immunity, the immunity that develops over time owing to exposure to an antigen, is an example of specific immunity [20]. Acquired immunity relies largely on the function of lymphocytes. Lymphocytes are white blood cells that typically come in two varieties, B and T.

B cells and T cells stem from the same type of stem cell, and acquire different names based on the regions in which they mature. T cells are known as such as they mature in the thymus from thymocytes, while B cells mature in the bone marrow (in adults) [21].

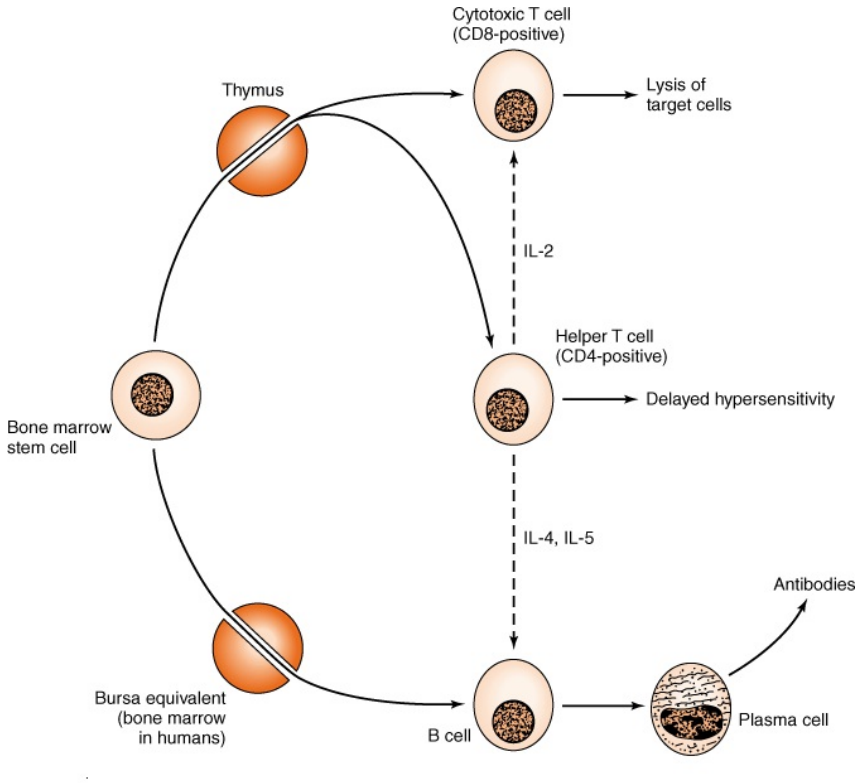

Figure 2.2: Development of T and B cells [22]

T cells can be split into two main classes - cytotoxic or killer T cells, and helper T cells. These cells are also referred to as CD8+ and CD4+ cells respectively [21]. CD4+ and CD8+ refer to the proteins exhibited on the surface of the cells, and the ”killer” and ”helper” labels refer to the specific functions of the cells.

CD4+ cells or T helper cells assist in two main forms of immunity; cell-mediated immunity and antibody-mediated immunity. Cell-mediated immunity is an immune response that does not involve antibodies, but instead relies on specific cells. CD4+ cells bind to the surface of antigen-presenting cells (APC) and release lymphokines (a subset of cytokines, which are a category of small proteins that are used in cell signalling). These attract more cells to the area. Antibody-mediated immunity is the subsection of humoral immunity relating to the role of antibodies in the immune response. CD4+ cells enhance the ability of B cells to produce antibodies[23]. They do this by binding to the B cells and releasing cytokines, which results in the B cells undergoing rapid mitosis, thus increasing their number. These cells either become memory cells or plasma cells. Upon re-infection, memory cells divide and form plasma cells. Plasma cells are responsible for the production of antibodies. A normal range for CD4+ cell count is 500 to 1500 cells per microlitre[24].

CD8+ cells are similarly known as T killer cells. Their function is to increase the cytotoxicity of the cells to which they bind, killing them. This is of particular importance when fighting off viral infections. Viruses often subvert the natural function of a cell by altering its DNA so that the cell produces more of the virus. In the early stages of this process, fragments of the virus’s proteins display on the surface of the cell. This attracts the CD8+ cell. By killing the cell, the new developing viruses are prevented from spreading.

It is clear that CD4+ and CD8+ cells play an important role in patient immunity and that quantification of these parameters provides valuable information when analysing a patient's ability to resist infection.

When examining immunity, both HIV and AIDS inevitably come to the fore. This stems from the fact that HIV targets the immune system directly by targeting CD4+ cells. AIDS refers to the state of a human being suffering from the effects of late-stage HIV infection, namely, that of being immunocompromised. In this state, the patient is highly vulnerable to all forms of infection and incapable of adequate defence. It is defined through either a CD4+ cell count of below 200 cells per microlitre of blood, or the occurence of specific diseases, such as pneumocystis pneumonia, in conjunction with an HIV-positive diagnosis. It is for this reason that CD4+ cell count is used to track HIV progress. Both the absolute value of the CD4+ cell count as well as the ratio of CD4+ to all leukocytes can be used. CD4+ to CD8+ ratio is also sometimes used to evaluate HIV progression and overall immune health. To quantify these cells, flow cytometry is used. Flow cytometry uses lasers and fluorescent labels to determine the physical and chemical characteristics of the particles in a fluid [25].

It should be noted that HIV/AIDS and the prevention of the development of HIV AMR have received a great deal of focus in recent years. The most notable example thereof is the action plan implemented by the WHO, aimed at controlling drug-resistance in HIV, tuberculosis and malaria [6]. This is of particular significance in a South African context as South Africa is home to 19% of the world's HIV patients and in 2016 saw 110 000 AIDS-related deaths [26] [27]. The development of a drug-resistant variant of HIV has the potential to decimate the South African population and as such CD4+ cell quantification in particular is of great importance.

2.4 Conclusion

It is clear that there is a great need for the development of strategies and technologies in all fields relating to the prevention of the development of AMR. This is made evident by the efforts put in place by international and national organisations like the WHO and the CDC, who are providing large-scale financial support to a variety of initiatives. The investment of money into the development of new antimicrobials serves to illustrate the severity of the problem, as it is clear that this type of research produces insufficient revenue for large pharmaceutical companies to invest in themselves.

The literature is also clear that appropriately managing current antimicrobial usage is the best recourse to address the problem of AMR development. The implementation thereof is not a trivial matter as it consists of various components. One component does stand out: diagnosis. Rapid and accurate diagnosis would allow for the swift implementation of targeted medicines. This would help to remove reliance on broad-spectrum antimicrobials, and thus help to decrease the rate at which resistance towards these drugs develop.

Another component to consider is overall patient immunity. Knowledge of how resistant a patient is to infection could serve as an important factor in cutting down on the over-prescription of antimicrobial agents. If a patient is known to be in good immune-system health, prescription of preventative medication can, under many circumstances, be avoided. Furthermore, one of the important factors governing the immunity of a patient, CD4+ cells, happens to be of vital importance in the analysis of HIV and AIDS.

It is thus evident that the development of a sensor capable of rapidly and accurately determining patient CD4+ cell count would be of great use in the fight against AMR, both in its entirety and with sppecific focus on HIV and AIDS.

Chapter 3

Biosensors

3.1 Introduction

Merriam-Webster defines a biosensor as, "a device that monitors and transmits information about a life process; especially: a device consisting of a biological component…that reacts with a target substance and an electrochemical or optical component that detects the resulting products or by-products and emits a signal"[28]. Biosensors are used to determine the presence and/or concentration of a target analyte in a substance. An example of a typical biosensor can be seen in Figure 3.1.

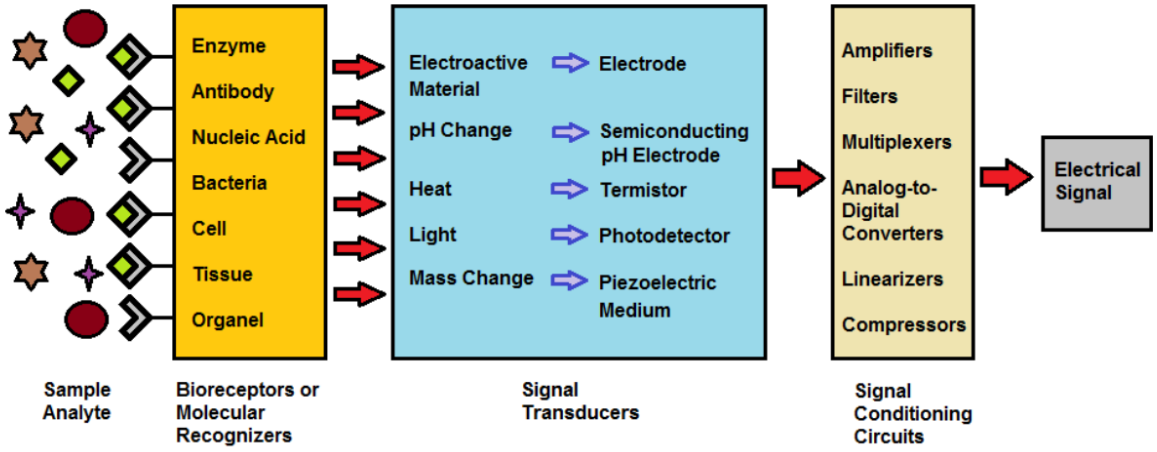

Figure 3.1: Biosensor Operating Principle: Main Subsystems [29]

This figure demonstrates a series of components, namely the Analyte, the Bioreceptor or Biorecognition element, the Transducer, the Conditioning Circuits and the Output Signal, each of which plays an important role in the analysis procedure.

This section disscusses the history of biosensors and highlights important factors that need to be considered when designing one. This chapter also discusses the design development procedure followed in this report.

3.2 Literature Review

3.2.1 History of Biosensors

One of the earliest documented implementations of a biosensor can be attributed to M. Cremer in 1906. Cremer proved that a potential difference is present between two liquids of different acidities separated by a glass membrane[30]. This was especially notable as the concept of pH was only established in 1909 by Søren Peder Lauritz Sørensen[31].

The literature indicates that the first 'true' biosensor (a biosensor containing a biorecognition element) was developed in 1956 by Leland C. Clark, Jr [32][33]. Clark is often heralded as the "Father of Biosensors", including at the 1992 World Congress on Biosensors in Geneva, Switzerland[34]. His sensor, eponymously named the 'Clark Electrode', was an oxygen sensor for use in conjunction with the heart-lung machine he had also developed. The electrode was required to determine the oxygen concentration in the blood exiting the heart-lung machine[34]. Clark realised that he could reduce the oxygen by means of a catalytic platinum electrode according to the following equation:

$$O_2 + 4e^- + 4H^+ \xrightarrow{\text{Pt}} 2H_2O \tag{3.1}$$

By connecting a voltage source to the platinum electrode, oxygen from the blood bound with hydrogen to form H_2O. This process is limited by the amount of electrons available and by the amount of oxygen flowing by. Increasing the voltage from zero will result in an increasing current, until eventually reaching saturation, whereafter increasing the voltage will not increase the current. This is because, in this instance, the oxygen is limiting the reaction. Thus, by determining the current saturation level, it is possible to determine the oxygen level present in the fluid flow.

In his initial experiment, Clark noted that the current draw decreased rapidly instead of maintaining a fixed level. He realised that this was as a result of the fouling of the electrode by the accumulation of particles from the blood. He then posited that a gas-permeable membrane should serve to protect the electrode. He proved this by making use of the cellophane wrapper from a pack of cigarettes[34].

Clark subsequently realised that he could develop a glucose sensor based on his oxygen sensor. Clark bound the enzyme glucose oxidase to the surface of the platinum electrode. When exposed to glucose, glucose oxidase converts oxygen into hydrogen peroxide. Consequently, increasing levels of glucose in the blood sample would result in decreased oxygen concentrations, which translates to a lower current draw. His paper on the subject coined the term "enzyme electrode" [33].

In 1969, Guilbault and Montalvo, Jr developed the first potentiometric biosensor for the detection of urea [35] and in 1975, Yellow Spring Instruments (YSI) produced the first commercial biosensor [32]. Since then, biosensor development has seen large-scale progress. Table 3.1 highlights certain significant advances in the development of biosensors:

3.2.2 Established Biorecognition Elements

While many advanced biorecognition elements exist, such as custom constructed DNA polynucleotides, this section of the report aims to highlight and detail only some of the

Table 3.1: Important milestones in the development of biosensors during the period 1970 to 1992

1970	Discovery of ion-sensitive field-effect transistor(ISFET) by Bergveld
1975	Fibre-optic biosensor for carbon dioxide and oxygen detection by Lubbers and Opitz
1975	First commercial biosensor for glucose detection by YSI
1975	First microbe-based immunosensor by Suzuki et al.
1982	Fibre-optic biosensor for glucose detection by Schultz
1983	Surface plasmon resonance (SPR) immunosensor by Liedberg et al.
1984	First mediated amperometric biosensor: ferrocene used with glucose oxidase for glucose detection
1990	SPR-based biosensor by Pharmacia Biacore
1992	Handheld blood biosensor by i-STAT

Reconstructed from [32]

most commonly used types of biorecognition elements. These are receptors, enzymes, antibodies, aptamers and peptide nucleic acids.

In this context, receptors refer to specialised protein molecules that receive chemical signals from outside a cell. The signal comes in the form of bonding between the receptor and a ligand. The use of receptors as biorecognition elements stems from the fact that, upon receiving the necessary signal, receptors initiate a specific cellular response, such as conformational changes. These changes can have subsequent effects, such as ion channel opening.

While high ligand specificity makes receptors seem appealing, various factors, such as low yield, relative instability and labour-intensive purification protocols of specific proteins have severely impeded development in receptor-mediated sensing [36].

Enzymes are very important macromolecules. The function of an enzyme is to act as a catalyst, meaning that it increases the rate at which certain chemical reactions take place, while not being consumed in the reaction itself. The products observed from the reaction are thus regulated entirely by the input chemicals, provided a sufficient amount of the catalysing agent is present. The aforementioned work by Clark (see Section 3.2.1) serves as a prime example of a biosensor employing enzymes as a biorecognition element.

As the signal corresponds to a rate of reaction, the use of enzymes is well-suited to flow-based sensors, such as those utilising microfluidics.

Most rapid-detection biosensing systems make use of antibodies as the biorecognition element for the purposes of recognition, identification and quantification of target analytes [36]. The use of antibodies saw a great rise in popularity after Kohler and Milstein established monoclonal antibody (MoAb) technology [36]. Their work enabled the use of cell clones that produce MoAbs of choice to produce large quantities of antibodies. This was achieved through a process that came to be known as hybridoma technology, which combined a type of cancerous cell with a cell producing the required antibody, thus endowing the antibody-producing cell with the ability to undergo rapid mitosis[37].

Antibodies are largely used for their very high specificity. Antibodies only bind to the antigen that they were designed for. Upon binding with the antigen, the antigen-antibody complex is formed. This binding can result in various optical and electrochemical changes.

As such, antibodies have been used in numerous ways, with the difficulty of implementation varying between methods.

Aptamers are small DNA or RNA ligands[38]. They are able to fold into three-dimensional structures and bind with high affinity and specificity to a range of target molecules[36]. Aptamers are produced synthetically through a complex process known as Systematic Evolution of Ligands by Exponential Enrichment (SELEX). Aptamers bind to their target based primarily on the target's shape, rather than its sequence[38].

Peptide Nucleic Acids (PNA) are very useful in terms of binding DNA strands. PNA are synthetic approximations of DNA which use a polyamide backbone in place of a sugar-phosphate backbone. PNA backbones are uncharged, which results in improved thermal stability during the formation of PNA-DNA duplexes when compared to DNA-DNA duplexes. The uncharged nature of the backbone also has the effect that it is not necessary to create a high-salt environment for hybridization to occur as the extra charge carriers are not required to overcome interstrand repulsion[36].

3.2.3 Established Methods of Biosensing

There are various different methods of biosensing, each suited to different applications. Figure 3.2 provides a useful overview of many of the established methods of biosensing currently available. This section briefly discusses piezoelectric sensing, opto-electronic sensing, thermistor-based sensing, electrochemical sensing and amperometric sensing.

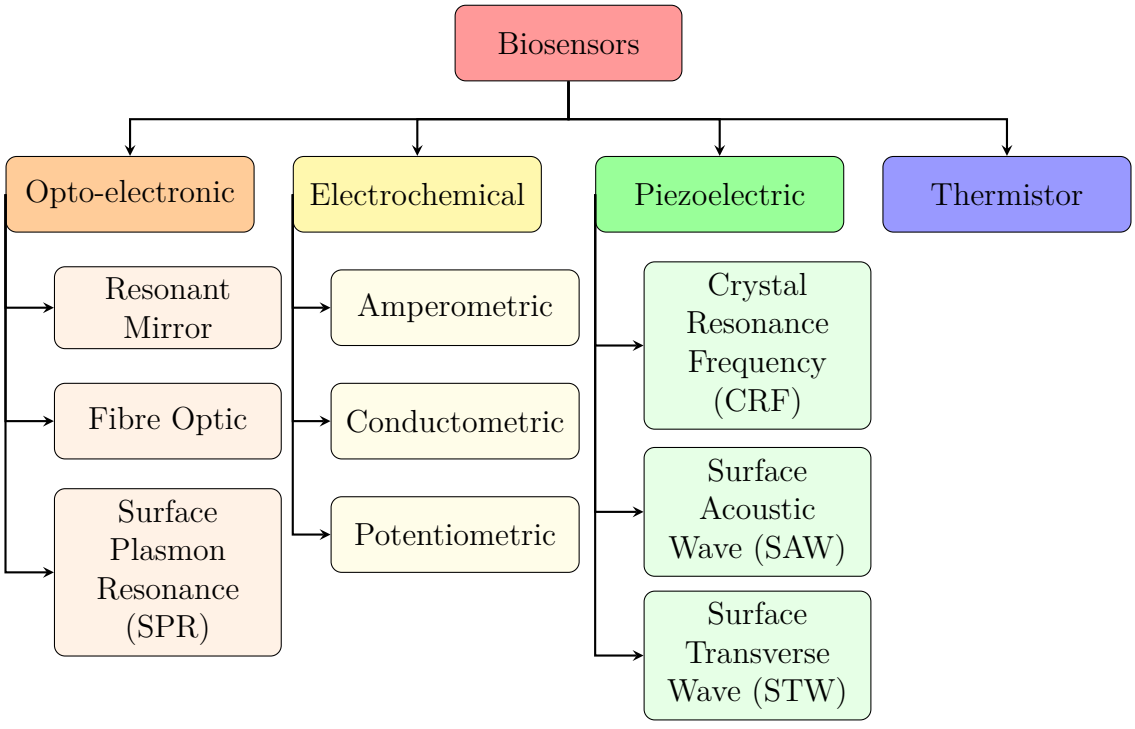

Figure 3.2: Types of Biosensors - Partial reconstruction from [29] and [39]

Piezoelectric biosensors rely on the piezoelectric effect. Piezoelectricity is the electric charge that develops in certain specific materials owing to mechanical stress. This occurs owing to the non-symmetrical nature of the unit cell in piezoelectric materials. When

stress is applied, the electrical balance of the crystal is disturbed, resulting in charge build-up proportional to the applied stress.

Opto-electronic sensors make use of the optic properties of the sample being analysed. These sensors require a light source and detection element. The difference between the light emitted and the light received is used to determine the effect of the analyte. A simple example is a pulse-oximeter, a device that is used to monitor oxygen saturation in patients, and from which heart-rate can be derived.

Thermistor-based sensors rely on changes in temperature. When certain chemicals react, heat is generated. By measuring the temperature change of a known reaction, it is possible to infer the concentration of the analyte in the substance.

Electrochemical sensors make use of the effect that certain chemical reactions have on the electrical characteristics of a known substrate. These sensors can typically be characterised as either amperometric, conductometric or potentiometric.

An amperometric biosensor measures the change in current brought about by the presence of the target analyte. A conductometric biosensor measures the change in conductivity of a medium brought about by the analyte. A potentiometric biosensor measures the accumulation or dissipation of charge brought about by the analyte [39].

3.2.4 Analysis of Method Applicability in the Context of this Thesis

As a concentration, not a force, is to be measured it stands to reason that piezoelectric sensors are not well suited. Furthermore, piezoelectric sensors operating at this scale are difficult to produce, and expensive to obtain commercially. While opto-electronic sensors could potentially produce accurate results, exceptionally fine control would need to be implemented in order to obtain accurate information on such a small scale. Thermistor-based sensors are also not ideal as many organic components are temperature sensitive, meaning that it is undesirable to bring about a change in the solution temperature as this could have various unforeseen results. Based on this, it was decided that an electrochemical sensor would need to be developed.

3.3 Theoretical Design Development

To design a biosensor, it is necessary to decide upon how the following aspects will be approached:

- Target analyte
- Biorecognition element
- Method of detection
- Substrate
- Intended Circuitry

3.3.1 Target Analyte

Based on the discussions in Chapter 2, it was determined that the target analyte of interest is CD4+ cells. In this thesis, human CD4 protein was selected as the target analyte, not CD4+ cells. The reasoning behind this decision is that the binding principle would be the same. Additionally, CD4+ cells are more expensive to obtain than CD4 protein. Furthermore, obtaining CD4+ cells requires an additional level of clearance that the protein alone does not. In addition to all of this, the CD4 protein is sufficient for proof-of-concept applications.

3.3.2 Biorecognition Element

Anti-CD4+ antibodies of the Immunoglobulin G (IgG) variety were selected as the biorecognition elements. Antibodies were selected for multiple reasons. Firstly, antibodies provide very high specificity. Secondly, these particular antibodies are readily available. Lastly, crosslinking of antibodies is a well-documented procedure. The decision to use the Ig variety corresponds to the fact that IgG antibodies constitute the vast majority of antibodies in the human body.

The crosslinking procedure will largely depend on the substrate used. The Fc portion of Ig antibodies express amine groups which can be used to bind the antibodies to a substrate. The substrate will determine if additional functionalisation is required and which type of crosslinker will be used.

3.3.3 Method of Detection

Various methods of analysis are available, such as voltammetry and resistive sensing. Ultimately, resistive sensing was selected as it is comparatively simple to implement, which helps to keep the overall cost of the sensor down.

3.3.4 Substrate

Two particular approaches were considered, namely thin films and nanofibres. Thin films are easy to produce and require little material. Thin films can be produced from a variety of materials and in various ways, such as spin-coating, deposition, sputter-coating and thermal evaporation.

Nanofibres also require very little material to produce. Production methods can range from simple to complex, and various different structures can be produced. The largest benefit of nanofibres is their incredibly large surface-area to volume ratio. This ratio makes them appealing in biosensing applications as a larger surface area corresponds to more available binding sites.

A potential drawback to nanofibres could be that there are limitations to the materials from which they can be produced.

Ultimately, nanofibres were selected as the substrate of choice owing to the high surface area to volume ratio. This is of particular importance because the concentrations of CD4+ cells can be very low, and an increase in the number of available binding sites increases the likelihood of the target cells binding.

These fibres would need to be conductive. The use of conductive nanofibres as the substrate for a biosensor has shown success in identifying target analytes in the work done by C.G.A. Viviers[40]. Ideally, the fibres should be intrinsically conductive, and not made conductive through a coating process. The reason for this is that the coating process, as documented by Viviers, introduces a degree of variability between samples as one cannot guarantee that all of the fibres are coated equally. This naturally decreases reproducibility.

The nanofibres used in this application should also, ideally, have appropriate mechanical properties. Viviers and N. Lawrenson[41] found that the carbon nanotubes used in their experiments were highly sensitive to physical stress, which often resulted in fibres breaking. Consequently, intrinsically conductive polymers were highlighted for analysis as the elastic properties of polymers could potentially result in increased reproducibility of samples as a result of increased robustness towards handling.

3.3.5 Intended Circuitry

As the solution may contain components other than the analyte that could affect the measured conductivity, it is desirable to perform a differential reading. This would compare the change in conductivity of a sample on a sensor without antibodies to a sample with antibodies. By obtaining the difference between the values, it is possible to obtain the effect of the analyte only.

To implement this analysis, a wheatstone bridge will be employed. The use of a wheatstone bridge is a staple in resistive sensing applications as it removes noise and amplifies the measured signal. If the configuration is adjusted appropriately, it is possible to obtain the difference between resistors.

The output from the wheatstone bridge will be fed through a low-pass filter to remove further noise, and then through an instrumentation amplifier to boost the signal to readable levels.

3.4 Conclusion

The final design intends to determine the change in conductivity caused by the concentration of CD4+ cells in a sample. It aims to achieve this by binding CD4+ cells to nanofibre substrates by means of antibodies. The sample solution will be placed on two sensors, one with antibodies and one without. The difference in the voltage at the two outputs will be filtered. The magnitude of this final signal should correspond to the concentration of cells in the sample.

Chapter 4

Nanofibres and Nanofibre Production

4.1 Introduction

Nanofibres can be comprised of various different materials and can be produced in a myriad of ways, such as drawing, electrospinning, self-assembly, template synthesis, and thermal-induced phase separation. This chapter discusses these different methods of nanofibre production, and explains why electrospinning was finally selected as the means of fibre production. Additionally, this chapter documents the system design and verification carried out to produce a simple electrospinning setup.

4.2 Literature Review

4.2.1 A history and review of some of the available nanofibre production methods

Producing nanofibres via a drawing process is a relatively new method, with the first professionally documented instance having taken place in 1998[42]. This process produces individual nanofibres, in contrast to many other methods that produce multiple fibres simultaneously. Naturally, this method lends itself to the study and characterisation of the individual fibre's properties. The drawing process works as follows: A fibre is pulled out of a microdroplet or from a micropipette just at the point of solidification owing to evaporation[42]. The narrowing of the fibre creates a large surface area which in turn enhances the rate of evaporation[43]. A severe limitation to the drawing process is the requirement that the material have pronounced visco-elastic properties, meaning that the material must exhibit both viscous and elastic characteristics, which translates to exhibiting time-dependant strain[42]. This is a problematic because few materials exhibit these properties.

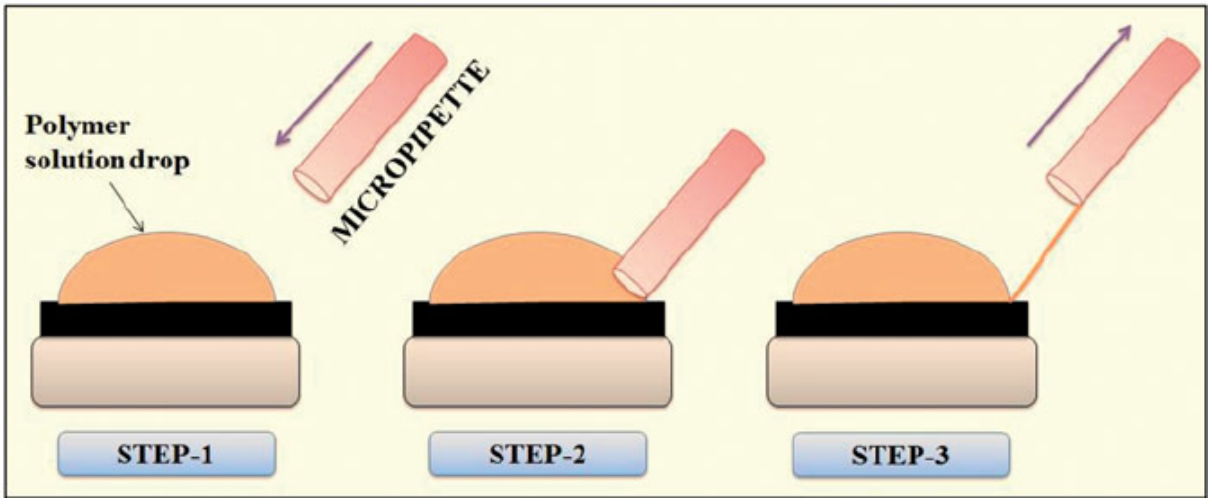

Figure 4.1: Nanofibre Drawing [44]

Electrospinning can be described as a dry spinning process whereby electrostatic forces are used in order to draw fibres from a liquid polymer solution or melt [45]. The first documented instance of electrostatic attraction of a liquid was made by William Gilbert. Gilbert's documentation of the effect of an electrostatic force on liquid came about as he was disproving the notion that electrostatic forces affected the air and not the object itself. In his experiment, Gilbert noted that the liquid formed a cone-shape[46]. This cone would eventually be referred to eponymously as the "Taylor Cone", in honour of Sir Geoffrey Ingram Taylor.

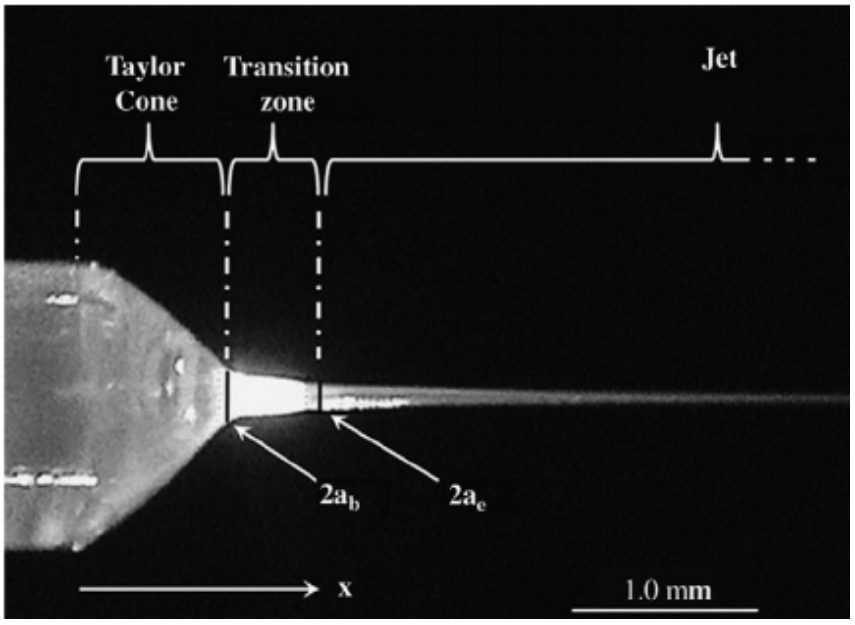

Figure 4.2: Taylor Cone [47]

The first solution used by the pioneers of electrospinning was a highly viscous substance known as collodion[45]. George Audemars produced fibres from this liquid in his earlier experiments in 1855 by simply placing a needle into the substance and drawing a long, rapidly drying filament. Collodion was readily available owing to its use in photography as

a medium for light-active chemicals. The main component required to produce collodion were also readily available owing to the great interest sparked by Christian Friedrich Schönbein's "schießbaumwolle" or "guncotton". The other components required were ether and ethanol. Schönbein apparently stumbled onto his invention after having spilled nitric and sulfuric acids which he cleaned up with his apron, which exploded after being hung up above the fireplace to dry. This explosion left behind no smoke or residue[48]. This "guncotton" was nitrocellulose. In Schönbein's experiment, the sulfuric acid served to catalyse the nitration of the cellulose and aid in the removal of water that would otherwise have limited the degree of nitration [45].

Lord Rayleigh conducted experiments on jets ejected from levitated microdroplets. He found that jets would be ejected when equilibrium was reached between surface tension and electrostatic force, and concluded that they should be observed when the ratio X given by 4.1 exceeds unity.

$$X = Q^2/((64 \cdot \pi^2 \cdot \varepsilon_0 \cdot \gamma \cdot r_0^3)) \tag{4.1}$$

In this equation, Q represents drop charge, ε_0 is vacuum permittivity, γ is surface tension and r_0 is the drop radius[49]. This has served as the backbone for a great deal of research into the effect of electric charge on droplet morphology, among many other topics. Recent research has found jets forming at $X = 1$, which indicates that new investigations into this problem must commence.

The popularity and expense of silk at the time served as an intense driving factor to produce large quantities thereof, or of very similar fabrics. It is to this end that Comte Louis-Marie Hilaire Bernigaud de Chardonnet, also known as Hilaire de Chardonnet, a student under Louis Pasteur, undertook to artificially replicate the process by which silkworms produce silk while researching a disease that was threatening the French silk industry [48]. Chardonnet devised a method of extruding collodion fibres by using a glass capillary. He was also able to decrease the flammability of the collodion using Joseph Swann's ammonium sulphide technique.

In 1888, Charles Vernon Boys designed and built an improved torsion-balance so as to measure the universal gravitational constant. This work required a suspension fibre that was suited to the task. He attempted to use "electrical spinning", and was able to produce beaded fibres from a variety of materials, such as sealing wax, collodion, and shellac. These fibres were, however, unsuited to his application, and he eventually decided on using fused quartz. By heating and drawing the quartz, Boys was able to produce fibres which he then wrapped around a wooden former. As both the force and speed required to draw the fibres was considerable, Boys made use of a crossbow and bolt. Boys drew the fibres by attaching the quartz to the bolt before heating the quartz and the firing the bolt. The fibre produced stretched 90ft (approximately 27 metres) long and the diameter was beyond the scope of available microscopes, however, estimates put the diameter at under 1/100 000 of an inch (approximately 254nm) [50].

The first electrospinning patent was filed by John Francis Cooley, an American inventor and electrician[51]. While his patents proposed different types of heads, all were intended for use with pyroxylin (nitrocellulose) in one way or another. In subsequent years, multiple individuals, such as Anton Formhals, developed patents of their own and contributed to the understanding of the electrospinning process.

Sir Geoffrey Ingram Taylor contributed greatly to the understanding of electrospinning between 1964 and 1969. Taylor mathematically modelled the shape of the cone formed by a fluid droplet under the influence of an electric field. He also worked with J.R. Melcher and developed the ”leaky dielectric model” for conductive fluids [45].

During the 1990s, several research groups, of which Reneker's stands most prominently, proved that many organic polymers could be electrospun. Consequently, there has been an exponential increase in the number of electrospinning publications each year. Many variations of electrospinning have been developed over the years but the core principle remains the same.

Today, simple electrospinning setups are comprised of three main components, namely a high voltage supply, a syringe pump and a collector plate. The polymer solution is loaded into a syringe which is placed in the syringe pump. The most important characteristics to consider when electrospinning are solution viscosity, flow rate, voltage, humidity, and the distance between the needle and collector plate.

Viscosity has a direct effect on the surface tension of the fluid. If the surface tension of the fluid is too low, there is insufficient time for long chains to develop, which results in spraying. If the viscosity is too high, the fluid will not eject a jet.

The flow rate needs to be fast enough to ensure that there is always a drop from which a jet can be ejected, while not so fast as to allow for the development of too large a drop that eventually breaks off. Similarly, the flow rate must not be so slow as to cause breaks in the fibre because not enough material is available.

The voltage determines the attractive force between the polymer and the collector plate, as well as the repulsive force between polymer chains in the droplet. The force of attraction makes the jet emerge from the droplet, while it is the repulsive force that is responsible for the fibres breaking apart from each other after a certain distance. The distance travelled is proportional to the amount of solvent that has evaporated, which directly affects the surface tension. At a certain critical distance, the repulsive force between the fibres overcomes the surface tension of the jet and the solution splits apart into finer fibres.

Humidity can affect the spinning process in two ways. Firstly, a higher humidity correlates with a larger quantity of ambient charge carriers, which can result in significant charge dissipation from the charged needle. Secondly, the humidity affects the evaporation rate of your solvent. A higher humidity would translate to a lower rate of evaporation.

The distance between the needle and collector plays an important role in fibre morphology. Shortening the distance decreases the amount of time available for solvent evaporation. Increasing the distance can thus decrease fibre diameter up until a critical point after which the distance is too great and beads begin to form.

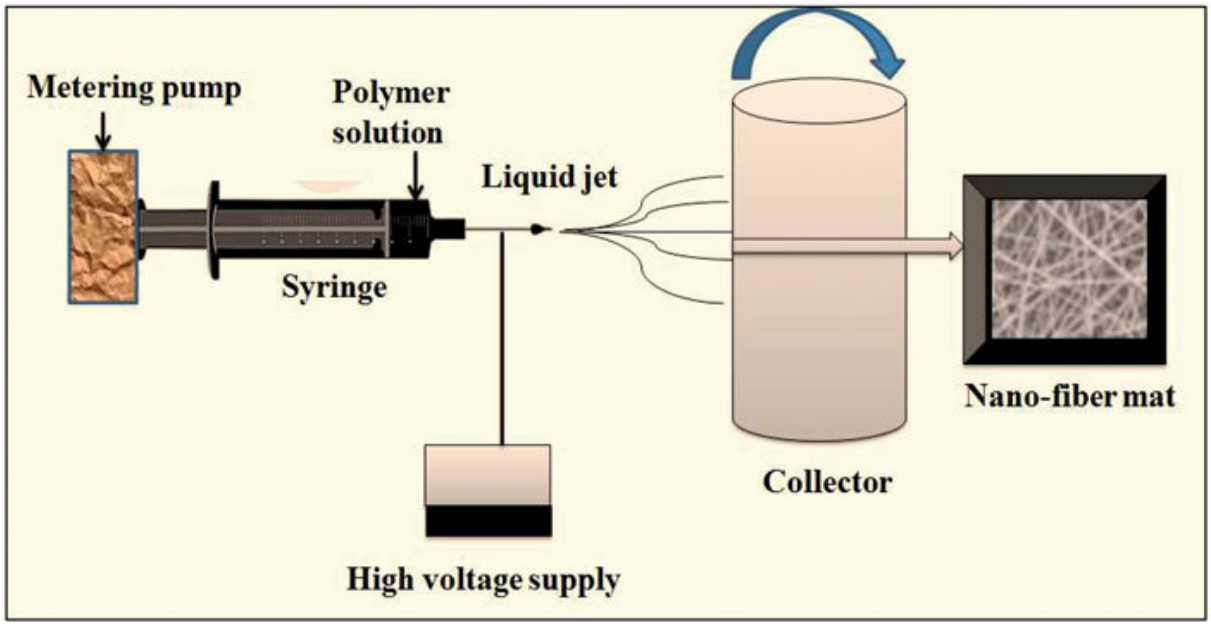

Figure 4.3: Electrospinning [44]

Self-assembly of nanofibres is a very complex procedure and produces peptide nanofibres. The procedure was inspired by a natural phenomenon, protein folding, specifically, the folding of amino acids to form unique 3-dimensional structures [52]. This method of nanofibre production is very new. Self-assembly is dependent on a number of important forces, such as hydrophobic interactions, electrostatic force, and hydrogen bonding. Ionic strength, pH and other factors can also greatly influence the produced fibres. The fibres produced from this process are typically very narrow, (7-100 nm) and short (approximately 20 micrometres).

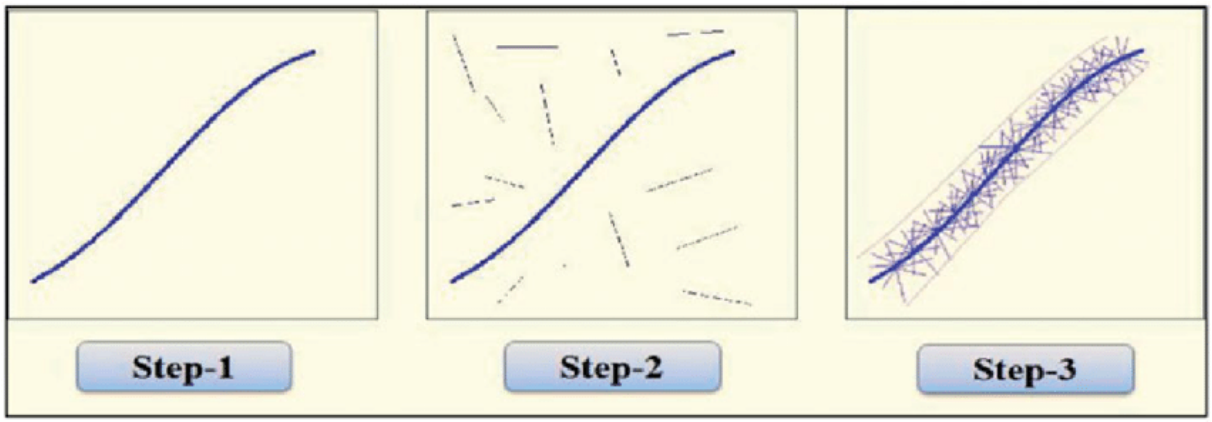

Figure 4.4: Self Assembly [44]

Template synthesis is a procedure that is based on the notion that the pores in a material can be used to direct the growth of another material. In order to be able to implement template synthesis, one needs access to metal sputtering and electrochemical deposition equipment. By developing a nanoporous membrane and forcing a polymer solution through the holes in this membrane into a solidification solution, one is able to obtain fibres of a specific and uniform diameter.

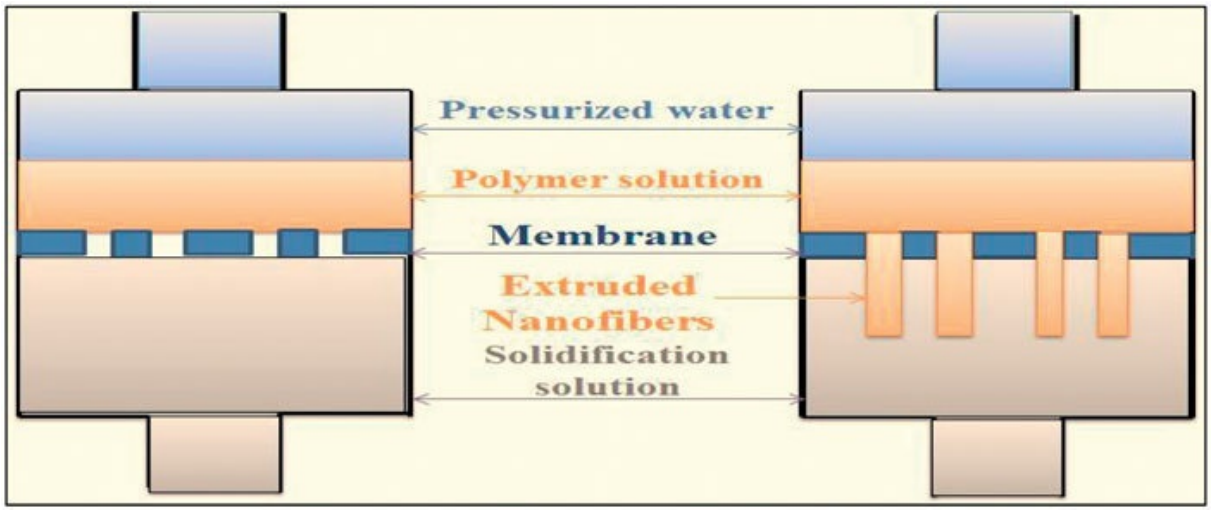

Figure 4.5: Template Synthesis [44]

Thermally Induced Phase Separation (TIPS) was first proposed by Castro in the 1980s [53]. TIPS is one of the most commonly used methods of producing polymeric materials with micropores for use in applications ranging from tissue scaffolds, to membranes, to foams. These all present a wide variety of potential uses, particularly in the fields of controlled drug delivery. Research has shown that during the TIPS process, parameters such as mass and heat transfer directly control the microporous structures created by the process [53]. By adjusting the preparation conditions, it is possible to control pore size. There are also means to control pore structure [54].

The TIPS process is based on making use of changes in thermal energy to de-mix a homogeneous polymer solution into a two or multi-phase domains [54], meaning that the original polymer blend splits into two or more blends of differing composition.

These different phases can typically be classified as either polymer-rich or polymer-poor. After separation has completed, the temperature is once again adjusted in order to allow for gelation to occur, meaning that polymer macromolecules (fibres) form. The solvent is then eluted with water, after which it is typically extracted via a freeze-drying process. Once this has occurred, the polymer-rich phase solidifies and forms the matrix while the polymer-poor phase forms the pores.

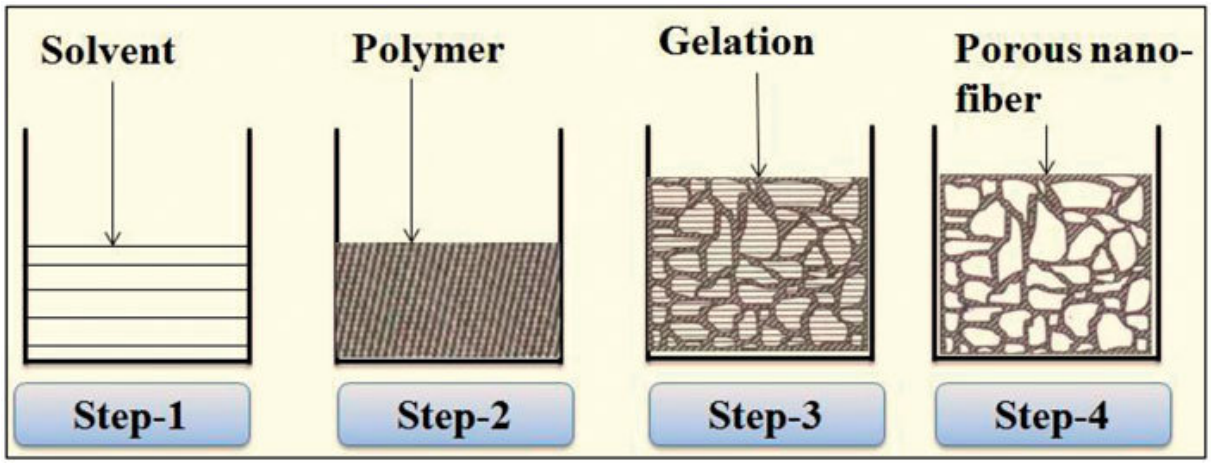

Figure 4.6: Thermally Induced Phase Separation [44]

From the information above, it is clear that each method of nanofibre production has its benefits and drawbacks. To determine which of these methods is most suited for the nanofibre production required in this thesis, it is necessary to evaluate all of the methods in terms of the requirements of the produced fibres.

Drawing allows for the characterisation of individual fibres, allowing for better model-design and approximations. Unfortunately, customising fibre diameter is extremely difficult. Furthermore, as the process produces individual fibres one at a time, it would be extremely time-consuming and tedious to produce enough fibres to make a biosensor from. Additionally, developing a sufficiently shielded setup to increase reproducibility would likely be an expensive process. Lastly, drawing fibres is typically a discontinuous process.

Electrospinning has been a popular method of nanofibre production from the 1990s owing to the relatively inexpensive setup costs and the wide variety of materials that can be spun [55]. Electrospinning can produce fibres varying in diameter from 10s of nanometres to several micrometres. A great deal of research has been conducted on the use of non-woven mats produced by electrospinning for use in applications such as filtration, tissue engineering, biotechnology and sensors. Electrospinning can be adapted in a myriad of ways to produce fibres with differing properties, such as co-axial electrospinning to produce fibres composed of multiple components or even to produce hollow fibres, or the use of a rotating collector to change fibre alignment. A drawback to electrospinning is that it is difficult to isolate individual fibres for characterisation.

Template synthesis allows for the control of fibre diameters. Furthermore, this method also enables one to control the length of the fibres developed. Unfortunately, access to sophisticated equipment is required to create the necessary membranes[56].

Self-Assembly is an incredibly difficult process to control. Ideal ambient conditions need to be maintained in order for successful fibre production to take place. Additionally, fibre diameter and length is very difficult to control. Furthermore, this method of nanofibre production is severely limited in that it can only be used to develop fibres of very specific composition. This method does, however, produce exceptionally narrow fibres. The comparative shortness of the fibres can also be beneficial in specific scenarios.

Thermally Induced Phase Separation is a very good method of producing large-volume nanofibrous structures. As this process consists of a number of phases, this procedure is innately complex. This process is comparatively expensive as there is a relatively large amount of material waste, in addition to which is the fact that achieving appropriate temperature control is costly. The requirement of freeze-drying apparatus also adds to the overall cost of such a setup.

4.2.2 Evaluation of Method Applicability

Electrospinning was selected as the means of nanofibre production for this project as it is the cheapest and most versatile of the methods listed above. While individual fibre characteristics may not be characterisable, the bulk material should be. In the context of a resistive sensor, this is an acceptable shortcoming as it is the overall change in resistance that is of greatest importance, not the changes caused in individual fibres. Furthermore, the morphology of the fibre mat produced by electrospinning is more appropriate for use as a sensor than the large-volume structure produced by thermally induced phase separation.

4.3 System Design

The electrospinning setup required for this thesis needed to be able to produce both aligned and unaligned fibres. To this end, the following components were required:

- Housing
- Collectors - Stationary and Rotating
- Syringe Pump
- High Voltage Power Supply
- Dehumidifier

4.3.1 Housing

The housing is comprised of wood, styrofoam, carbon-fibre rods, ABS plastic and plexiglass. All of these materials were chosen for their non-conductive nature. While the electricity used in electrospinning is static in nature, using these materials would likely serve to avoid any potentially harmful current flow through the frame. A frame was built from locally available squared pine dowels. Two black plexiglass plates, 3mm in thickness, were cut and affixed to the frame using adhesives. These plates have a central hole through which the needle can pass. The inside of the frame was lined with styrofoam.

A third plexiglass plate, 5mm thick, was used as the mount for the two collectors. Four linear ball bearings were affixed to the plate via 3D-printed ABS brackets. Additional 3D-printed mounts were affixed to the two 3mm thick plates on either end of the electrospinner. These mounts serve to hold the carbon fibre rods which were passed through the linear ball bearings. This allowed the mounting plate to be positioned at any desired distance from the needle tip by simply sliding it along the carbon fibre rails.

4.3.2 Collectors - Stationary and Rotating

The stationary collector is a petri dish affixed to one side of the mounting plate with adhesives. The rotating collector or mandrel is affixed to the opposite side of the mounting plate.

The rotating collector consists of an acetal barrel, acetal brackets, ball bearings, a brass end ring and contact, a 3D-printed motor mount and an aluminium base plate. The motor mount houses a 19.6 W, 7.3 V DC motor rated at 19 000 rpm, obtained from RS Components. This motor is press-fitted onto the shaft, owing to the narrowness of the exposed motor-shaft. This necessitates that the motor be sped up slowly, which is implemented via a microcontroller, namely an Arduino UNO R3. The brass ring on the end of the acetal barrel allows for the material attached to it to be grounded properly. A 4.4 to 5.5 V Broadcom Incremental Encoder was used to monitor the speed of the rotating collector. The result was fed to an Adafruit 0.96" OLED screen. The motor was controlled by a PWM Driver board from MikroElektronika which received an input from the UNO to determine the output voltage. Speed control was achieved by using buttons to indicate the desired action to the UNO. The whole system is powered by a 5V 10 A DC Power Supply obtained from Micro Robotics. This was connected directly to the external input of the PWM driver board, as well as to the UNO via a 12V step-up voltage regulator and barrel-jack connector, both of which were also obtained from Micro Robotics.

4.3.3 Syringe Pump

A syringe pump was fortuitously available for use at the University of Stellenbosch's faculty of Engineering. It is particularly fortunate as a good syringe pump is typically the most expensive component in a simple electrospinning setup. This pump is capable of outputting at a minimum of tens of microlitres per hour, and a maximum of several mililiters per minute.

4.3.4 High Voltage Power Supply

A high-voltage DC power supply was required. Based on the literature, most experiments seldom exceeded 22.5 kV. To this end, this was chosen as the minimum acceptable value for the supply that was to be obtained. After much research, a supply was obtained from Gamma High Voltage, Florida. There was only a small difference in price between the 330 μA version and the 660 μA version. This resulted in the 660 μA version being selected owing to the increased potential for use in alternate applications. This device has built-in surge protection and can be fed by both 110 V at 60 Hz and 220 V at 50 Hz.

4.3.5 Dehumidifier

Owing to the relatively high humidity in Stellenbosch, it was deemed necessary to obtain a dehumidifier as humidity plays a large role in the electrospinning process. A household, low energy, GMC Aircon unit with a capacity of 26 ℓ/Day and rated at 320 W was obtained. The complete system, together with the dehumidifier, was placed in a repurposed fume-hood so as to maximise the effectivity of the dehumidifier.

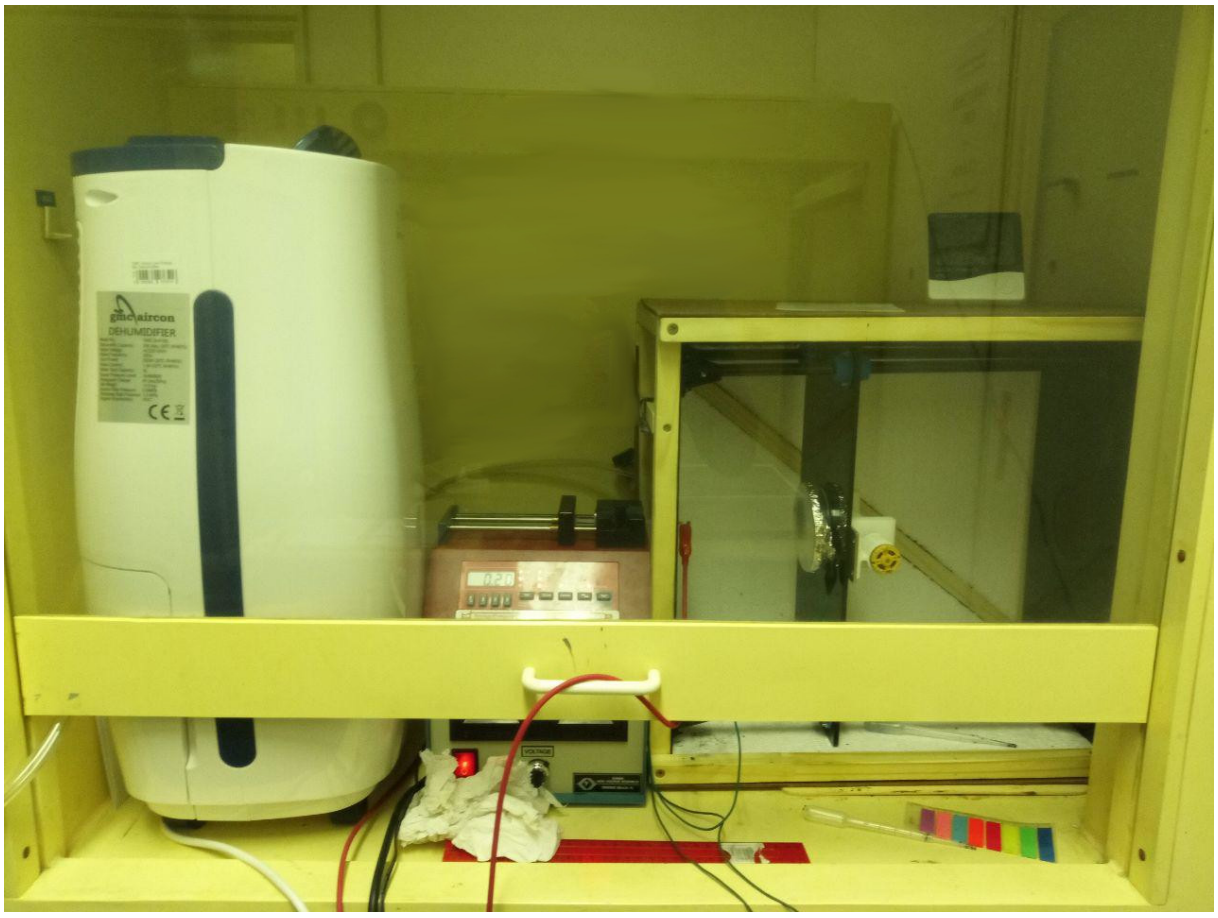

Figure 4.7: Electrospinning Setup in Modified Fume-hood

4.4 System Verification

In order to verify that the electrospinning setup was capable of producing nanofibres, a 5 wt% solution of PVA in DI water was prepared by heating the solution in a beaker to approximately 90 °C and simultaneously mixing it by making use of a magnetic stirrer. After a homogeneous solution was obtained, the solution was allowed to cool while the mixing continued. After 30 minutes, the solution was deemed sufficiently mixed for the purposes of verification.

The PVA solution was taken up in a syringe with a 15 G blunt-tip needle and placed in the syringe pump. Aluminium foil was wrapped around the stationary collector and connected to the ground of the high voltage (HV) supply. The HV crocodile clip was connected to the tip of the needle. The distance between the needle tip and the collector was set to 10 cm. The syringe pump was set to eject the fluid at a rate of 1.2 mℓ/h. The HV supply was then switched on, and the voltage taken up to 20 kV. After 10 minutes, the following fibres were produced.

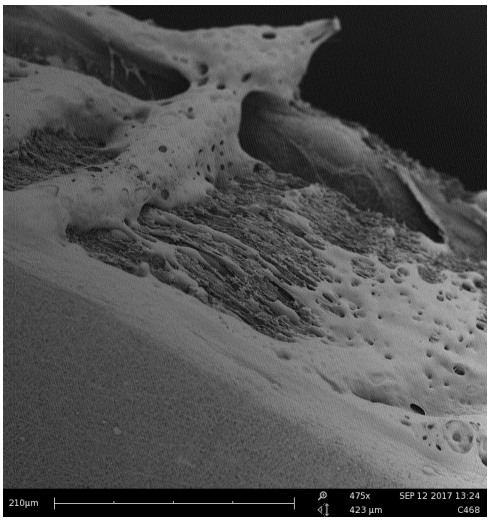

Figure 4.8: PVA Unaligned Fibres 1

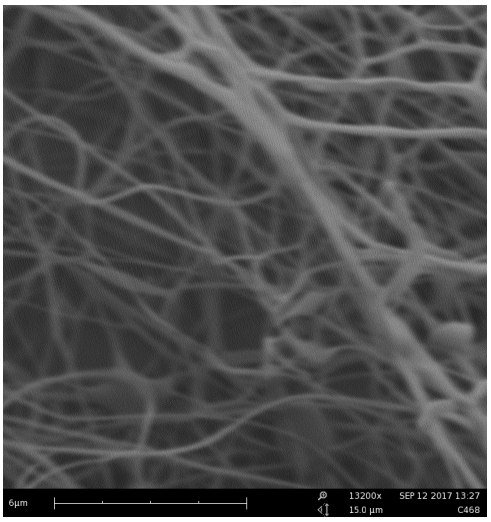

Figure 4.9: PVA Unaligned Fibres 2

Figure 4.8 shows the edge of a section of the nanofibre mat that was laser-cut while figure 4.9 shows a closer view of the unaligned nanofibres.

To test the rotating collector, aluminium foil was wrapped around the rotating mandrel and secured with double-sided tape. The electrode connected to the brass end of the mandrel was connected to the HV supply's ground terminal. Again, a 5 wt% PVA in DI water solution was made and placed in a 15 G blunt-tip syringe. The fluid ejection rate was again set to 2.1 mℓ/h and the distance between needle-tip and collector was again set to 8 cm. The HV supply was also set to 20 kV. The following fibre formations were produced.

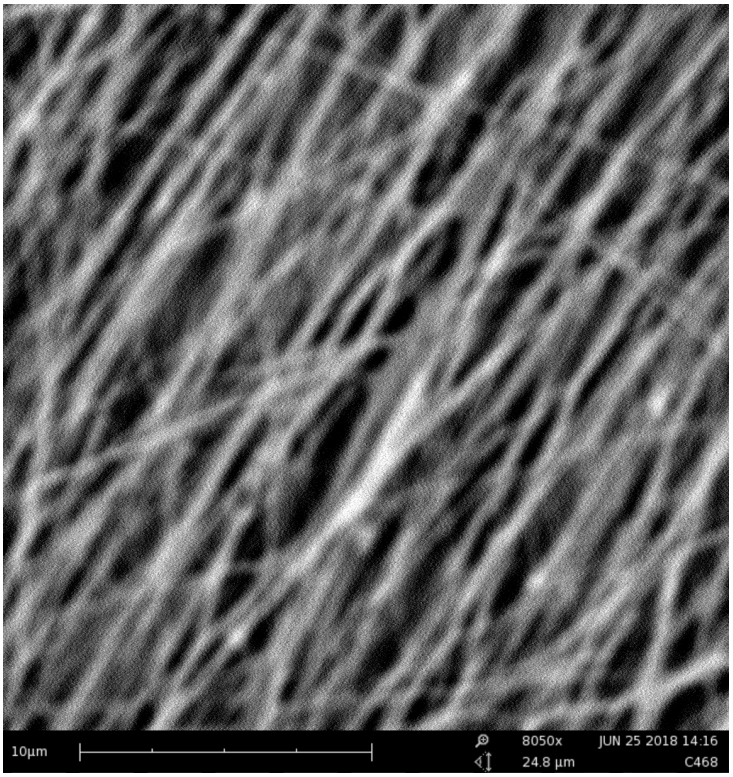

Figure 4.10: PVA Aligned Fibres

4.5 Conclusion

Analysis of the fibres found on the stationary collector shows that uniform fibres were indeed formed. The average fibre diameter is approximately 150 nm. Sharp bends at intersections between fibres indicate that the fibres had dried sufficiently during the spinning process, ensuring that the fibres did not recombine.

Analysis of the fibres found on the rotating collector shows fibres of a similar diameter to those found on the stationary collector, with a distinct degree of alignment. This proves that the produuced electrospinning setup functions as it was designed to.

Chapter 5

Development of Intrinsically Conductive Nanofibres

5.1 Introduction

For the purpose of this thesis, intrinsically conductive nanofibres are desirable as their electrical characteristics per volume typically correspond to the uniformity of mat thickness and fibre diameter. When a coating step is required to make non-conductive fibres conductive, it becomes very difficult to achieve reproducibility between samples as the coating process itself is not easily governable. Two of the most common types of intrinsically conductive nanofibres are carbon nanofibres and intrinsically conductive polymer (ICP) nanofibres. Carbon nanofibres offer very high levels of conductivity, however, their rigid nature leaves them very brittle. In the work by Lawrenson and Viviers[40][41] they found it necessary to use carbon nanofibres on carbon microfibre backing to provide sufficient mechanical strength to survive handling. The effect of the microfibre layer on the overall conductivity was not discussed. While polymers are not typically considered conductive, there are a number of ICPs whose methods of conducting electricity have been well-documented. In this thesis, ICP nanofibres were selected as they provided superior mechanical robustness.

5.2 Literature Review

ICPs are generally considered to be a rather new development in chemistry. In fact, in 2000, the Nobel Prize in Chemistry was awarded to Alan J. Heeger, Alan G. MacDiarmid and Hideki Shirakawa "for the discovery and development of conductive polymers".[57] Interestingly, however, it can be argued that conductive polymers had been developed long before this. Polyaniline and polypyrrole (two well-known ICPs), were being prepared as early as the 19th century[58]. The difficulty in establishing when exactly ICPs were first truly developed is, as noted by György Inzelt in *Conducting Polymers: A new Era in Electrochemistry* [58], attributed to the fact that the history of scientific development itself plays a role. In particular, the fact that the existence of macromolecules was not accepted until the 1920s makes this a very difficult issue.

In this thesis, PEDOT:PSS was selected as the ICP of choice. PEDOT:PSS is a polymer mixture consisting of two oppositely charged ionomers. The PEDOT is charged with positive holes while the PSS chains have sulfate anions that act as the negative counterions

[59]. Together the two form a macromolecular salt. It has been used in various different applications, ranging from polymer electrolytic capacitors[60], to antistatic linings[61], to flexible electronics[62] and many more. PEDOT:PSS is one of the most popular materials for conductive layer applications [63]. Some of its most notable characteristics, in addition to conductivity are, transparency when in thin layers (thick layers have a distinct dark blue colour[64]), high ductility, water solubility[65] and biocompatibility[65]. It is typically obtained as a dispersion in water. The conductivity of PEDOT:PSS can be greatly increased (by one or two orders of magnitude) via the addition of secondary dopants, such as dimethyl sulfoxide (DMSO) or *N,N* DMF[63]. PEDOT:PSS has also been successfully electrospun by B. Bessaire, M. Mathieu, V. Salles *et al*[66] and K. Khanum, S.Hedge and P. Ramamurthy[67]. Secondary dopants are dopants that increase the conductivity of an already doped material (in this case the PEDOT is doped with PSS) permanently, even after their removal[63].

The approach used by Salles *et al* was adopted in this thesis as it made use of the Clevios PH1000 PEDOT:PSS solution, which is, at the time of this thesis, the highest conductive grade version of PEDOT:PSS that is commercially available. Additionally, this methodology made use of *N,N* DMF, a secondary dopant, which would stand to increase overall conductivity. Lastly, while both articles made use of poly(ethylene oxide) (PEO), this article forewent the use of polyvinyl alcohol (PVA), another polymer used in the work by Ramamurthy *et al*. This meant that the fibres produced by Salles *et al*'s method would have a higher percentage of PEDOT:PSS than the fibres produced by Ramamurthy *et al*'s method. It was believed that PVA would serve to lower conductivity as it is a non-conductive polymer.

In the article by Salles *et al*, fibres were electrospun from a mix of Clevios PH1000 PEDOT:PSS, PEO with a Mw of 900 000, and *N,N* DMF.

PEO is a water-soluble polymer commonly used in electrospinning. In this context, the PEO served to increase the solution viscosity as it has a high molecular weight and is typically obtained in powder form.

The use of the DMF solvent would serve to increase fibre conductivity as it would act as a secondary dopant. During the electrospinning process, as well as in baking and desiccation steps, the DMF would be removed from the polymer mixture. The DMF's effect on conductivity, however, would remain. The DMF would also have the effect of lowering the mixture viscosity as the DMF solvent has a viscosity of only 0.802 mPa.s at 25 °C[68].

5.3 Initial Customisation of Solution

Salles et al used PEO with a Mw of 900 000. In this thesis, PEO with a Mw of 600 000 was obtained as it was significantly cheaper. The change in molecular weight lowered the solution viscosity. This change in viscosity needed to be addressed as solution viscosity is a key parameter in electrospinning. As the viscosity of the solution used by Salles was not available, an appropriate alternative mixture was obtained experimentally (see Appendix A).

The mixing procedure followed in the fibre development steps took the following form. The PEO was dissolved into the PEDOT:PSS by mixing over 24 hours. After the mixture was sufficiently blended, the DMF was added and mixed for another 24 hours.

Initially, the quantity of DMF, which has a low viscosity, used in the prepared solutions was decreased in successive batches to attempt to account for the lowered viscosity caused by the lower molecular weight PEO.The amount of PEDOT:PSS used in each batch was 2.560 g and the PEO used was 0.06 7g. Relative humidity was kept constant at approximately 20%, the needle used was 22 gauge and the solutions were tested at varying feed rates and varying potential differences. The distance between the needle and collector plate was held at 10 cm.The change in DMF concentration had little to no effect on the results as only electrosprayed beads were deposited on the collector.

During secondary attempts, the PEO concentration was reduced. PEDOT:PSS was set at 2.560 g and DMF was set to 0.345 g per batch. As with the previous experiments, relative humidity was kept at approximately 20%, the needle used was 22 gauge and the distance between needle and collector was 10 cm. The first of these attempts used 0.075 g of PEO. This proved unspinnable as the solution was too viscous as it produced only droplets of solution that would be ejected off of the needle, irrespective of feed rate. The next attempt used 0.068 g of PEO which resulted in beads interspersed with fibres. With a feed rate of 0.1 mℓ/h, a potential difference of 15 kV and the addition of 0.07 g of Mw 600 000 PEO to the solution, fibres were eventually produced. It should be noted that some of these fibres would intertwine and stand off from the collector plate, branching towards the charged needle.

5.4 Primary Nanofibre Electrode Production

In order to use these nanofibres as a resistive sensing element, it was necessary to connect the fibres to electrodes and measure conductivity. Ideally, the fibres would be deposited directly onto the electrodes; this process would eliminate the need to remove the fibres from the collector and then affix them to electrodes by other means. This is advantageous because this handling could potentially damage the fibres. To this end, specialised interdigitated electrodes were produced. These electrodes were produced by Mr Daniël Retief with his modified inkjet printer.

These electrodes took the form of silver interdigitated electrodes on a paper substrate. Paper was used because it provided an easily and cheaply obtainable substrate with tremendous flexibility. Silver-ink was deposited onto semi-hydrophobic paper. Line widths of under 150 μm and line spacings of under 100 μm were achieved. The exposed terminals for connection were placed apart to match the spacing of a standard USB type A connector. This would allow for the electrode to be connected to a measurement setup via a standard female USB type A port.

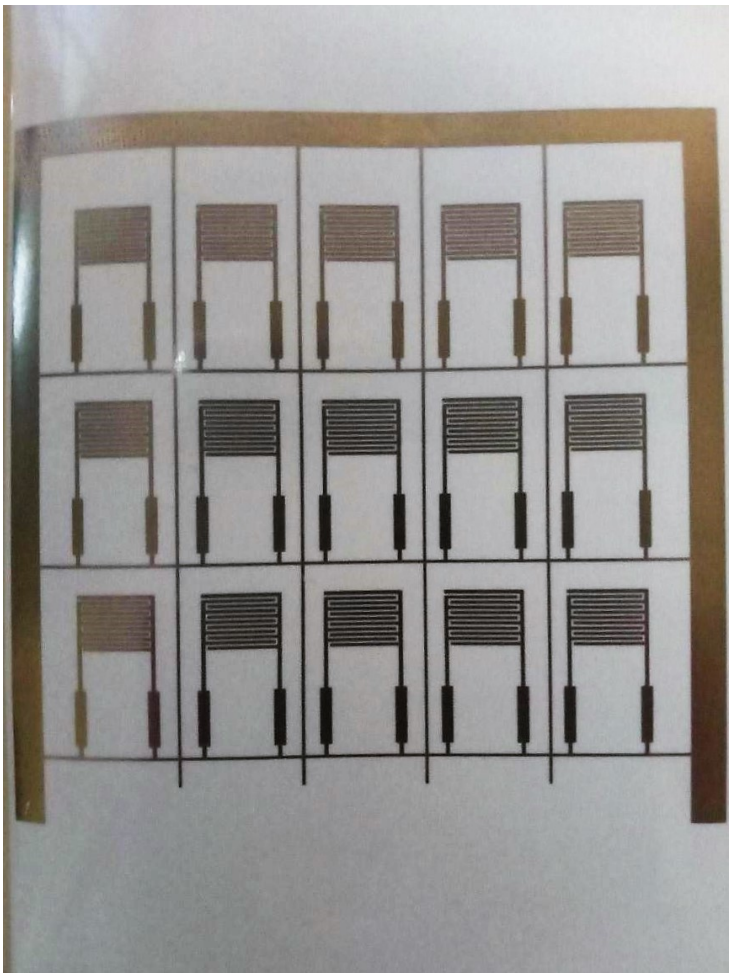

Figure 5.1: Printed IDEs

Semi-hydrophobic paper was used for the following reasons. Firstly, non-hydrophobic paper simply absorbed the ink, causing discontinuities and low reproducibility. Furthermore, the treatment steps that would later need to occur to enable the binding of antibodies to the fibres would greatly affect the non-hydrophobic paper, as many of these steps require the deposition of solutions for varying periods of time. The addition of solutions in this manner would then compromise the structural integrity of the paper. Secondly, fully hydrophobic paper was not used as the ink could not bind properly to the surface of the paper, which would mean that the electrodes would be too vulnerable to handling. A casual brush would be sufficient to distort the ink. Semi-hydrophobic paper served as an appropriate balance, as it allowed for the ink to absorb into the paper just enough to enable secure binding, but not enough to compromise the structural integrity of the paper. Once the electrodes had been printed, the sheets were placed in an oven at 100°C and baked for 30 minutes. This allowed sintering to take place, thereby ensuring conductivity in the electrodes.

To measure the conductivity of these fibres, a sheet of these electrodes was mounted to the stationary collector and fibres were spun for 15 minutes directly onto the electrodes. The following electrodes were produced.

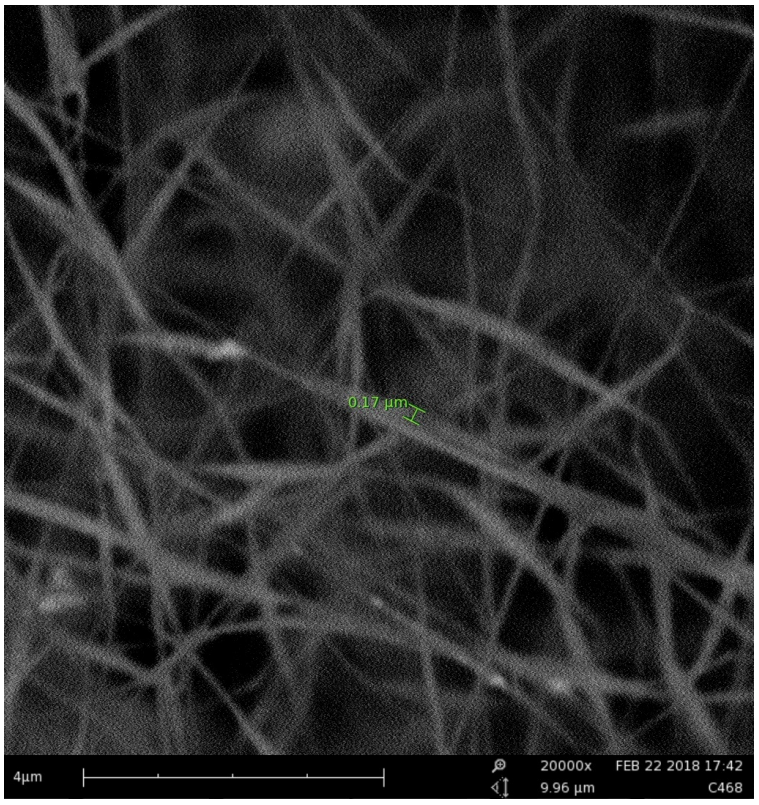

Figure 5.2: Unaligned Fibres 1

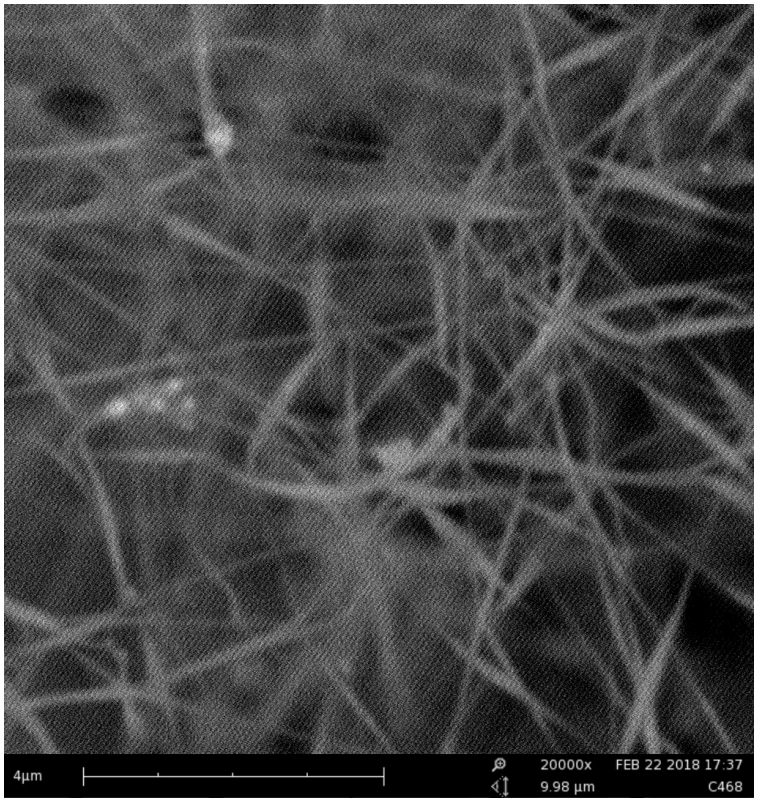

Figure 5.3: Unaligned Fibres 2

Thereafter, the production of aligned fibres was attempted. A mandrel was coated with a sheet of aluminium foil affixed by double-sided tape and set to spin at 15 000 rpm. As the rotation of the mandrel provided an additional drawing force, the feed-rate of the polymer solution was adjusted to 0.9 mℓ/h. Once this electrospinning process had been completed successfully, the process was repeated. In this attempt, a sheet of electrodes was wrapped over the mandrel and fibres were once again spun directly onto the electrodes for 15 minutes. The spin time was limited to 15 minutes as the double-sided tape would lift off if spun for a longer period. The following electrodes were obtained.

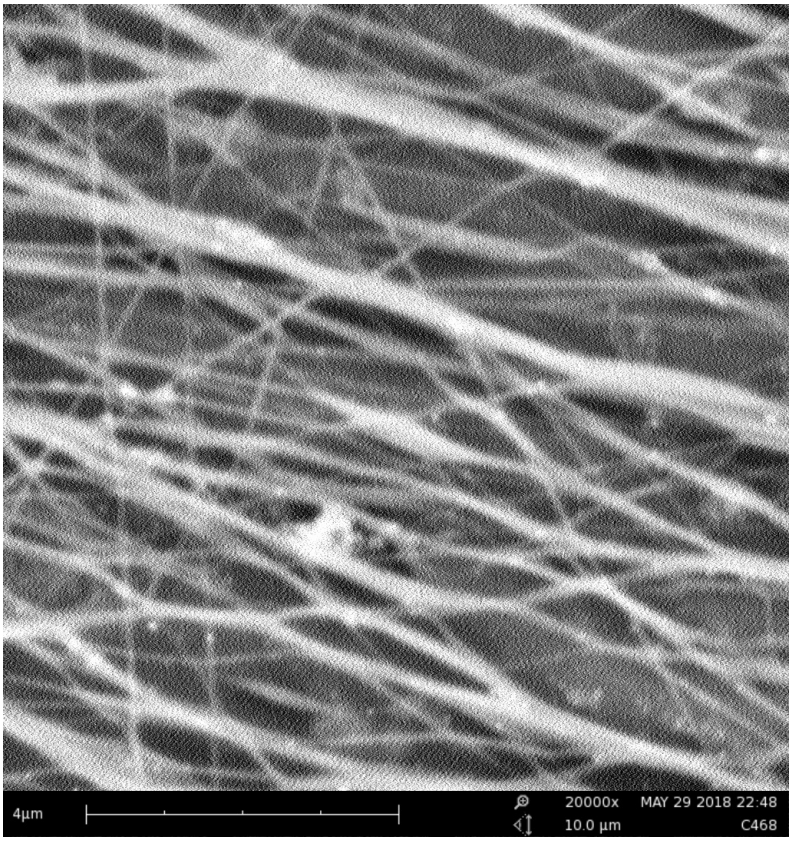

Figure 5.4: Aligned Fibres 1

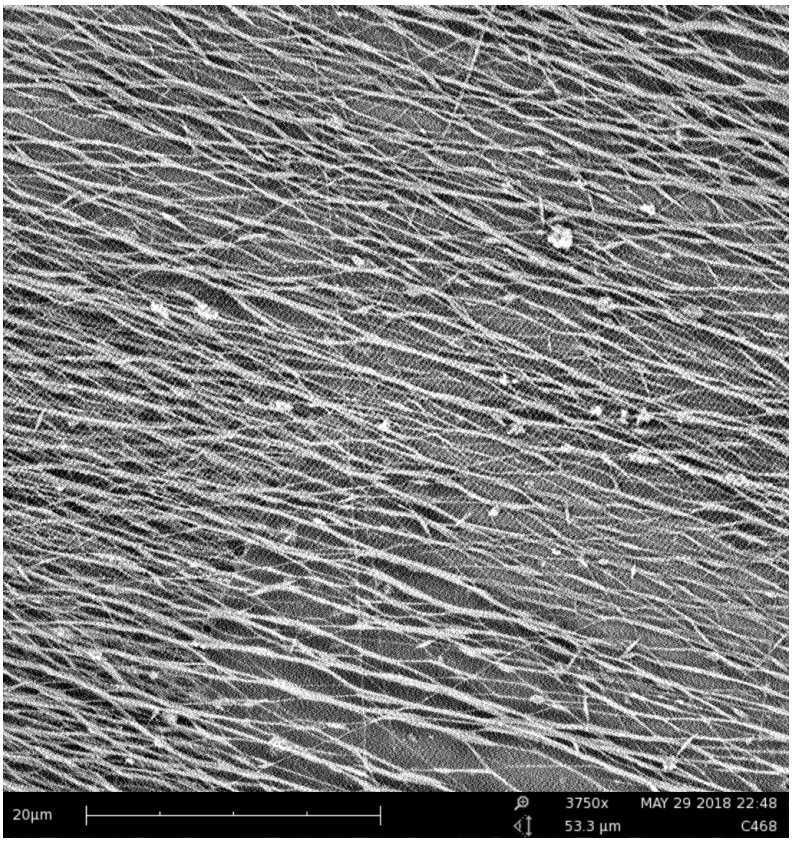

Figure 5.5: Aligned Fibres 2

5.5 Primary Fibre Characteristics (Verification)

The nanofibre mats produced were distinctively blue owing to the PEDOT:PSS. The fibres were desiccated and placed under a SEM and the average diameter was found to be between 100 and 300 nm. This confirmed that these were indeed nanofibres. The fibres were also confirmed to be continuous and distinct. Additionally, the fibres deposited on the rotating mandrel were found to have a distinct general alignment in the direction of rotation.

The samples were tested for conductivity by connecting a multimeter to the exposed terminals of the silver electrodes. Conductivity of the aligned fibre mats was much higher and more uniform than the unaligned fibre mats. This conformed to expectations as the alignment would assist in carrying charge from one electrode to another by keeping the length of travel, and, therefore, resistance, as small as possible. Additionally, the aligned fibre mats were noticeably thicker than the unaligned fibre mats. This corresponds to the increased feed rate necessitated by the drawing force generated by the mandrel, and also accounts for the increased conductivity owing to better fibre coverage.

5.6 Secondary Nanofibre Solution Customisation and Electrode Production

When the electrodes were exposed to DI water, two issues became apparent. Firstly, the hydrophobic layer of the semi-hydrophobic paper was insufficient. Water was, over time,

absorbed into the paper, which distorted the silver electrodes. Discontinuities were formed and liftoff occurred. To address this issue, a hydrophobic layer was needed that would cover the paper, but not the silver electrodes. Mr Retief found that a dilution of S1818 photoresist in Acetone would serve this purpose. As such, the two were blended in a wt% ratio of 1:4. This mixture was then spin-coated onto the sheet of electrodes. This was done at 700 rpm for 40 s. Two layers proved to provide sufficient hydrophobicity whilst also remaining clear of the silver. The photoresist was then soft-baked on a hotplate for 2 minutes at 100 °C. The following figure 5.6 shows the exposed silver and the photoresist covered paper. Close examination reveals a slight overlap of photoresist on the silver at the very-edge of the silver, but no further.

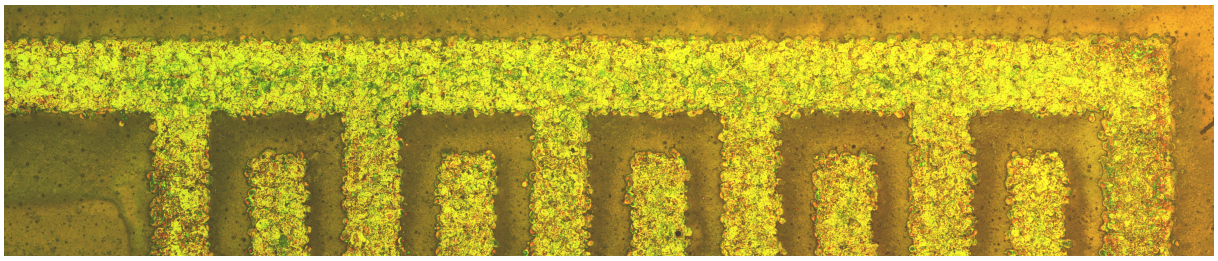

Figure 5.6: Photoresist-treated Electrode

The second discovery was the tendency of the nanofibres to dissolve and wash off from the paper. Consequently, it was necessary to bind the nanofibres to the electrodes, as well as address the solubility of PEDOT:PSS in water, a polar solvent. To this end, a chemical known as GOPS/GOPTS was employed. GOPS is a well-known crosslinking agent and has been used to crosslink with PEDOT:PSS in various experiments, and as such is noted in various articles such as those by Mahmoudy *et al*[69] and Håkansson *et al*[59]. In this role, the GOPS acts not only as a crosslinking agent, but serves to prevent PEDOT:PSS from dissolving in polar solvents[59]. A thin film of GOPS was spin-coated over the photoresist layer at a speed of 1000 rpm for 40 s once. The electrodes were then baked for 30 minutes at 100 °C in an oven to enable crosslinking between the GOPS and the photoresist layer.

After the completion of these preparatory steps, the sheet of electrodes was mounted to the mandrel and the PEDOT:PSS nanofibres were spun directly onto them. As before, the mandrel was set to rotate at 15 000 rpm, the distance between needle and collector was 10 cm, the needle used was 22 gauge, the feed rate was 0.9 mℓ/h and the potential difference was set to 15 kV. After electrospinning for 15 minutes, the electrodes were removed from the mandrel and placed in the oven once again to bake at 100 °C for two hours. This step ensured that crosslinking occurred between the GOPS and the PEDOT:PSS. Sample conductivities were measured after the requisite two hours had passed and found to correspond with the initial values. After measuring, the samples were rinsed with DI water. While at first glance it appeared that the fibres had once again washed off completely, SEM imaging confirmed the presence of a very thin layer of PEDOT:PSS nanofibres which coated the electrodes. Conductivity was measured after the rinsing process and found to have increased considerably (see table 5.1) This is likely owing to the absence of unbound nanofibres that would otherwise have caused interference.

5.7 Secondary Fibre Characteristics (Verification)

The secondary fibre morphologies and conductivities are as follow:

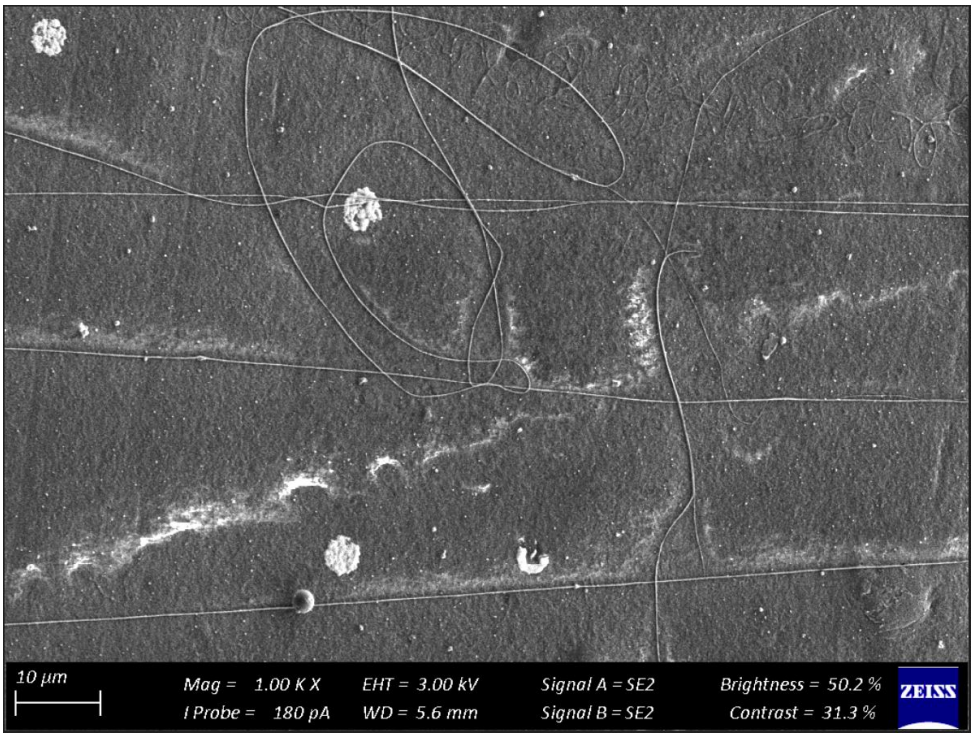

(a) Unaligned Fibres

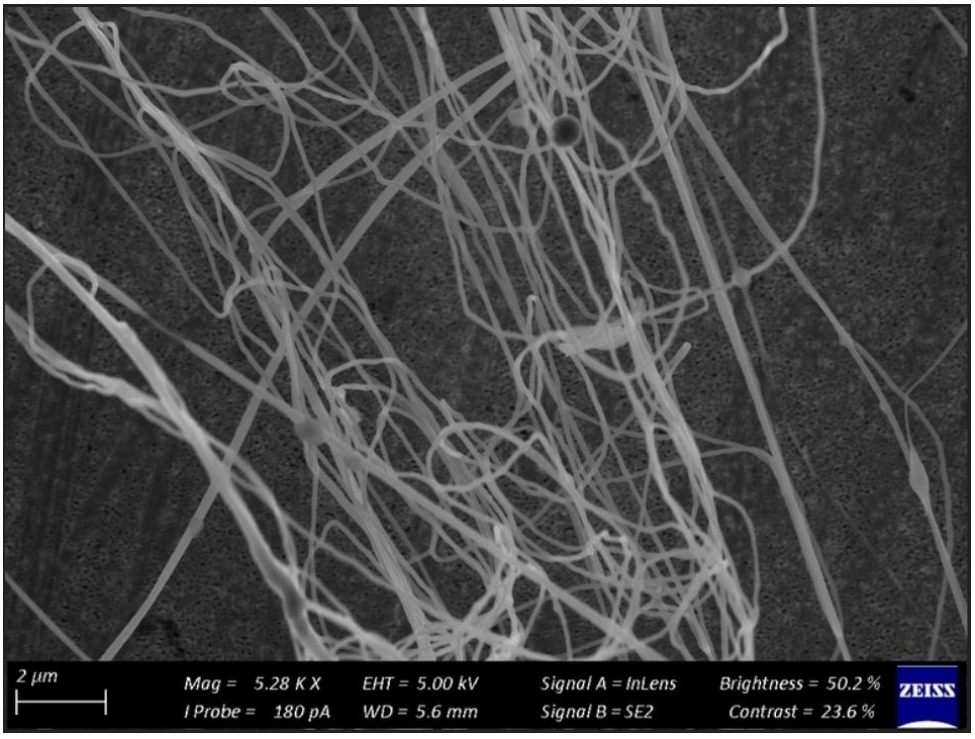

(b) Unaligned Fibres

Figure 5.7: Secondary Fibres - Unaligned - Pre-Rinse

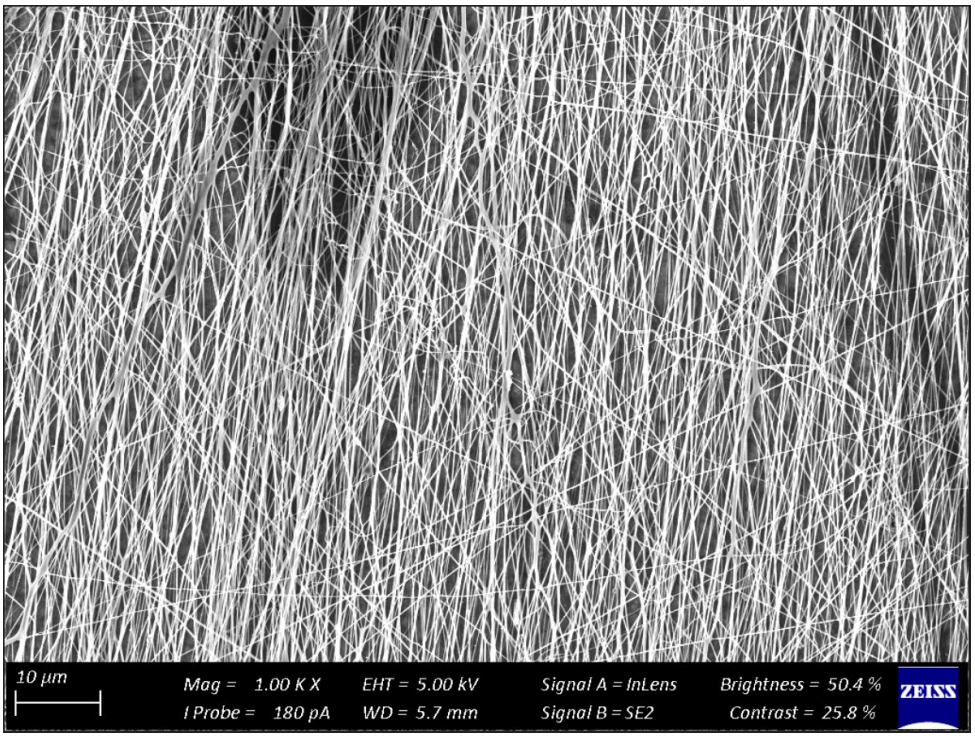

(a) Aligned Fibres

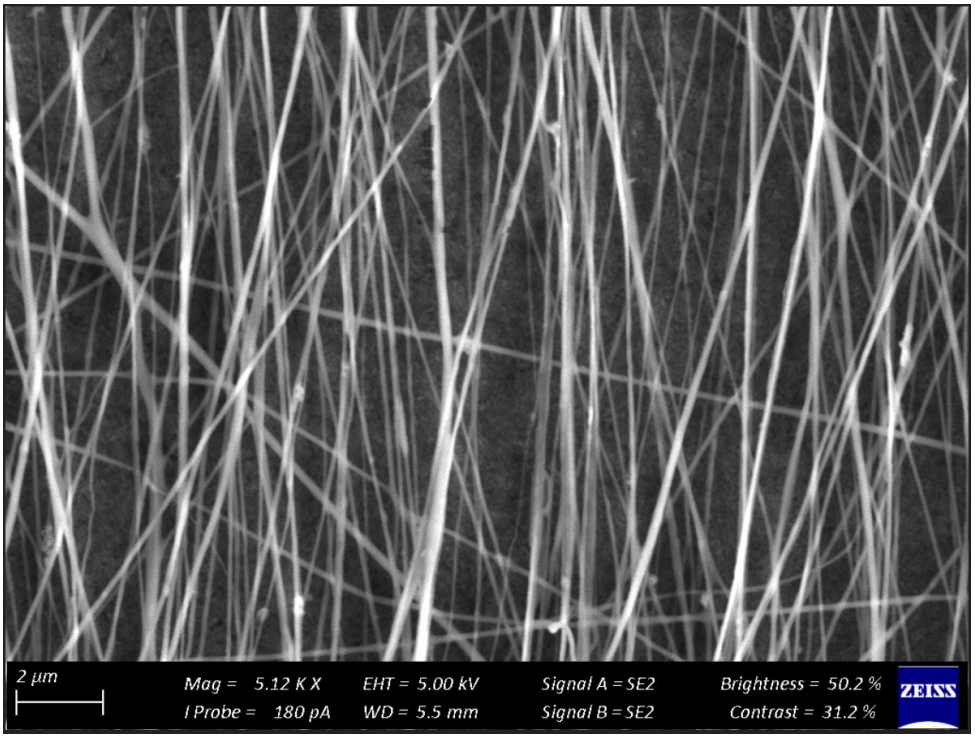

(b) Aligned Fibres

Figure 5.8: Secondary Fibres - Aligned - Pre-Rinse

Table 5.1: Secondary Fibre Characteristics (Aligned) Post Rinse

Column 1	Column 2	Column 3	Column 4	Column 5
1980Ω	520Ω	360Ω	550Ω	1250Ω
4270Ω	650Ω	510Ω	730Ω	1870Ω
2420Ω	510Ω	300Ω	580Ω	1210Ω

These resistances correspond to the following graph, Figure 5.9, which shows how the conductivities per column correspond well to a normal distribution.

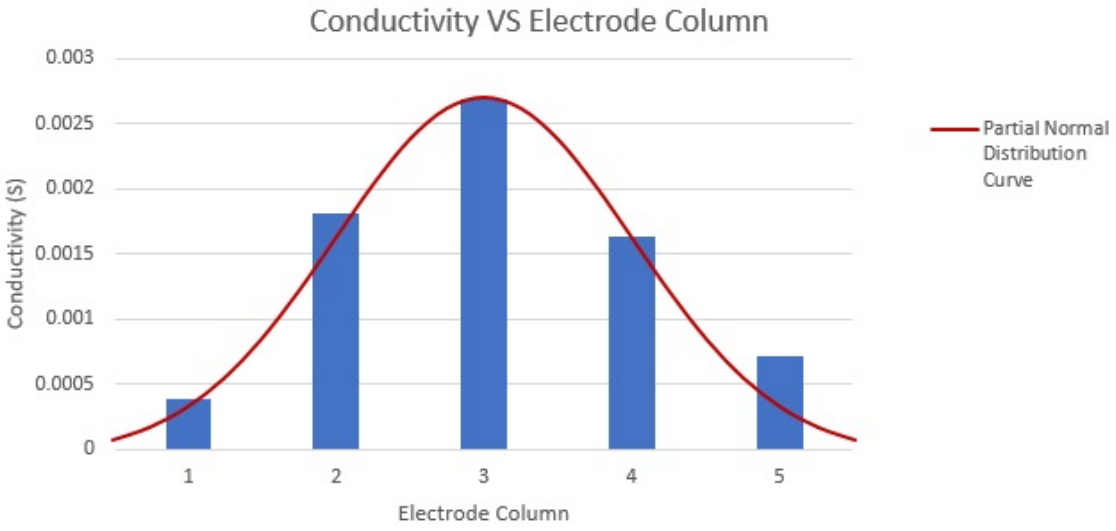

Figure 5.9: Conductivity VS Electrode Column

As will be discussed in a later chapter in this thesis, the chosen method of functionalisation made use of a compound known as APTES. After functionalising the electrodes, it was found that the base resistance of the electrodes increased dramatically, typically by an order of magnitude or more. To offset this, it was deemed necessary to provide the APTES with additional binding sites.

5.8 Final Fibre Solution Customisation and Electrode Production

It has been found that APTES binds with hydroxyl groups [70] which can be found in compounds such as PVA. It was found that the initial fear concerning the effect of PVA on fibre conductivity was unfounded, as experiments have found that the addition of PVA to fibre solutions not only increases tensile strength, but also conductivity [71]. To this end, 5mg of PVA (mw 98 000) was added to the solution. As this would increase the solution viscosity, the amount of DMF was also increased to 0.35 g. This mixture was produced with the same mixing procedure as before, with the addition of one step, namely heating the mixture during mixing to 80 °C for 10 minutes to facilitate the dissolving of the PVA into the mixture. This mixture was then electrospun directly onto a sheet of electrodes with the exact same parameters as before.

5.9 Final Fibre Characteristics (Verification)

The final fibre conductivities and morphologies are as follow:

Table 5.2: Final Fibre Characteristics Post Rinse

Column 1	Column 2	Column 3	Column 4	Column 5
1650Ω	530Ω	230Ω	450Ω	930Ω
1720Ω	450Ω	280Ω	580Ω	1520Ω
2070Ω	430Ω	410Ω	390Ω	890Ω

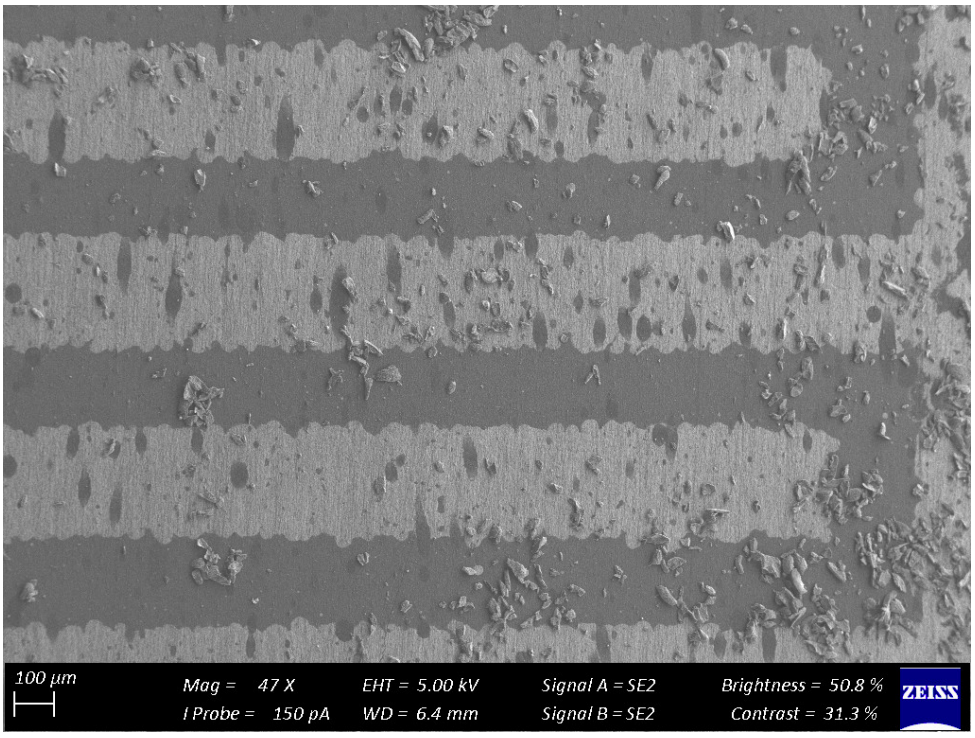

(a) Aligned Fibres over Electrode

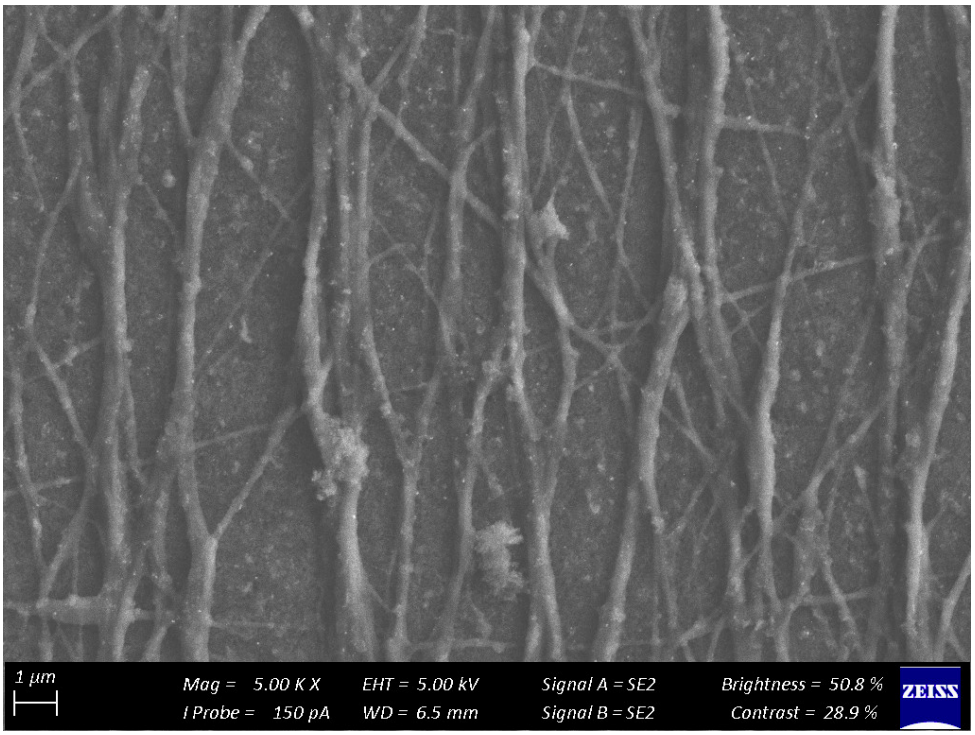

(b) Aligned Fibres Closeup

Figure 5.10: Final Fibres Over Electrode Post Rinse

Chapter 6

Developing Sensors From Polymer Nanofibres

6.1 Introduction

While the previous chapter details the procedures followed to produce a resistive sensing element, this chapter delineates the design employed to incorporate the resistive sensing element into an electrical circuit for the purpose of measuring the response of the resistive sensing element when exposed to the target antigen. While the means of connection has already been established, this section will discuss the noise mitigation and prevention strategies that were employed in the final design of the measuring circuit. This design was made based on the assumption of a linear output from the resistive sensing elements.

6.2 Literature Review

Resistive sensing is a well-established means of detection. It is employed in a wide variety of applications, such as sliding contact devices, thermistors, thermocouples and, most notably, strain gauges. As strain gauges are axiomatic examples of resistive sensing elements, and owing to the fact that the implementation of resistive sensing elements in this thesis is similar to the use of strain gauges, this review will often draw on the considerations made when implementing strain gauges. The principle of operation in a strain gauge is that, when strain is applied and deformation occurs, the electrical pathway of the strain gauge is affected, changing its resistance[72] . Similarly, in this thesis, it is proposed that the binding of the target analyte to the resistive sensing element will cause a change in conductivity.

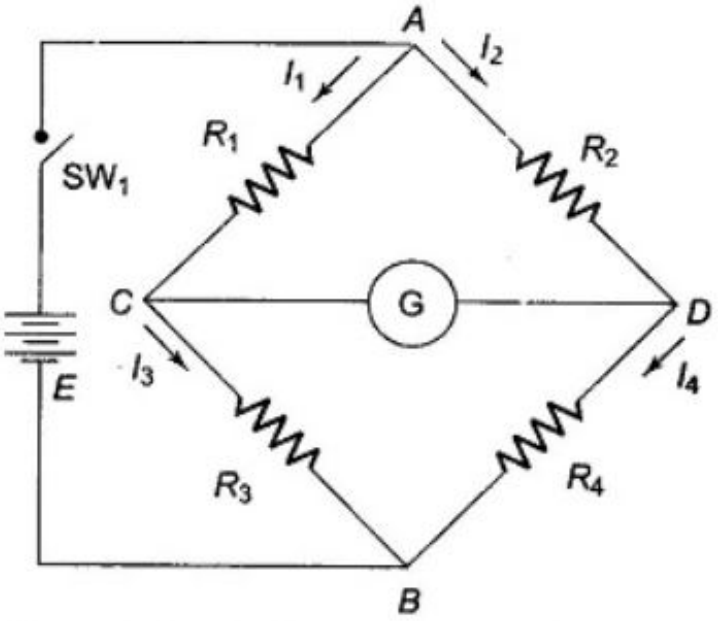

Figure 6.1: Wheatstone Bridge Circuit[73]

When developing a measurement setup, it is important to eliminate noise as early in the process as possible, while ensuring that as little noise as possible is added to the system in subsequent steps. To this end, strain gauges are typically employed in a variation of a wheatstone bridge configuration. The wheatstone bridge configuration (see Figure 6.1), is an elegant means of noise mitigation. Wheatstone bridge configurations are used to ensure that the outputs are directly proportional to a specific direction of applied strain[74]. This is achieved by cancelling out the effect of strain in other directions. Thermal effects can also be compensated for[72]. For the purpose of this thesis, a modified wheatstone bridge configuration will be employed to mitigate noise from the sensor and allow for a direct differential measurement over two electrodes, one with antibodies and one without.

The parameter of interest for this thesis is the change in resistance brought about by the binding of CD4 proteins to their corresponding antibodies. Therefore, it makes sense to take a differential measurement. Comparing one electrode that does not have the CD4 specific antibodies to an electrode that does have CD4 specific antibodies will allow for the determination of the effect of the binding alone. Any other changes in resistance brought about by other particulates in solution would affect both electrodes similarly, provided that the manufacturing process has produced electrodes with an appropriate degree of repeatability. Thus, by taking the difference, these contaminants are accounted for.

Another potential source of noise to consider is noise transmitted via the AC input from the wall source. This should be accounted for with the appropriate placement of either capacitors or filters, or both.

6.3 Design

This chapter serves to expand on the decision-making process used to develop a resistive sensing setup. The various subsections analyse specific portions of the design, after which all of these sections are consolidated.

6.3.1 Connection to Circuit

As mentioned in the previous chapter, a USB type A connector (see Figure 6.2) was chosen as the means by which the resistive sensing elements would be connected to the system. The justification for this decision is that this type of connection is ubiquitous, and as such has been proven to be both stable and convenient. Furthermore, this means of connection is both cheap and easy to implement.

Figure 6.2: USB Type A Male to Female [75]

6.3.2 Sensor Configuration

The sensor configuration is that of a modified wheatstone bridge. The purpose of this configuration is to enable control of current, to account for base variance, to reduce noise, and to provide the potential for a differential measurement to be made.

As seen in the circuit diagram below, Figure 6.3, the sensors (VS1 and VS2) are each to be connected in series with a known resistor and a potentiometer. These two branches would be in parallel, being supplied by an adjustable voltage source which is, in turn, powered by a 12V DC power supply. The two potentials of interest are those marked on the diagram as V1 and V2.

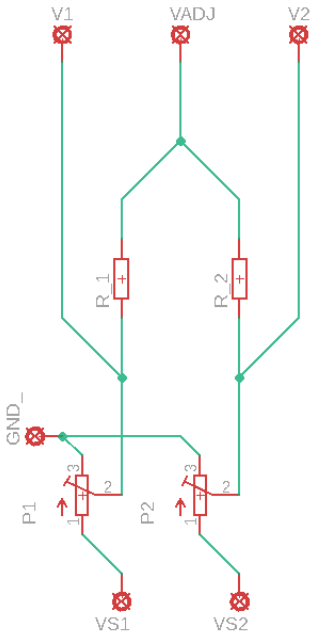

Figure 6.3: Circuit Diagram: Wheatstone Bridge

The purpose of the potentiometers P1 and P2 are to account for minor base variances in the resistance of the resistive sensing elements. This will be used to ensure that any variation in resistance caused by, for example, the lack of antibodies on one of the electrodes, can be accounted for, ensuring an initial difference of zero between the signals.

6.3.3 Signal Amplification

Before the signals can be amplified, it is necessary to ensure that appropriate noise mitigation steps are taken. By removing noise before amplification, one prevents the amplification of the noise itself; this results in a more accurate representation of the data.

To this end, the two voltages of interest will be fed through low-pass filters set to 40 Hz. The purpose of the low-pass filters is to remove any noise contribution brought about by the voltage supply. These filters will serve to remove any trace of the 50 Hz signal from standard South African power lines.

After having been filtered, the signals will be fed into an instrumentation amplifier. This type of amplifier takes two input signals and subtracts them from each other. The output of the amplifier is the result of this difference, multiplied by a factor determined by a specified resistor. A typical instrumentation amplifier circuit can be seen below, Figure 6.4. In this figure, P3 represents the potentiometer controlling the degree of amplification. Also note the reference voltage VREF that is typically an offset applied to the output. The aim thereof is to enable the appropriate biasing of the internal circuit.

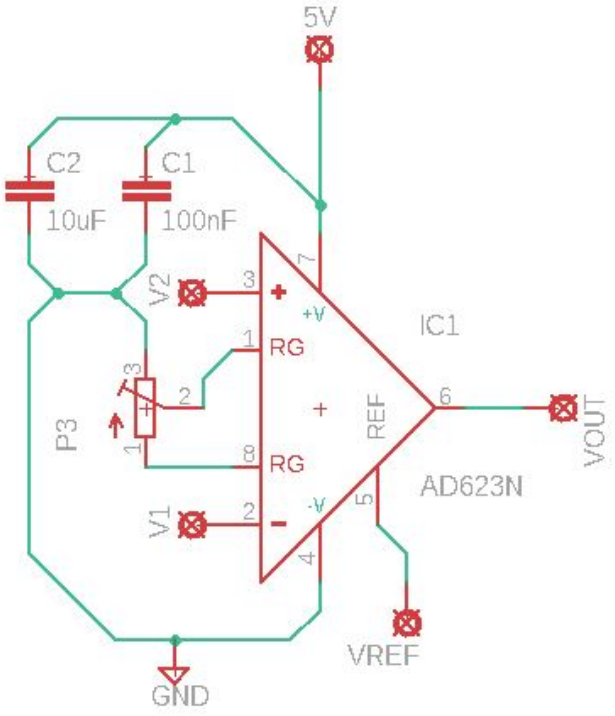

Figure 6.4: Circuit Diagram: Instrumentation Amplifier

6.3.4 ADC Protection

The value at the output would need to be read in by an ADC. It is necessary, however, to ensure that the ADC is protected from an overly high voltage. To this end, the following voltage clamp is to be implemented. This design makes use of a zener diode to clamp the voltage as soon as it reaches 5V. The output is modelled alongside Figure 6.5.

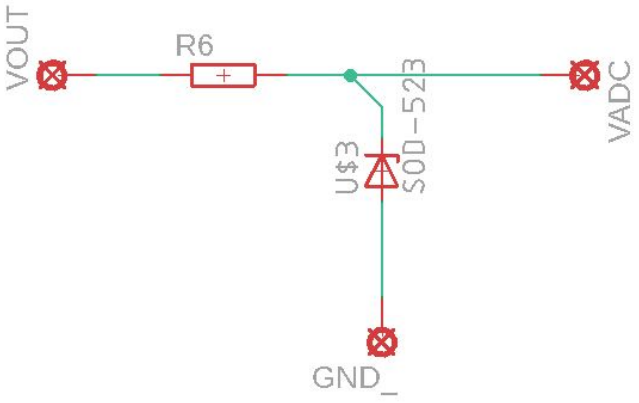

Figure 6.5: Circuit Diagram: Voltage Clamp

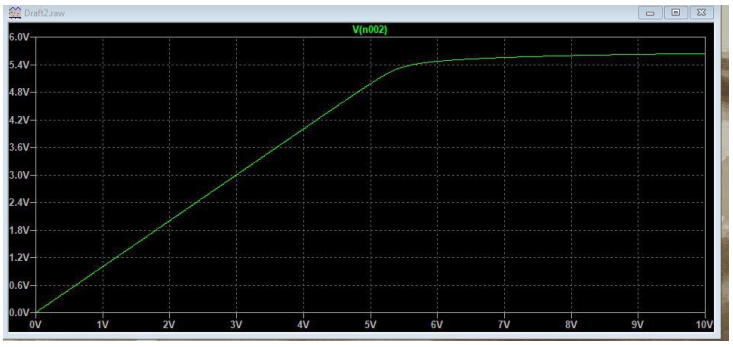

Figure 6.6: Example: 5.36V Zener Diode in this Configuration

6.3.5 Final Design

The final design for the measurement apparatus to be used in conjunction with the sensor can be found in Appendix B.

The microcontroller used in this design is an Arduino UNO. The UNO has a 10 bit ADC which provides sufficient resolution for the measurement at this scale as it can resolve 5 mV changes. Additionally, the UNO makes use of 5 V logic which corresponds to the level required by the LPFs chosen for this design. This microcontroller is also inexpensive to obtain and has a great deal of support available.

In terms of power, a single 12 V 4.2 A 50 W switching mode DC power supply from Micro Robotics powers the entire system. This drives the Arduino UNO, an adjustable DC-DC power supply from Micro Robotics, and a series of low dropout regulators. For the sake of power dissipation, a 7 V low dropout regulator (TO-220 package) from ROHM Semiconductor is used as an intermediary between the 5 V regulator (TO-220 package) from Texas Instruments and the 12 V supply. The 5 V regulator powers the internal logic of the ICs used on this board, namely the LPFs and the Instrumentation Amplifier. The 5 V regulator also supplies a 0.9 V Voltage reference (SOT-23 package) from RS components that is used as an offset to bias the instrumentation amplifier.

The filters chosen for this application are Maxim MAX7400CSA+ active, 8th order, low-pass filters. These filters are in 8-pin SOIC form and can have their cut-off frequency set by a 5 V clock signal anywhere from 0.001 to 10 kHz. This signal can be produced by the Arduino UNO.

The instrumentation amplifier chosen for this application is the AD623ANZ from Analog Devices. This IC comes in an 8-pin DIP package and has a 0.2 mV offset. This means that there is very little distortion at its output, which makes it ideal for this application.

The value of the Trimmer Potentiometers selected for this application would depend on the base variance between the electrodes, and as such could not be decided upon until functionalisation and antibody binding steps had been completed.

6.4 Conclusion

Unfortunately, the assumption that the electrodes would behave like normal resistors after the appropriate chemistry had been conducted proved to be false. As will be discussed in later chapters, a periodic electrochemical response was noted on many of the resistive sensing elements, with the implication that this measurement setup could not be implemented. Instead, a digital multimeter, namely the Agilent 34401A, was used in conjunction with the Keysight Benchvue Digital Multimeter software package.

Chapter 7

Sensor Functionalisation and Crosslinking

7.1 Introduction

This chapter outlines the procedures employed to modify the electrodes produced in the previous chapters so that they react with the appropriate degree of specificity. The following sections explain the function of each step and how these steps, collectively, serve to convert the base electrodes into sensors that react only to the presence of the prescribed antigen. Firstly, a short literature review provides the necessary background to the principles involved. Secondly, a section details the steps undertaken to functionalise the electrodes. Thirdly, the immobilisation procedure is discussed. Lastly, verification in the form of fluorescent microscopy is documented.

7.2 Literature Review

This thesis aims to verify if antigen-antibody binding causes a proportional change in resistance on the developed electrodes. It is, therefore, necessary to bind antibodies as the biorecognition element to the nanofibre substrate strongly, thus forming the transducer.

Strong chemical bonds typically come in the form of covalent bonds. It is very difficult to form covalent bonds with PSS. There is little in the literature which examines this approach. Consequently, adsorption was considered for the purpose of functionalisation. Functionalisation is the process whereby a target is treated in such a manner that, after treatment, it expresses specific functional groups on its surface.

This thesis considered two compounds for functionalisation, specifically PEI and APTES. PEI is a cationic polymer with a repeating unit which contains an amine group.

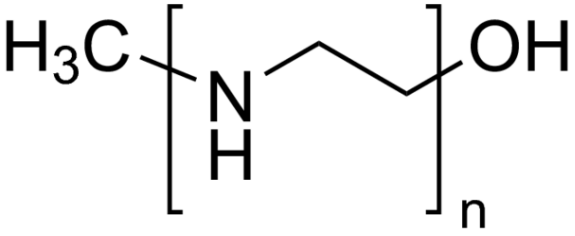

Figure 7.1: PEI[76]

PEI has been used in various experiments to react with PEDOT:PSS [77][78]. The PEI adsorbs to PEDOT:PSS owing to the strong opposing charges between the PEI and the PSS. This can be considered an electrostatic binding.

Much like PEI, APTES can be adsorbed onto PEDOT:PSS owing to the strong opposing charge of the PSS. APTES is a an aminosilane that is commonly used in silanization. As an aminosilane, it expresses an amine group.

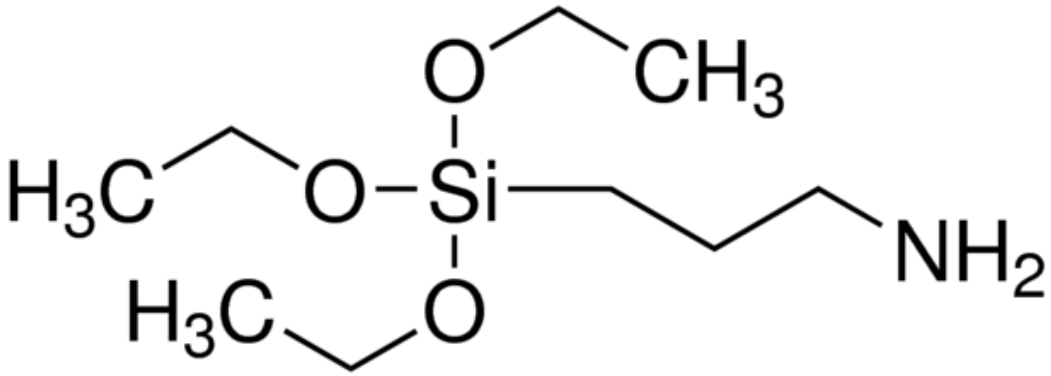

Figure 7.2: APTES[79]

When functional groups are available for covalent bonding, crosslinking chemistry can occur. Crosslinking is, "...the process of chemically joining two or more molecules by a covalent bond"[80]. Crosslinking reagents are often referred to as crosslinkers. These reagents have two or more reactive ends. These reactive ends determine the classification of the crosslinker in question. As the target molecule, anti-CD4+ antibodies of the IgG variety, express amine groups on the Fc portion of the antibody, a homobifunctional crosslinker is required that binds to amine groups on both ends.

According to the literature, a commonly used homobifunctional crosslinker that could serve this purpose is Glutaraldehyde[80].

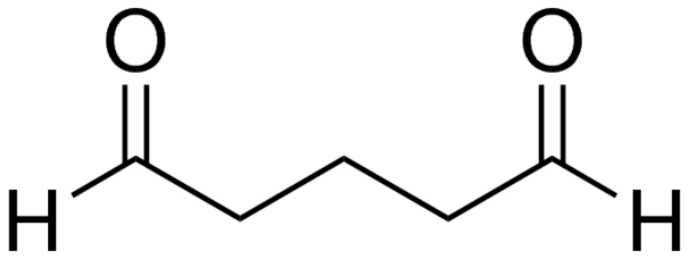

Figure 7.3: Glutaraldehyde[81]

On its own, Glutaraldehyde is often used as a disinfectant and to sterilise surgical instruments[82]. To this end, it features on the WHO's Model List of Essential Medicines[83]. As a crosslinker, glutaraldehyde is considered aggressive[84] owing to its carbonyl groups. A drawback to the use of glutaraldehyde is that its aggressive nature can result in the deactivation or denaturisation of antibodies or enzymes[84] [85].

Another homobifunctional crosslinker that binds with amine groups is BS3.

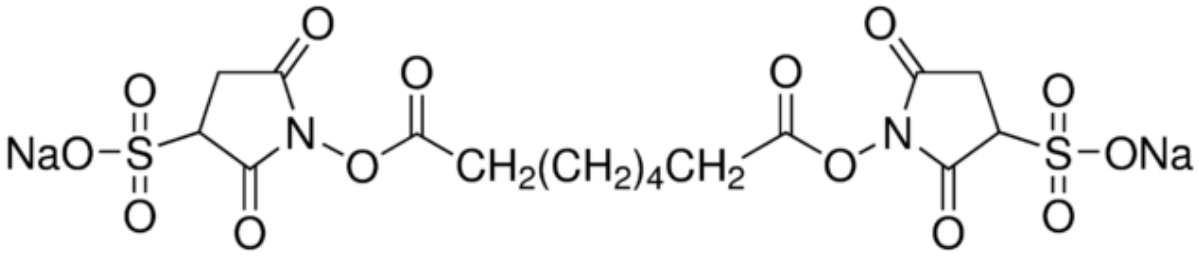

Figure 7.4: BS3[86]

BS3 is far less aggressive than glutaraldehyde owing to the means with which it binds to amine groups. Instead of carbonyl groups bonding directly to the amine groups, BS3 has amine-reactive N-hydroxysulfosuccinimide (NHS) esters at each end. These NHS esters react with amine groups and form stable amide bonds [87]. Upon forming these bonds, NHS groups break off into the solution.

In order to determine the effect of a target analyte, it is necessary to ensure that all potential non-specific binding sites have been blocked [88]. While any protein that does not bind specifically to the antibodies used for testing can be used as a blocking agent, it is common practice to make use of an established blocking buffer. BSA-based blocking buffers are commercially available and commonly employed for this purpose. To further reduce the likelihood of non-specific antibody binding, Polysorbate 20 or Tween® 20 can be used as a washing agent. Tween® 20 is a surfactant with 20 repeat units of polyethylene glycol.

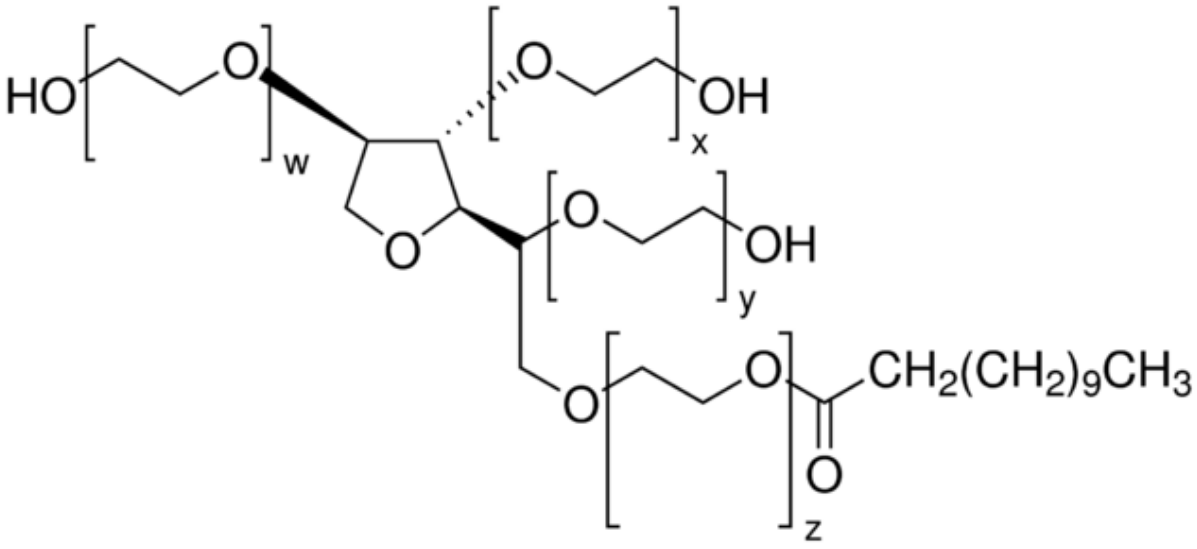

Figure 7.5: Polysorbate (Tween®) 20[89]

Another important solution to note is PBS. PBS is a balanced salt solution used for various cell-culture applications[90]. PBS 7.4 refers to PBS with a pH level of 7.4. This corresponds to the average pH level found in human blood.

7.3 Functionalisation Methodology

The electrodes were functionalised by means of the following steps:

1. Produce Electrodes
   Sheets of electrodes were produced as outlined in the previous chapters.

2. Electrode Sorting
   Electrodes with a base resistance exceeding 1 kΩ were deemed failures and discarded.

   Plexiglass or Poly(methyl methacrylate) wells were laser cut and affixed onto the electrodes with cyanoacrylate and allowed to dry (see Figure 7.6).

3. Functionalise with APTES
   80 $\mu\ell$ of 10 wt% APTES in Toluene was pipetted into each well. These wells were then sealed with masking tape to prevent evaporation. The electrodes were then left for four hours.

4. Rinse
   100 $\mu\ell$ of PBS 7.4 was pipetted into the wells. This was then taken up in the pipette and then pipetted back into the wells. This was repeated two more times, thereafter the wells were emptied.

   At this point, another 100 $\mu\ell$ of PBS 7.4 was added. The aforementioned rinsing procedure was followed.

   This entire procedure was repeated a third time.

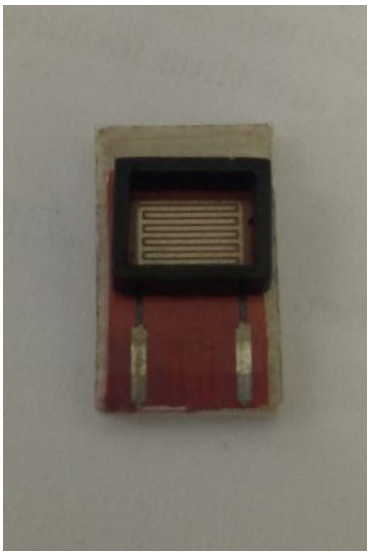

Figure 7.6: Electrode with well

At this juncture, the electrodes were measured a second time. The base resistance of all of the electrodes had risen considerably. When this was first discovered, the change in resistance was typically an increase of an order of magnitude or more. Consequently, the solution was adjusted, as described earlier, so as to include PVA. This provided additional binding sites for the APTES, allowing for a decreased change in resistance. This was confirmed when the above methodology was repeated with the new mixture. The change in resistance was now typically 10 times or more. Additionally, it was at this juncture (after functionalisation) that it was noted that not all of the electrodes produced a linear resistance. In fact, it was noted that after functionalisation, the resistance on some of the electrodes had become periodic. This will be discussed later in this chapter.

7.4 Functionalisation Confirmation

After the functionalisation procedure was completed for the first time, it was necessary to determine whether functionalisation had indeed occurred. To this end, fluorescent microscopy was used.

The available functional group is typically the determining factor when choosing a fluorescent marker for fluorescent microscopy. As amine groups were expected to be available for binding, FITC was selected as the fluorescent marker. FITC binds to specific functional groups, such as amine and sulfhydryl groups. It has an excitation wavelength of 490 nm (maximum) and an emission wavelength of 525 nm (maximum). It should be noted that FITC, like many fluorescent markers, is light-sensitive.

In order to prepare a 1 mg/mℓ FITC in PBS solution, FITC was dissolved into a PBS buffer and stirred for 15 minutes. 100 $\mu\ell$ of this solution was pipetted onto each of the sensors. The sensors were subsequently kept in a dark room for two hours to allow for binding to occur. After this had been completed, the sensors were rinsed with DI water in a manner similar to step 4 in section 7.3.

The results of the fluorescent microscopy were as follows:

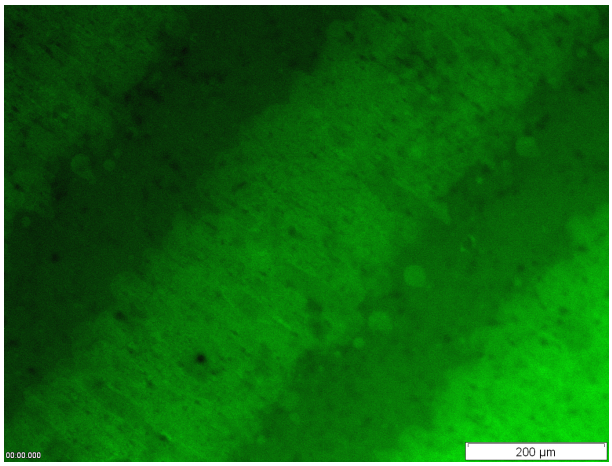

(a) Fluorescent 1

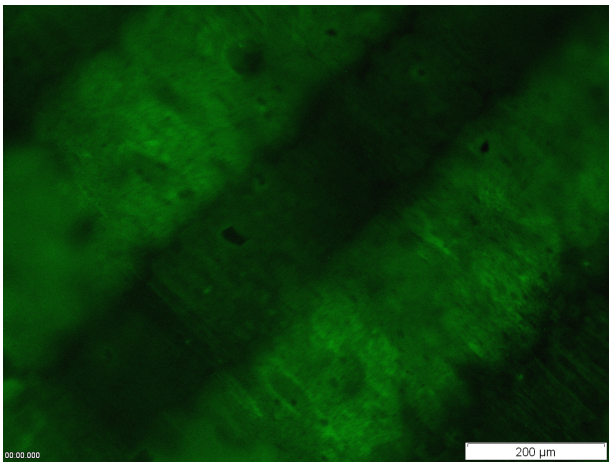

(b) Fluorescent 2

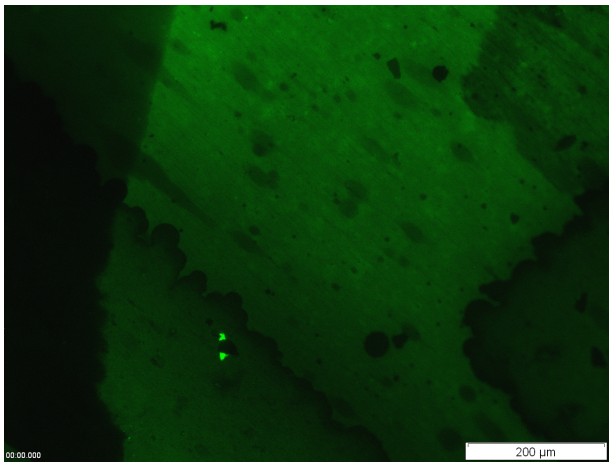

(c) Fluorescent 3

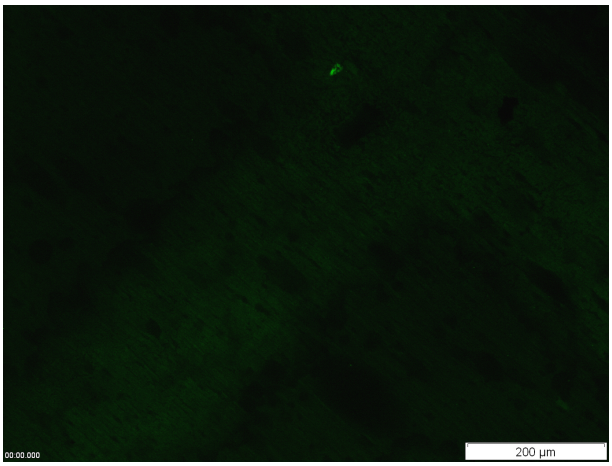

(d) Fluorescent 4

Figure 7.7: Fluorescent Microscopy Results

The vibrant green light in the above images is a clear indication that amine groups were successfully bound to the surface of the PEDOT:PSS fibres. Additionally, the direction of alignment of the fibres can be discerned, further re-affirming the hypothesis that the amine groups were bound to the distinct fibres. In figure c, the darker semi-circular region shows where the drop of FITC ended. This serves as a clear indication of the difference between the FITC exposed region and the non-exposed region.

7.5 Antibody Crosslinking Chemistry

This procedure follows directly on the functionalisation steps described in 7.3. To assist with proof-of-concept, an additional set of tests was conducted. This set of tests would make use of anti-lysozyme antibodies and lysozyme protein.

Polyclonal anti-CD4 antibodies were obtained from abcam, Cambridge, United Kingdom. The host-species was rabbit and species reactivity tests had proven that these antibodies reacted with human CD4 protein.

Recombinant human CD4 protein was also obtained from abcam.

Two avenues of testing were available. Firstly, the concentration of antibodies could be held constant and the concentration of proteins varied over the electrodes. Alternatively, the concentration of antibodies could be varied and the concentration of proteins held constant. For complete characterisation of a sensor, both methods need to be followed, however, for proof-of-concept, one of these avenues would be sufficient. The anti-CD4 antibodies proved to be more expensive than their protein counterpart. Consequently, antibody concentration was varied and protein concentration was held constant so as to reduce the amount of antibodies required.

1. Add BS3: 100 $\mu\ell$ of 6 mg/10mℓ BS3 in PBS was added to each well. The wells were then covered in masking tape once again and the electrodes were left to incubate at room temperature for two hours.

2. Rinse: The same rinsing procedure documented in step 4 of section 7.3 was repeated at this juncture.

3. Antibody Immobilisation: At this stage, the two separate sets of tests began. An unknown concentration of anti-lysozyme antibodies was made available by the microbiology department at the University of Stellenbosch for this thesis.

   The anti-lysozyme was administered as follows:

   - 50 $\mu\ell$ of 4%volume of the unknown concentration of antibodies was added to one row of wells.
   - 50 $\mu\ell$ of 2%volume of the unknown concentration of antibodies was added to a second row of wells.
   - 50 $\mu\ell$ of 1%volume of the unknown concentration of antibodies was added to a third row of wells.

   The anti-CD4 was administered as follows:

   - 100 $\mu\ell$ of 10%volume of the 1 mg/mℓ anti-CD4 antibodies in PBS was added to one row of wells.
   - 100 $\mu\ell$ of 1%volume of the 1 mg/mℓ anti-CD4 antibodies in PBS was added to a second row of wells.
   - 100 $\mu\ell$ of 0.1%volume of the 1 mg/mℓ anti-CD4 antibodies in PBS was added to a third row of wells.

4. Add BSA: 100 $\mu\ell$ of 3 wt% BSA was added to each well. The electrodes were left to incubate for two hours.

5. Tween 20 Rinse: The electrodes were rinsed with 0.0005 vol% Tween 20 in PBS in a manner similar to the rinse described in step 4 of section 7.3. This was done in a darkened room owing to the light-sensitive nature of Tween 20.

6. Rinse: The electrodes were rinsed with PBS as described in step 4 of section 7.3.

Thereafter, the electrodes were measured. The observation of the electrodes pre and post antibody addition served to prove that antibody binding did indeed take place. This is evidenced by the change in resistance documented and discussed in the following sections. Periodic functions were analysed and compared by means of Matlab's *trapz* function which is suited to integrating discrete data sets by means of the trapezoid method.

7.6 Lysozyme Analysis: Pre and Post Antibody Addition

As each row has had a different concentration of antibodies bound to it, the analysis of the electrodes will be taken row by row. It should be noted that the fibre density is most dense at the centre of each row, decreasing in density towards the extremities. It should also be known that the original concentration of the antibody is unknown.

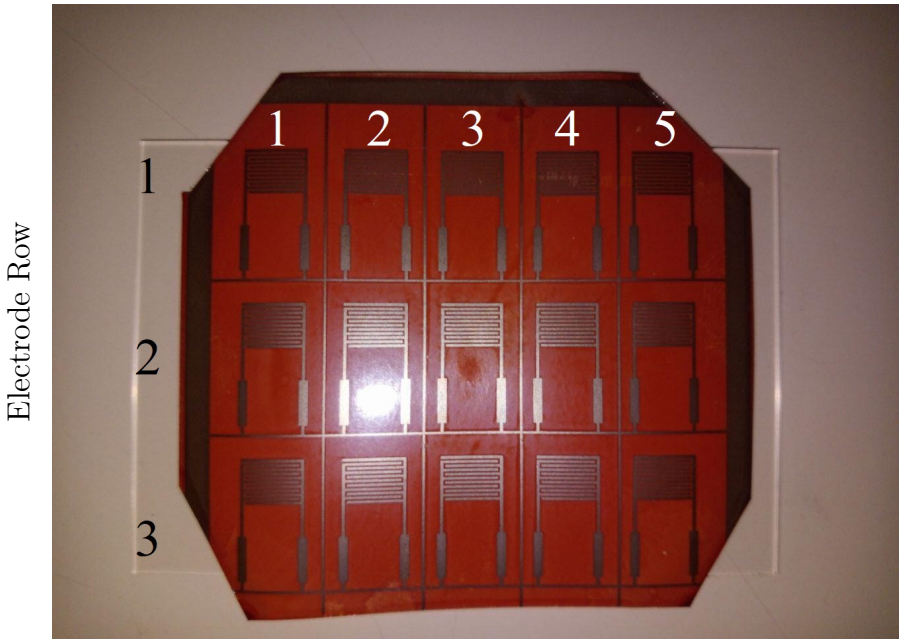

Figure 7.8: Electrode positioning system used in analyses.

7.6.1 Row 1 - 4% Anti-lysozyme Antibody Solution in PBS 7.4

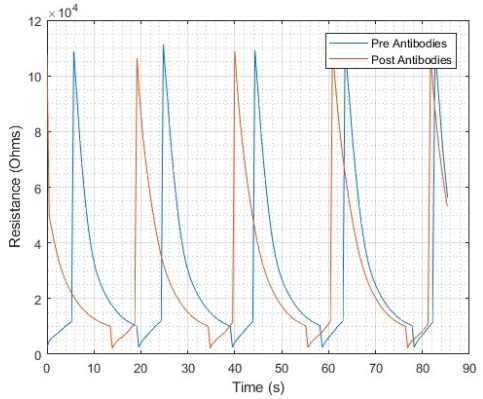

(a) Lysozyme Pre and Post Antibodies: Test 0

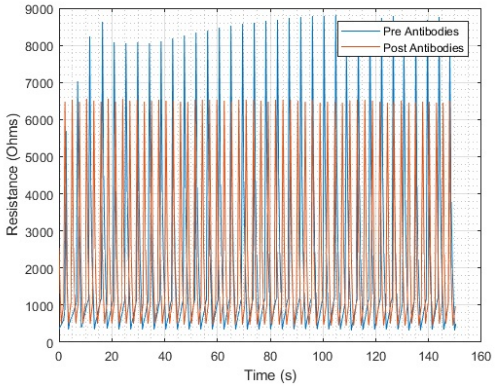

(b) Lysozyme Pre and Post Antibodies: Test 1

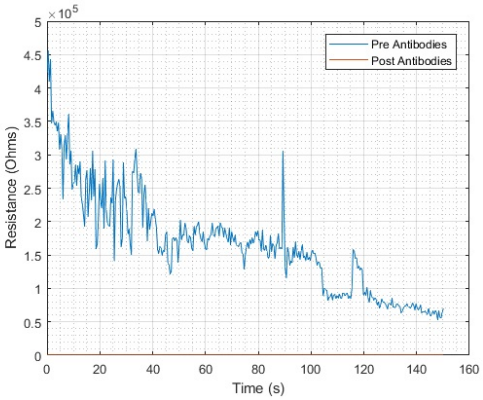

(c) Lysozyme Pre and Post Antibodies: Test 2

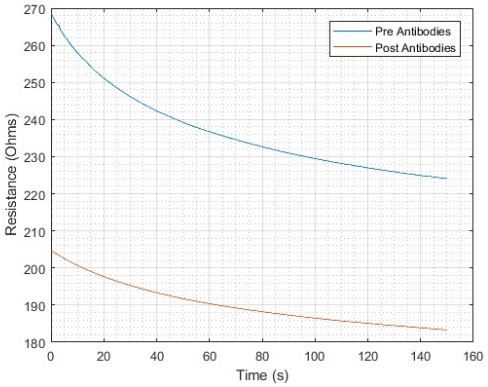

(d) Lysozyme Pre and Post Antibodies: Test 3

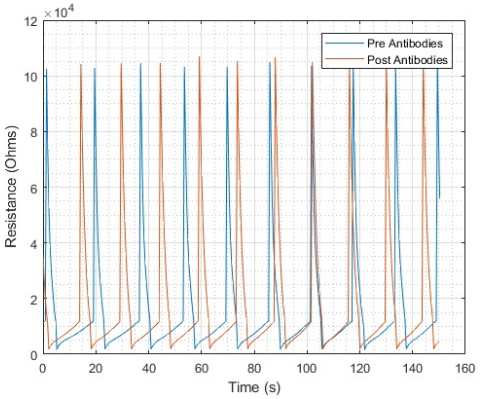

(e) Lysozyme Pre and Post Antibodies: Test 4

Figure 7.9: Resistance over time of electrodes before and after the addition of anti-lysozyme antibodies. Tests are arranged in order across one row of electrodes.

Test 0 found periodic signals both pre and post antibody addition. This test showed little change in frequency (approximately 0.05 Hz) or signal amplitude. Integration of the

signals over the time period showed only a small change in base resistance, approximately 1.04%.

Test 1 also found periodic signals and showed an increase in frequency. The frequency before antibody addition was approximately 0.22Hz. The overall amplitude decreased. Integration yielded a small increase in resistance of approximately 2.79%.

Test 2 saw two signals that stabilised to fixed values. A very substantial decrease in resistance was noted, with the resistance decreasing by 99.78%.

Test 3 also found signals that approached steady-state values. A decrease of approximately 18.18% was noted.

Test 4 found periodic signals. There was a small increase in frequency, and the amplitudes were also similar. Integration found an overall increase in resistance of approximately 8.69%.

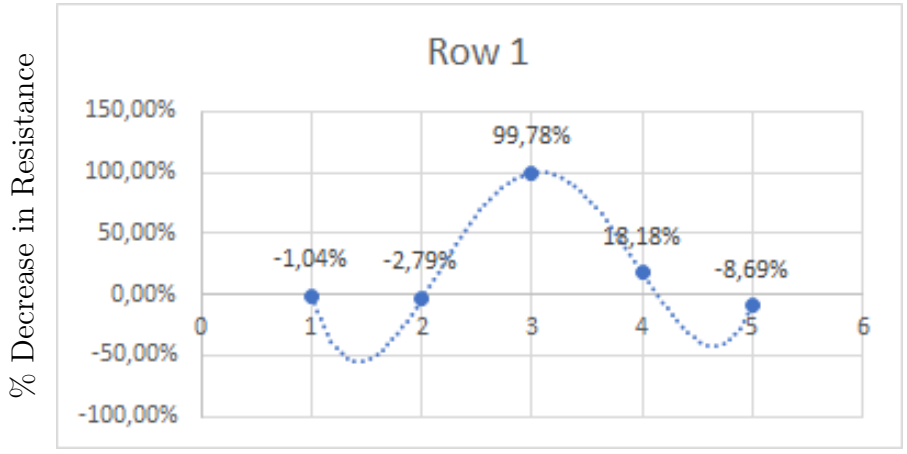

Figure 7.10: Lysozyme Pre and Post Antibodies: Row 1. % Decrease in resistance across the electrode row.

Analysis of these signals would suggest that at a higher fibre density in this row, a non-periodic output curve can be expected. As fibre density decreases, periodic functions are observed with ever-decreasing frequency. Antibody addition seems to increase frequency in general. The overall effect on this row would seem to indicate that, on non-periodic sensors, antibody addition decreased the overall resistance significantly. Sensors exhibiting periodic outputs, on the other hand, seem to experience a small increase in resistance. Base resistances also increase from the centre of the row outwards, similar to pre-functionalisation.

A plot of the % decrease in resistance corresponding to each electrode in row 1 can be seen in Figure 7.10.

7.6.2 Row 2 - 2% Antibody Solution in PBS 7.4

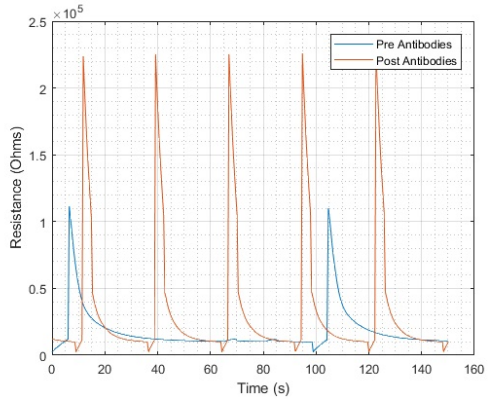

(a) Lysozyme Pre and Post Antibodies: Test 5

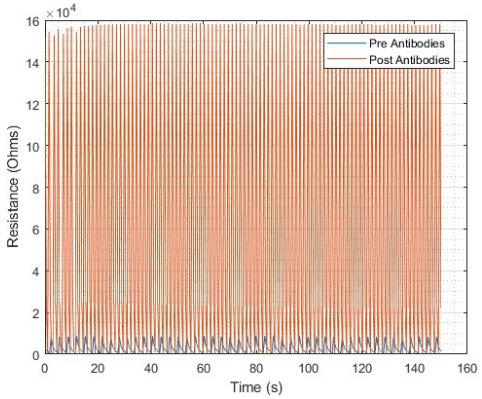

(b) Lysozyme Pre and Post Antibodies: Test 6

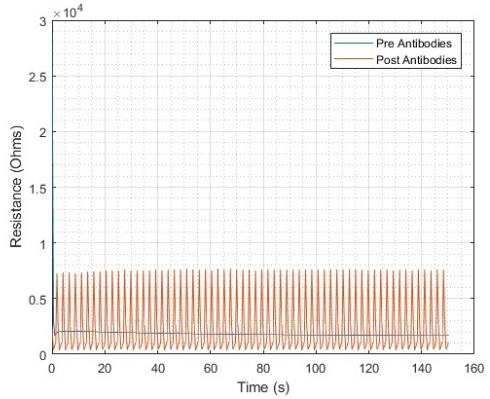

(c) Lysozyme Pre and Post Antibodies: Test 7

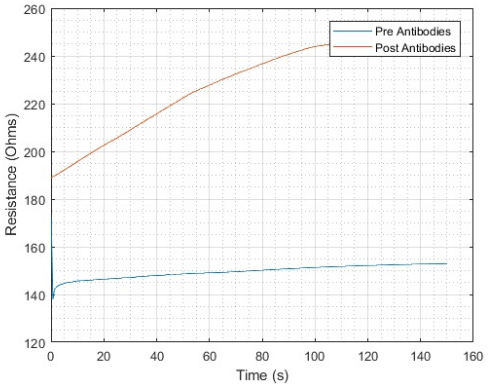

(d) Lysozyme Pre and Post Antibodies: Test 8

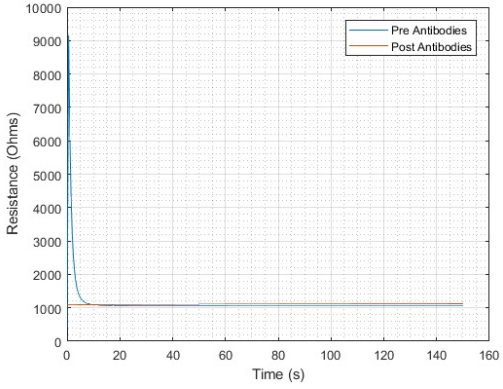

(e) Lysozyme Pre and Post Antibodies: Test 9

Figure 7.11: Resistance over time of electrodes before and after the addition of anti-lysozyme antibodies. Tests are arranged in order across one row of electrodes.

Test 5 saw sensors with periodic responses. Antibody addition increased frequency notably, and there was a very large increase in amplitude. Integration found an increase of approximately 83.75% in base resistance.

Test 6 saw sensors with periodic responses. Frequency increased greatly and there was again a notable increase in signal amplitude. Integration found an increase in base resistance of 1833.62%.

Test 7 saw a non-periodic sensor become periodic after the addition of the antibodies. This would suggest that the PBS aided the transformation to a periodic signal. Integration found an overall increase in resistance of approximately 29.88%.

Test 8 found a non-periodic response that remained non-periodic after antibody addition. A nett decrease of approximately 37.25% was noted in the stabilised response values.

Test 9, similarly, found a non-periodic signal that remained non-periodic. This time an increase of approximately 6.26% was noted from the steady-state values.

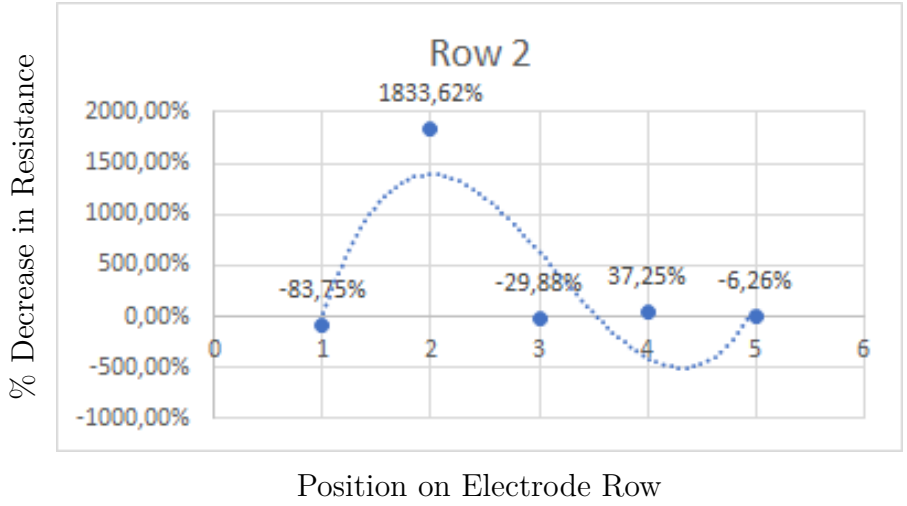

Figure 7.12: Lysozyme Pre and Post Antibodies: Row 2. % Decrease in resistance across the electrode row.

The response from test 8 was similar to the response from test 3, which is significant as both have similar fibre densities and both are non-periodic in nature. Their steady-state values are also similar, however, test 8 noted a larger change in resistance than test 3. This could suggest that the blocking buffer has a greater effect on base resistance as the buffer should have bound to more sites on test 8 than on test 3. All of the periodic signals saw an increase in frequency owing to antibody addition, and the base frequency, much like in the row above, decreased from the centre of the row towards its extremities. Base resistances, determined by integration, also seem to decrease from the centre towards the extremities, which corresponds to expectations.

A plot of the % decrease in resistance corresponding to each electrode in row 2 can be seen in Figure 7.12.

7.6.3 Row 3 - 1% Anti-lysozyme Antibody Solution in PBS 7.4

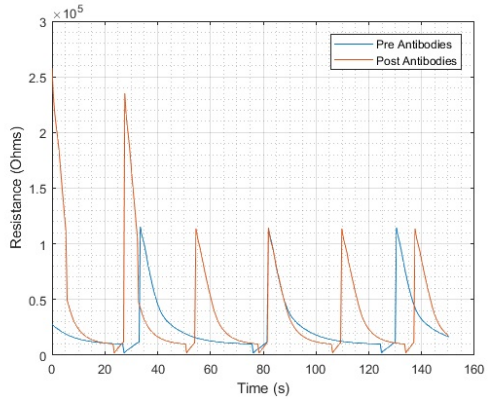

(a) Lysozyme Pre and Post Antibodies: Test 10

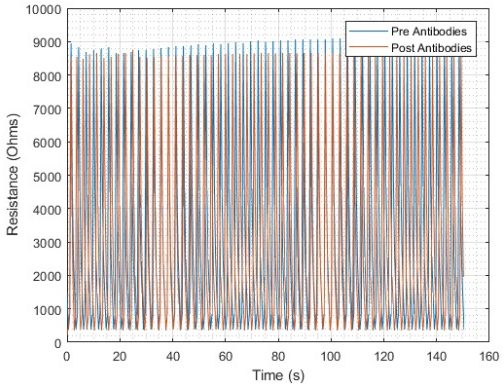

(b) Lysozyme Pre and Post Antibodies: Test 11

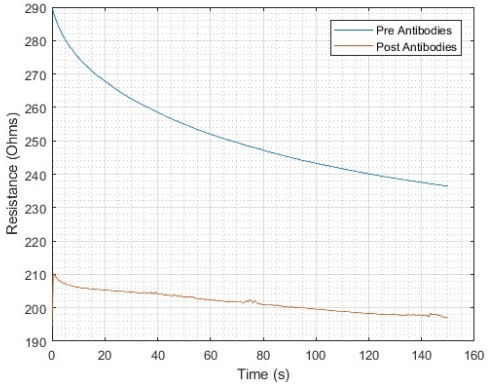

(c) Lysozyme Pre and Post Antibodies: Test 12

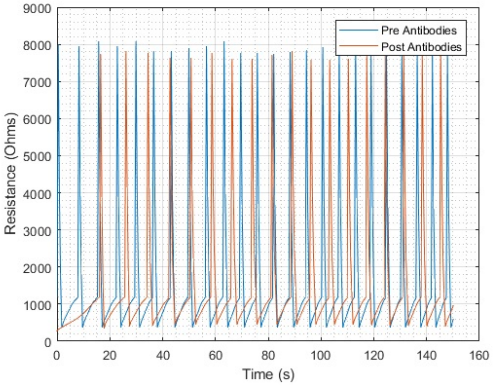

(d) Lysozyme Pre and Post Antibodies: Test 13

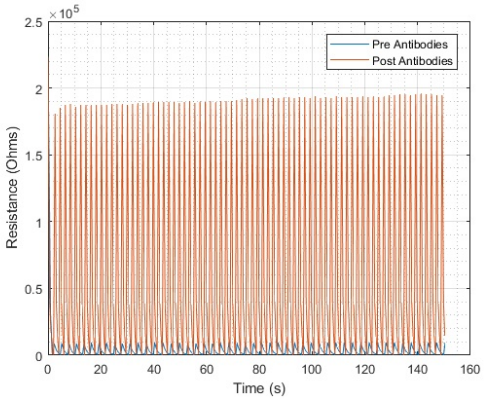

(e) Lysozyme Pre and Post Antibodies: Test 14

Figure 7.13: Resistance over time of electrodes before and after the addition of anti-lysozyme antibodies. Tests are arranged in order across one row of electrodes.

Test 10 saw periodic resistances whose frequency increased after antibody addition. This frequency increase was sufficient to cause an increase in average resistance of approxi-

mately 57.3%. It should be noted that this figure may have been exaggerated by the effect of response stabilisation on the integration period.

Test 11 also saw periodic responses. Similarly, the frequency increased and there was a decrease in amplitude. The result was an overall decrease of approximately 5.15%. It must be noted that this value may be understated owing to stabilisation occuring at the onset of the integration period.

Test 12 saw non-periodic responses. A comparison of these steady-state values showed a decrease in resistance of 14.78%.

Test 13 saw periodic responses with a decrease in frequency post antibody addition. A small decrease in amplitude is also noted. An overall decrease over the integrated period of approximately 9.33% was observed, although this difference may be slightly exaggerated owing to stabilisation occuring in the integrated period.

Test 14 saw a significant increase in frequency from periodic responses. Similarly, a dramatic increase in amplitude was noted. This resulted in an overall increase in resistance of approximately of 1328.10%.

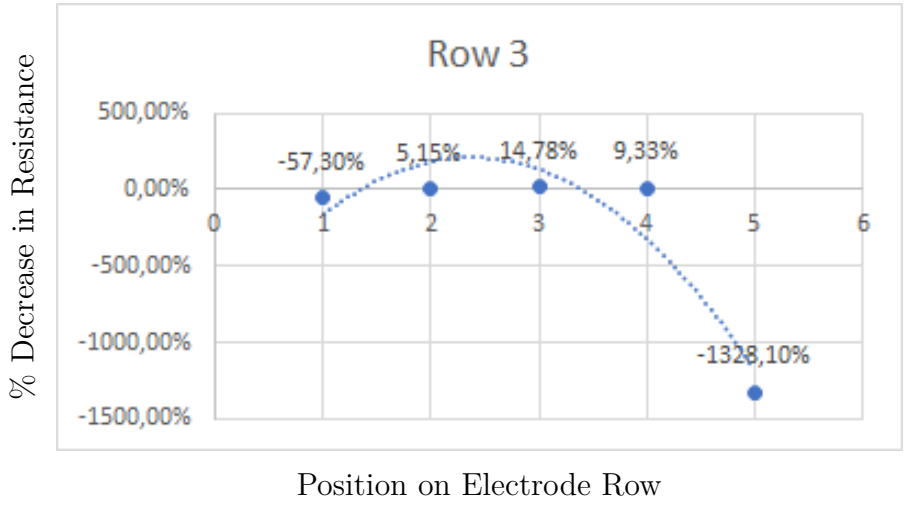

Figure 7.14: Lysozyme Pre and Post Antibodies: Row 3. % Decrease in resistance across the electrode row.

Analysis of this row shows the greatest decrease occurring at test 12, with the decrease decreasing towards the extremities of the row. This corresponds to the fibre density of this row. Based hereupon it is believed that a greater prevalence of antibody binding corresponds to a greater decrease in resistance of the electrodes. As fibre density decreases, the responses become periodic with decreasing frequency. In these periodic responses, the antibody binding seems to cause a general increase in resistance when evaluating the integral of the response. This would correspond to the antibodies serving as a resistive factor to the periodic, electrochemical response taking place.

A plot of the % decrease in resistance corresponding to each electrode in row 3 can be seen in Figure 7.14.

7.7 CD4 Analysis: Pre and Post Antibody Addition

7.7.1 Row 1: 10% 1mg/mℓ CD4 Antibodies in PBS 7.4

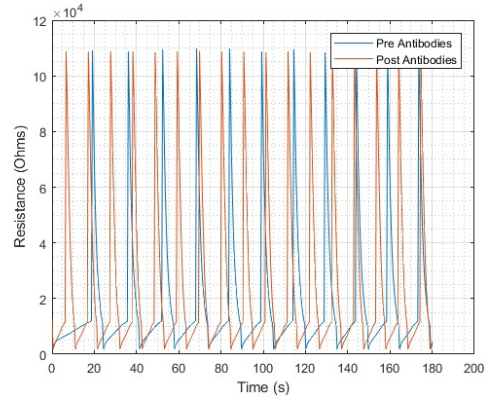

(a) CD4 Pre and Post Antibodies: Test 0

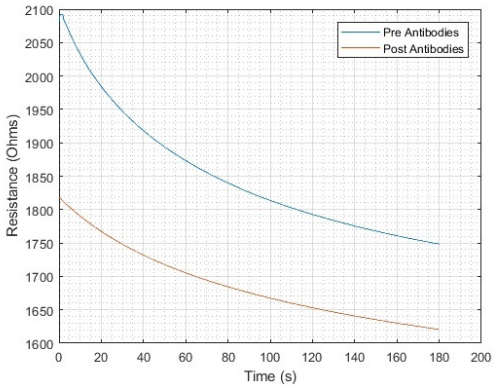

(b) CD4 Pre and Post Antibodies: Test 1

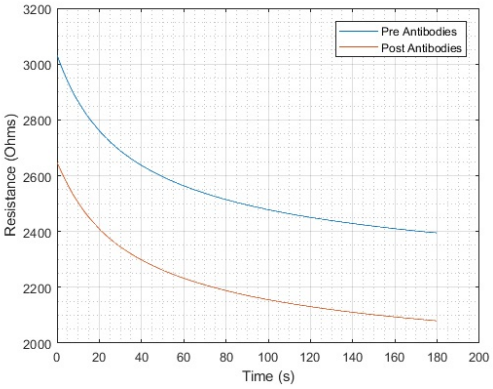

(c) CD4 Pre and Post Antibodies: Test 2

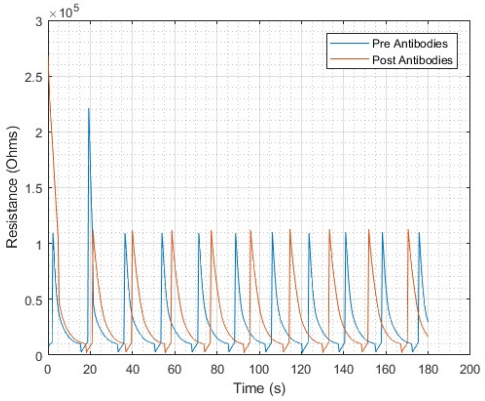

(d) CD4 Pre and Post Antibodies: Test 3

Figure 7.15: Resistance over time of electrodes before and after the addition of anti-CD4 antibodies. Tests are arranged in order across one row of electrodes.

Test 0 found periodic responses with an increase in frequency post antibody addition from 0.0625 Hz. Integration yielded an average increase in resistance of approximately 25.11%.

Test 1 found non-periodic responses and an overall decrease in amplitude at steady-state of approximately 10%.

Test 2 also found non-periodic responses with an overall decrease in amplitude noted at approximately 13.33%.

Test 3 saw a periodic response with a very small decrease in frequency from 0.0625 Hz occurring post antibody addition. Integration yielded an increase average increase in resistance of approximately 23.14%.

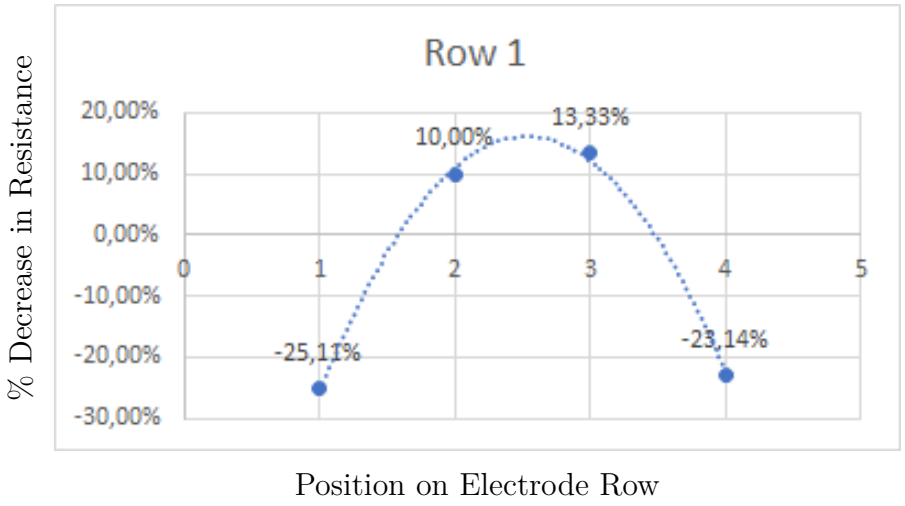

Figure 7.16: CD4 Pre and Post Antibodies: Row 1. % Decrease in resistance across the electrode row.

Overall, this row showed a somewhat parabolic response with the largest decrease in resistance present at the highest fibre density, with ever-increasing changes in resistance towards the extremities, i.e. as the fibre density decreased.

A plot of the % decrease in resistance corresponding to each electrode in row 1 can be seen in Figure 7.16.

7.7.2 Row 2: 1% mg/mℓ CD4 Antibodies in PBS 7.4

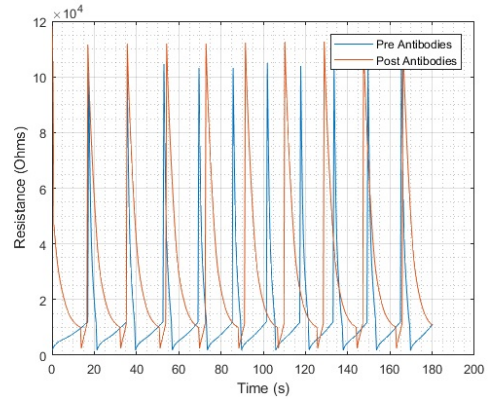

(a) CD4 Pre and Post Antibodies: Test 4

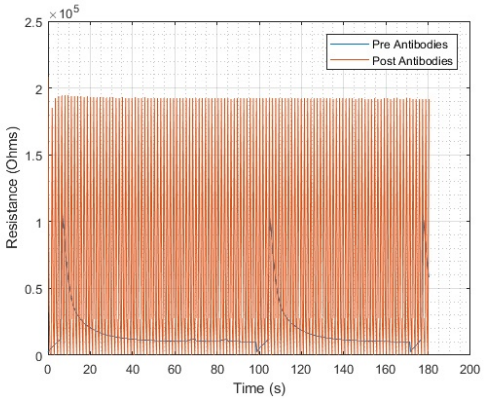

(b) CD4 Pre and Post Antibodies: Test 5

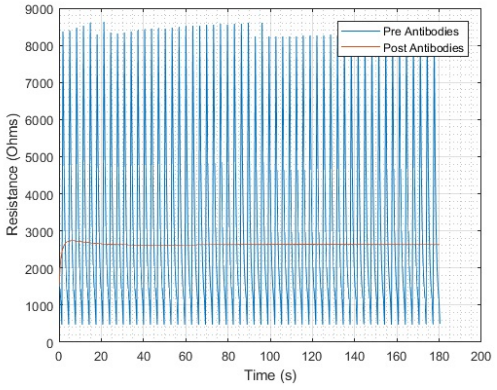

(c) CD4 Pre and Post Antibodies: Test 6

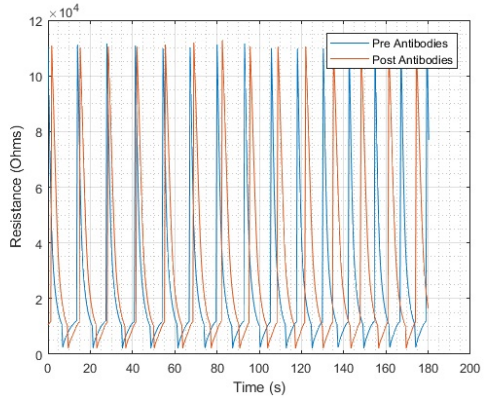

(d) CD4 Pre and Post Antibodies: Test 7

Figure 7.17: Resistance over time of electrodes before and after the addition of anti-CD4 antibodies. Tests are arranged in order across one row of electrodes.

Test 4 showed a periodic response with frequency increasing from approximately 0.0667 Hz. The amplitude of the response also increased. Integration yielded an average increase in magnitude of approximately 99.32%.

Test 5 saw a marked increase in frequency of the periodic responses observed. Integration, however, found that a net decrease in resistance of approximately 58.18% was observed.

Test 6 showed a periodic response at approximately 0.3 Hz that became non-periodic after the addition of the antibodies. An average decrease in magnitude of approximately 15.71% was noted by integration.

Test 7 saw a periodic response at approximately 0.0667 Hz that increased in frequency post antibody addition. While the amplitudes remained relatively similar, an overall increase in resistance of approximately 19.94% was observed from the comparison of the integrated results.

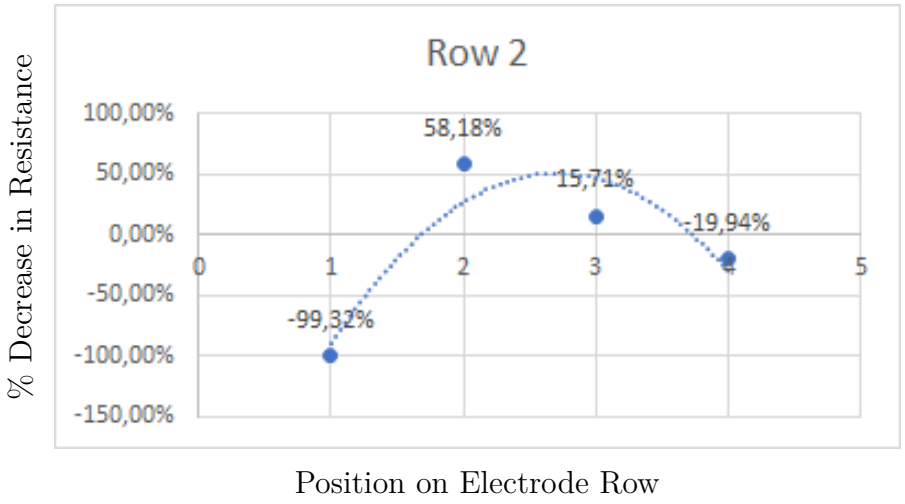

Figure 7.18: CD4 Pre and Post Antibodies: Row 2. % Decrease in resistance across the electrode row.

Overall this row showed a similar parabolic response to the first row. The magnitudes, however, are also typically larger, suggesting that the blocking agent may have a more significant impact than the antibodies.

A plot of the % decrease in resistance corresponding to each electrode in row 2 can be seen in Figure 7.18.

7.7.3 Row 3: 0.1% 1mg/mℓ Anti-CD4 Antibodies in PBS 7.4

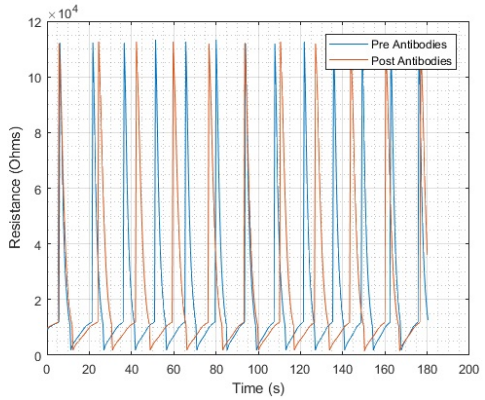

(a) CD4 Pre and Post Antibodies: Test 8

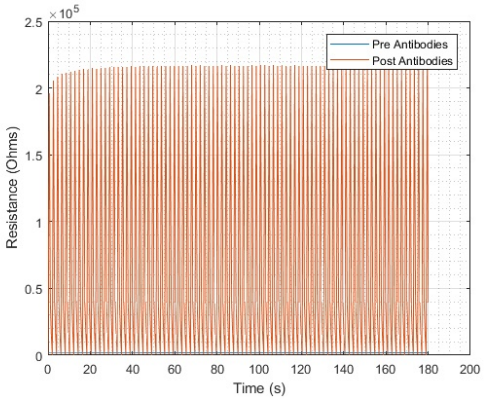

(b) CD4 Pre and Post Antibodies: Test 9

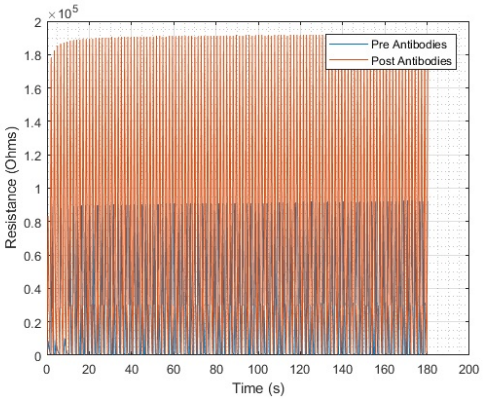

(c) CD4 Pre and Post Antibodies: Test 10

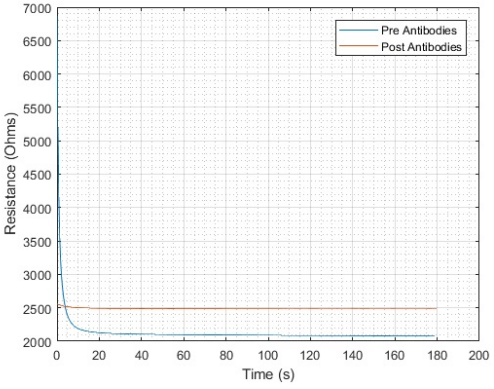

(d) CD4 Pre and Post Antibodies: Test 11

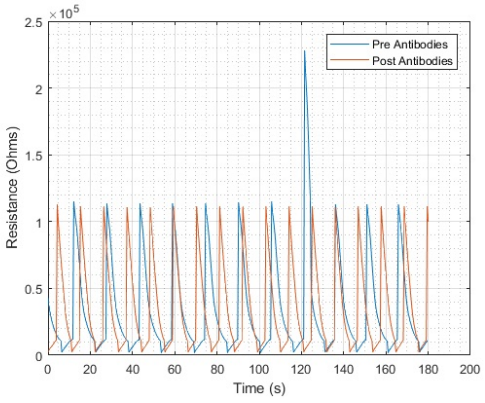

(e) CD4 Pre and Post Antibodies: Test 12

Figure 7.19: Resistance over time of electrodes before and after the addition of anti-CD4 antibodies. Tests are arranged in order across one row of electrodes.

Test 8 saw a periodic response with an increase in frequency occuring post antibody addition. The amplitudes in this response were similar, and an overall increase of approximately 6.64% was noted.

Test 9 saw a non-periodic response become periodic post antibody addition. The periodic response was relatively fast, in comparison to other observed signals, at 0.5 Hz. Integration

over the period saw an increase in resistance of over 4000%. This increase is cause for concern with respect to the subsequent test and should be noted as it could imply that the electrode has been damaged.

Test 10 saw periodic responses where antibody addition caused an increase in frequency from approximately 0.575 Hz. A very large increase in amplitude was noted. Through integration, an increase in the average resistance of approximately 148.86% was noted.

Test 11 saw non-periodic responses. An increase in amplitude at steady-state of approximately 19.05% was noted.

Test 12 saw periodic functions at low frequencies. The initial frequency was approximately 0.0555Hz and increased slightly post antibody addition. While the amplitude remained fairly similar, integration yielded an average overall increase in resistance of approximately 17.48%.

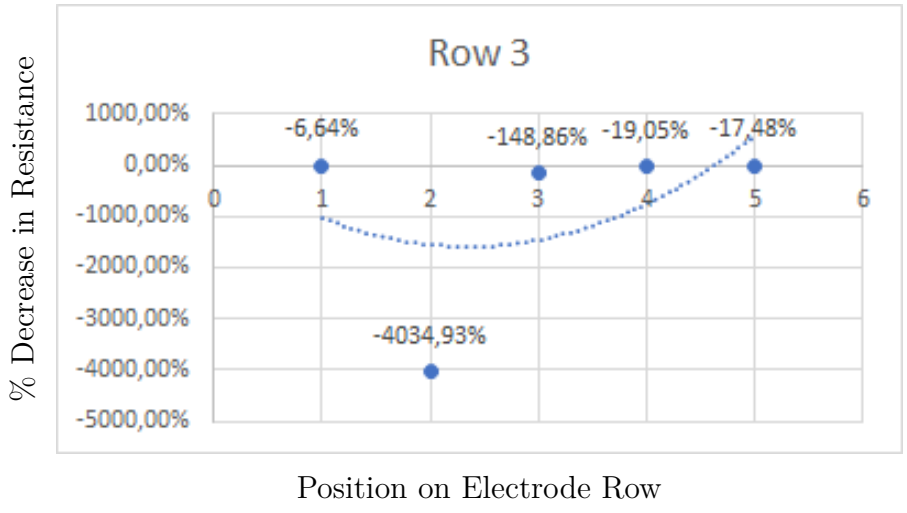

Figure 7.20: CD4 Pre and Post Antibodies: Row 3. % Decrease in resistance across the electrode row.

This row followed a parabolic trend similar to the previous two rows, only inverted in direction. This would suggest that the blocking buffer is more likely to cause an increase in resistance than the antibodies, as the blocking buffer occupied far more of the potential binding sites than the antibodies did.

A plot of the % decrease in resistance corresponding to each electrode in row 3 can be seen in Figure 7.16.

Chapter 8

Characterisation of Nanofibre-based Biosensors

8.1 Introduction

This chapter will present the results obtained after analysis was performed on the completed biosensors. Furthermore, analysis will be performed on the results to aid interpretation thereof. Integration is performed using Matlab's *trapz* function, which uses the trapezoid method to integrate discrete data sets.

8.2 Lysozyme Analysis: Pre and Post Protein Addition

8.2.1 Row 1

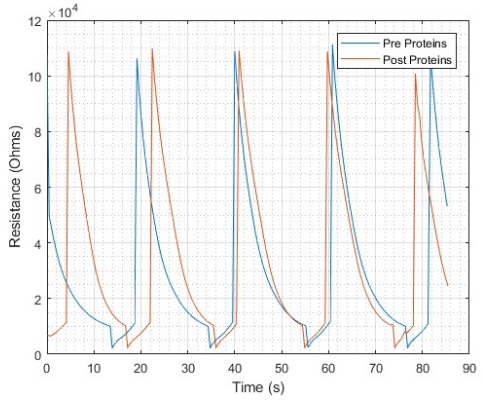

(a) Lysozyme Pre and Post Proteins: Test 0

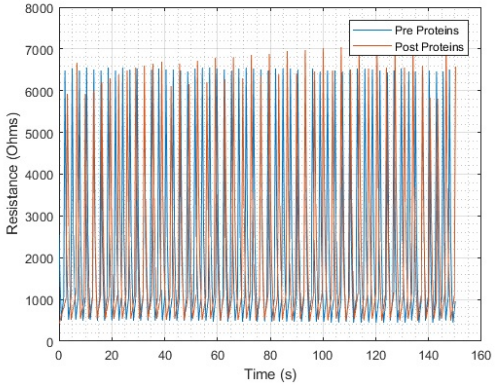

(b) Lysozyme Pre and Post Proteins: Test 1

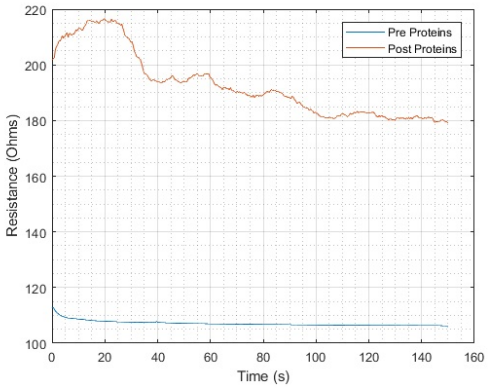

(c) Lysozyme Pre and Post Proteins: Test 2

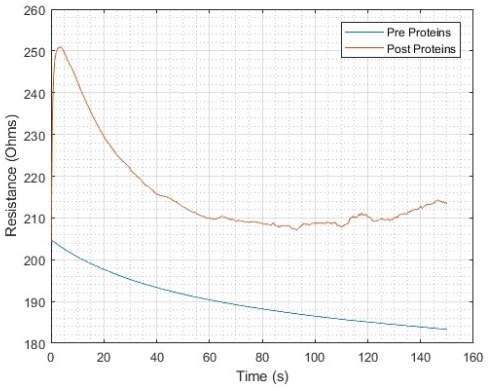

(d) Lysozyme Pre and Post Proteins: Test 3

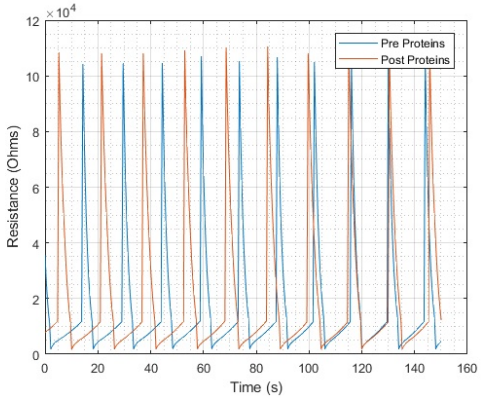

(e) Lysozyme Pre and Post Proteins: Test 4

Figure 8.1: Resistance over time of electrodes before and after the addition of lysozyme proteins. Tests are arranged in order across one row of electrodes.

Test 0 saw a periodic response with an increase in frequency post protein addition. The amplitudes remained similar. Comparison of the integrals over the period of evaluation determined an increase in resistance of approximately 13.32%.

Test 1 also saw periodic responses with an increase in frequency post protein addition. An increase of 4.16% was noted over the integration period, however, this may be understated owing to stabilisation occurring at the onset of the integration period.

Test 2 saw non-periodic responses. An increase in resistance of approximately 63.64% was noted at steady-state.

Test 3 also saw non-periodic responses. An approximate increase of 19.44% was noted at steady-state

Test 4 saw periodic responses with an increase in frequency post protein addition. Integration over the interval saw an increase in resistance of approximately 17.45%.

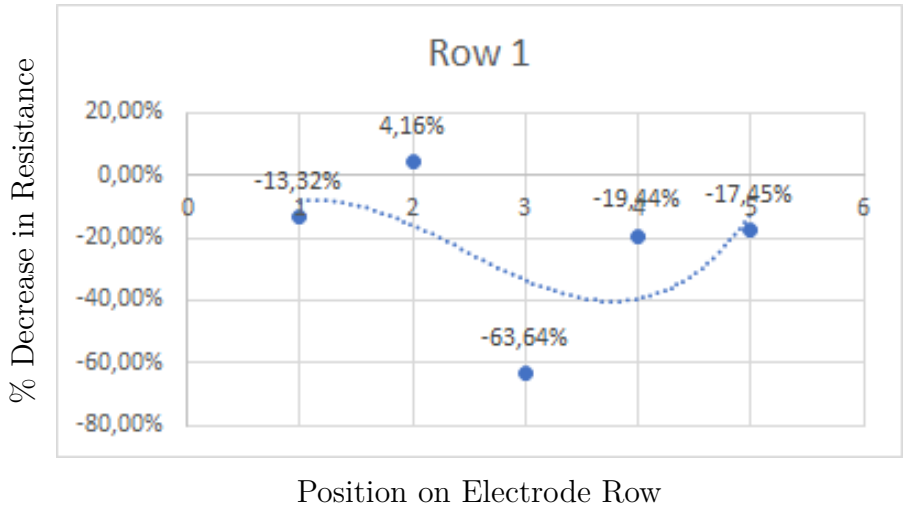

Figure 8.2: Lysozyme Pre and Post Proteins: Row 1. % Decrease in resistance across the electrode row.

At higher fibre density, the waveforms obtained are typically non-periodic. A large increase in resistance was noted where fibres were most dense. This increase decreased as fibre density decreased. Upon the responses becoming periodic, there seems to be a certain frequency below which the binding starts to increase resistance in response to decreasing frequency.

A plot of the % decrease in resistance corresponding to each electrode in row 1 can be seen in Figure 8.2.

8.2.2 Row 2

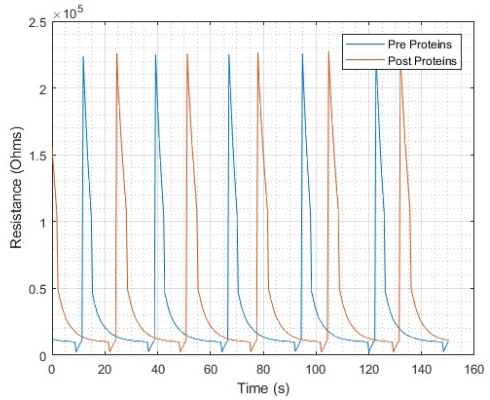

(a) Lysozyme Pre and Post Proteins: Test 5

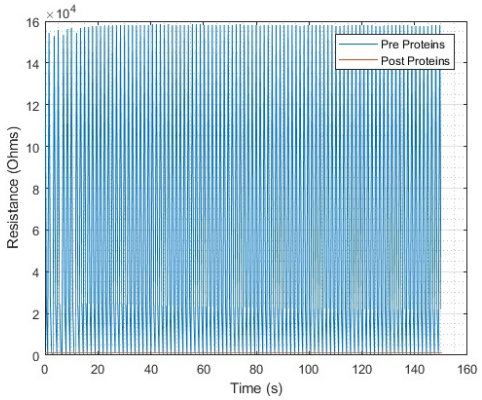

(b) Lysozyme Pre and Post Proteins: Test 6

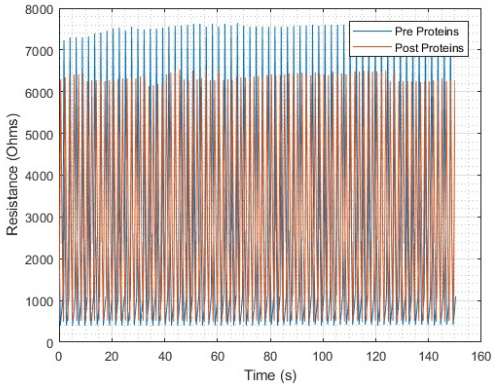

(c) Lysozyme Pre and Post Proteins: Test 7

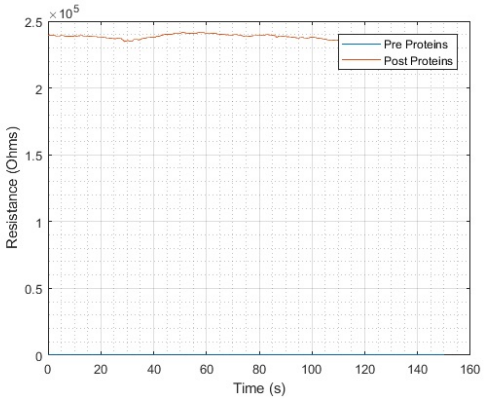

(d) Lysozyme Pre and Post Proteins: Test 8

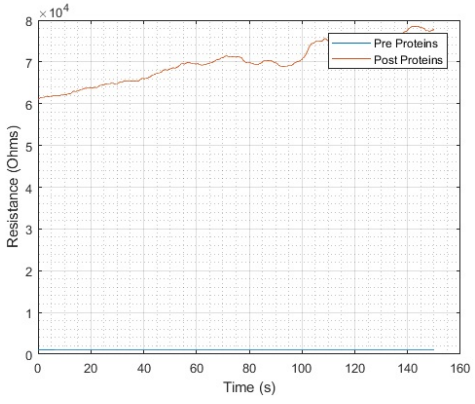

(e) Lysozyme Pre and Post Proteins: Test 9

Figure 8.3: Resistance over time of electrodes before and after the addition of lysozyme proteins. Tests are arranged in order across one row of electrodes.

Test 5 showed periodic responses with a decrease in frequency post protein addition. Integration over the evaluation period. While amplitude remained fairly unchanged, the change over the integration period showed an increase of approximately 18.51%.

Test 6 showed a change from periodic to non-periodic waveforms. Integration yielded a decrease in resistance of approximately 98.24%.

Test 7 showed relatively fast responses, with the frequency increasing from 0.5 Hz after protein addition. Integration yielded an overall increase of approximately 27.57%.

Test 8 showed non-periodic responses. The increase in resistance, however, was 117900%. Because of this drastic increase, it is believed that this electrode broke during testing.

Test 9 also showed non-periodic responses. The increase in resistance, however, was 12566.67%. Because of this drastic increase, it is believed that this electrode broke during testing.

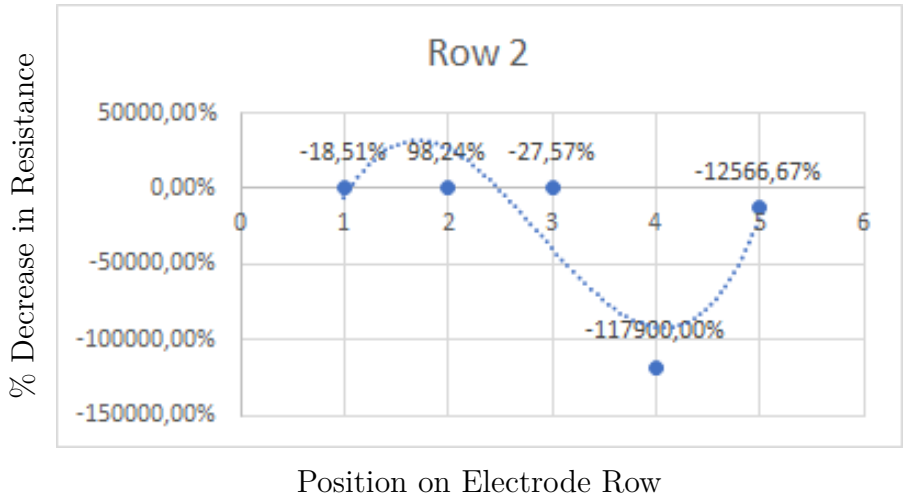

Figure 8.4: Lysozyme Pre and Post Proteins: Row 2. % Decrease in resistance across the electrode row.

The overall trend of the change in resistance seems to match that of the previous row (see section 8.3.1). The very large changes in tests 8 and 9, however, are cause for concern as they could indicate that these electrodes had broken, making the observed trend unreliable.

A plot of the % decrease in resistance corresponding to each electrode in row 2 can be seen in Figure 8.4.

8.2.3 Row 3

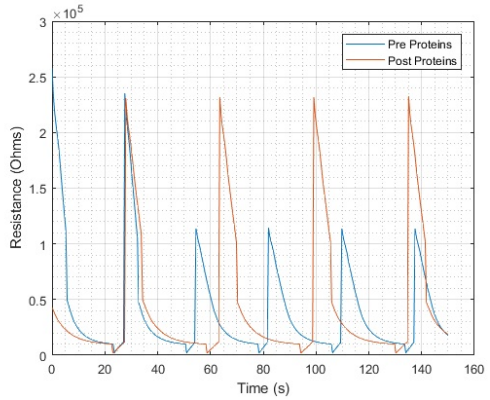

(a) Lysozyme Pre and Post Proteins: Test 10

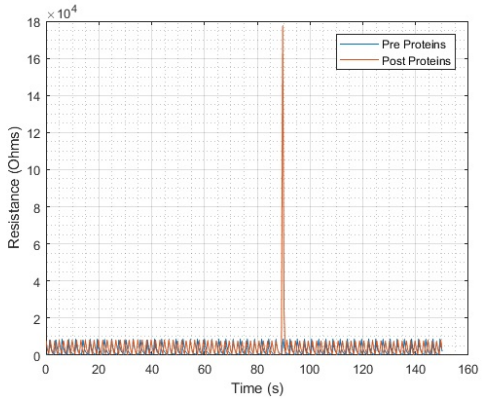

(b) Lysozyme Pre and Post Proteins: Test 11

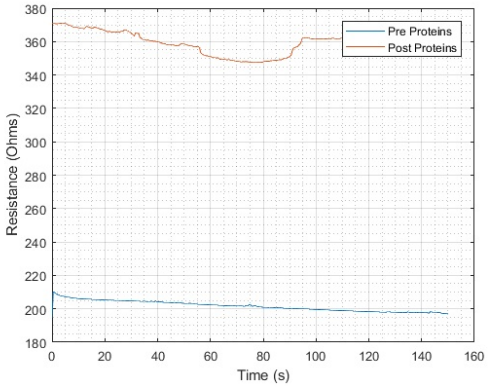

(c) Lysozyme Pre and Post Proteins: Test 12

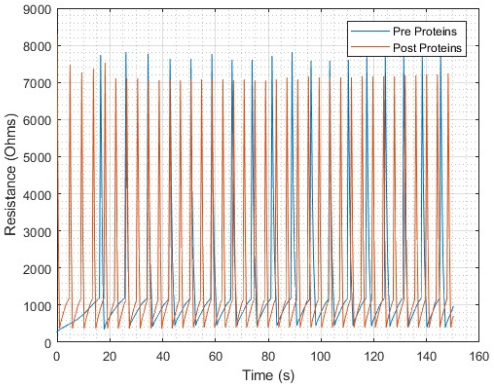

(d) Lysozyme Pre and Post Proteins: Test 13

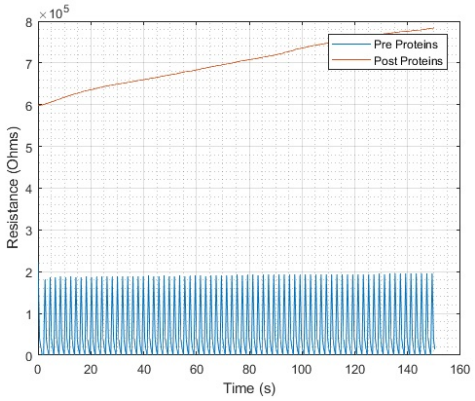

(e) Lysozyme Pre and Post Proteins: Test 14

Figure 8.5: Resistance over time of electrodes before and after the addition of lysozyme proteins. Tests are arranged in order across one row of electrodes.

Test 10 showed periodic responses with frequency falling slightly from approximately 0.04Hz. The amplitude of the functions also doubled, resulting in a large increase in resistance.

Test 11 showed periodic functions with increasing frequency from 0.375Hz. Integration yielded an increase of 57.34%.

Test 12 showed non-periodic functions. The increase in resistance noted at steady-state was approximately 85%.

Test 13 showed periodic responses with frequency increasing from 0.1125 Hz post protein addition. The overall increase determined by integration was approximately 17.21%. Stabilisation during the integration interval may have affected this result to a small degree.

Test 14 saw a non-periodic function become periodic. The percentage increase noted via comparison of the integrals over time, 1008.83%, would suggest that this electrode broke.

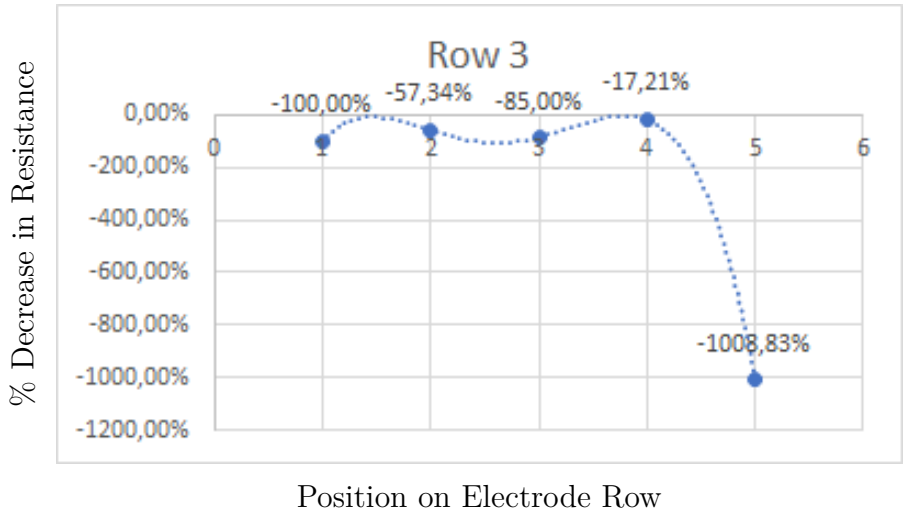

Figure 8.6: Lysozyme Pre and Post Proteins: Row 3. % Decrease in resistance across the electrode row.

Overall, the responses of all three rows seem to indicate a general pattern that can be described by a fourth-order polynomial. While no distinct values can be compared between electrodes, likely owing to the variance in the base electrodes, the general trend observed between rows suggests promise for further work, as discussed in Chapter 10.

A plot of the % decrease in resistance corresponding to each electrode in row 3 can be seen in Figure 8.6.

8.3 CD4 Analysis: Pre and Post Protein Addition

8.3.1 Row 1

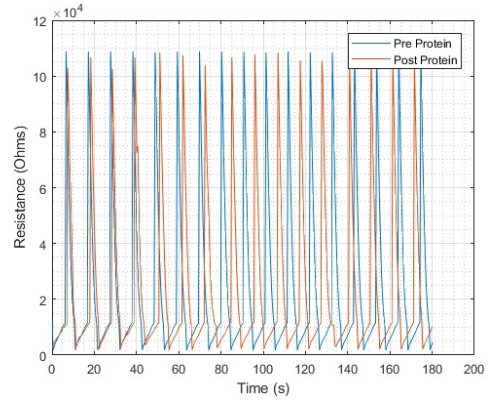

(a) CD4 Pre and Post Proteins: Test 0

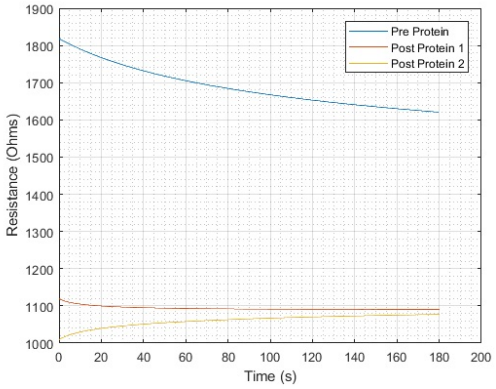

(b) CD4 Pre and Post Proteins: Test 1

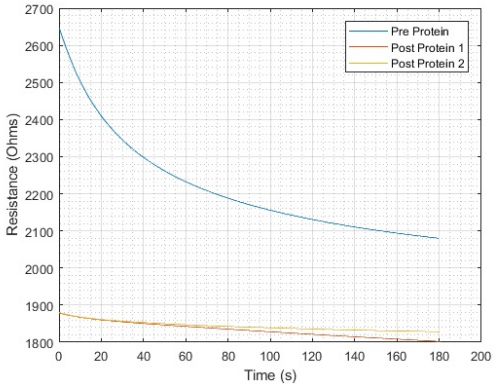

(c) CD4 Pre and Post Proteins: Test 2

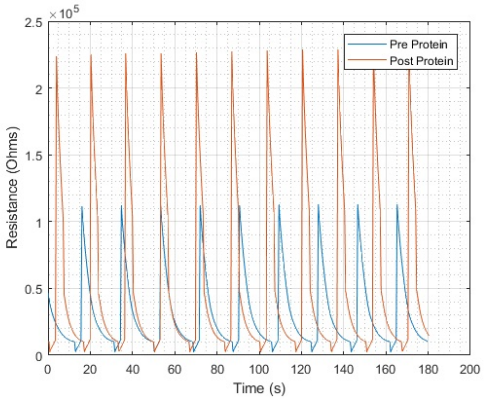

(d) CD4 Pre and Post Proteins: Test 3

Figure 8.7: Resistance over time of electrodes before and after the addition of CD4 proteins. Tests are arranged in order across one row of electrodes.

Test 0 saw periodic responses, with frequency increasing slightly post protein addition from approximately 0.1Hz. The amplitude of the signal decreased slightly, as can be seen in the above figure. An overall decrease in resistance of approximately 3.91% was noted when integrals over the period were compared.

Test 1 saw non-periodic responses whose magnitude at steady-state saw an overall decrease of 31.25%.

Test 2 also saw non-periodic responses. These saw a decrease of approximately 28% at steady-state.

Test 3 saw periodic responses, with frequency increasing from approximately 0.0677 Hz post protein addition. A large increase in amplitude was noted and integration yielded an overall increase of approximately 52.41%.

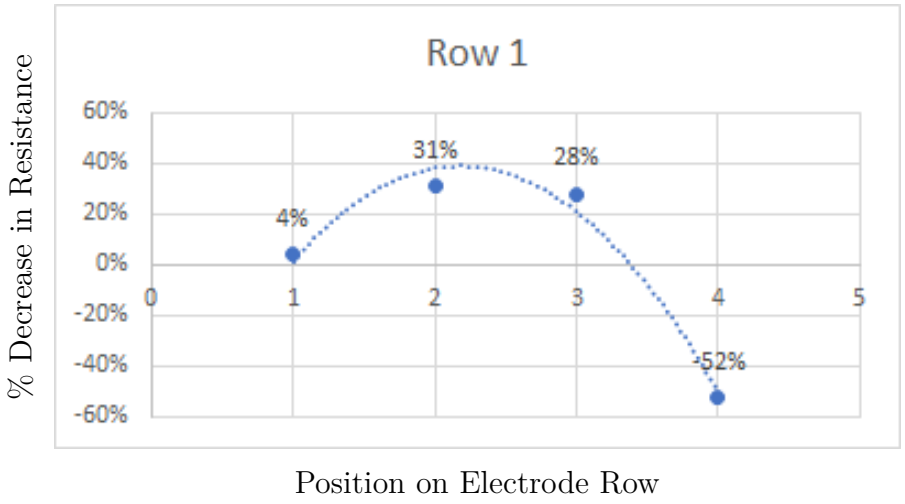

Figure 8.8: CD4 Pre and Post Proteins: Row 1. % Decrease in resistance across the electrode row.

Overall this row's output seemed to match a parabolic curve with decreasing change in magnitude corresponding to decreasing fibre density.

A plot of the % decrease in resistance corresponding to each electrode in row 1 can be seen in Figure 8.8.

8.3.2 Row 2

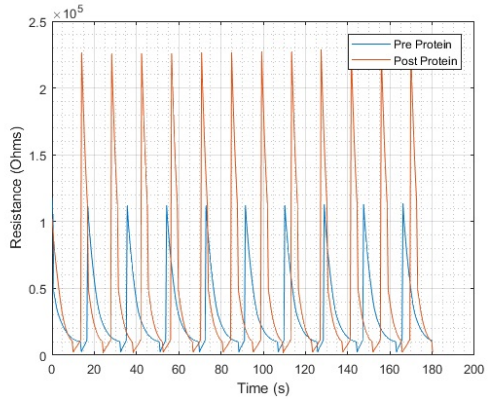

(a) CD4 Pre and Post Proteins: Test 4

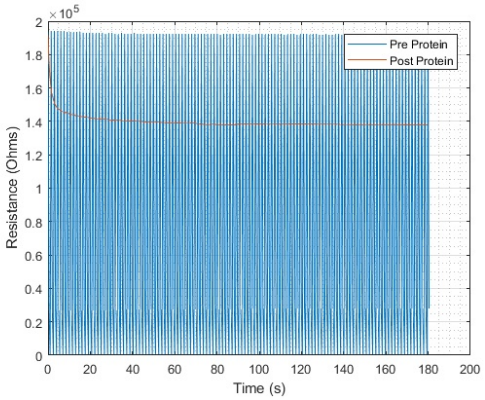

(b) CD4 Pre and Post Proteins: Test 5

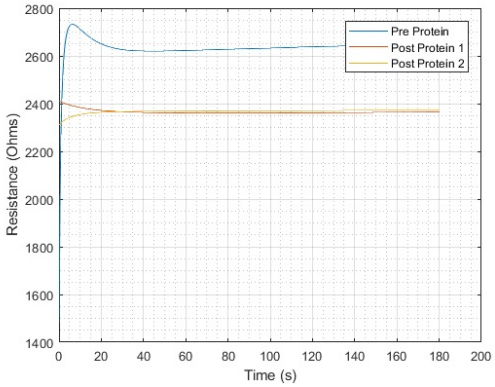

(c) CD4 Pre and Post Proteins: Test 6

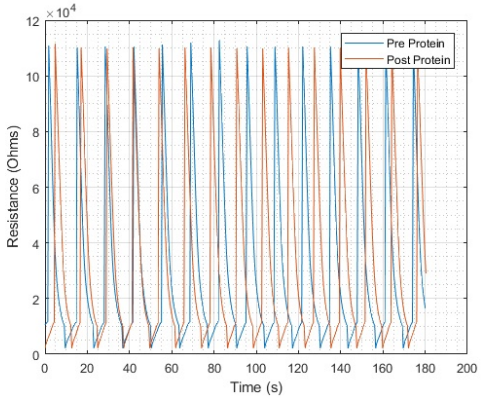

(d) CD4 Pre and Post Proteins: Test 7

Figure 8.9: Resistance over time of electrodes before and after the addition of CD4 proteins. Tests are arranged in order across one row of electrodes.

Test 4 saw periodic responses with response frequency increasing from approximately 0.0667 Hz post protein addition. A large increase in amplitude was noted, and integration yielded an overall increase in average resistance of 52.41%.

Test 5 saw a periodic function, at a frequency of approximately 0.7 Hz, become non-periodic post protein addition. The integral for the steady state result was determined in two ways, firstly, the *trapz* function, which included the variance caused by signal settling, and secondly, a conservative estimate of the steady-state value multiplied with the integration period. The average of the two results was compared to the integral of the periodic function, and an overall increase in resistance of approximately 86.47% was noted.

Test 6 saw non-periodic functions. The overall difference at steady state was a decrease in resistance of approximately 11.85%.

Test 7 saw periodic functions where the frequency increased slightly from approximately 0.1 Hz. The change in amplitude was similarly small, and integration determined that there was only approximately a 5.17% difference between the overall resistances.

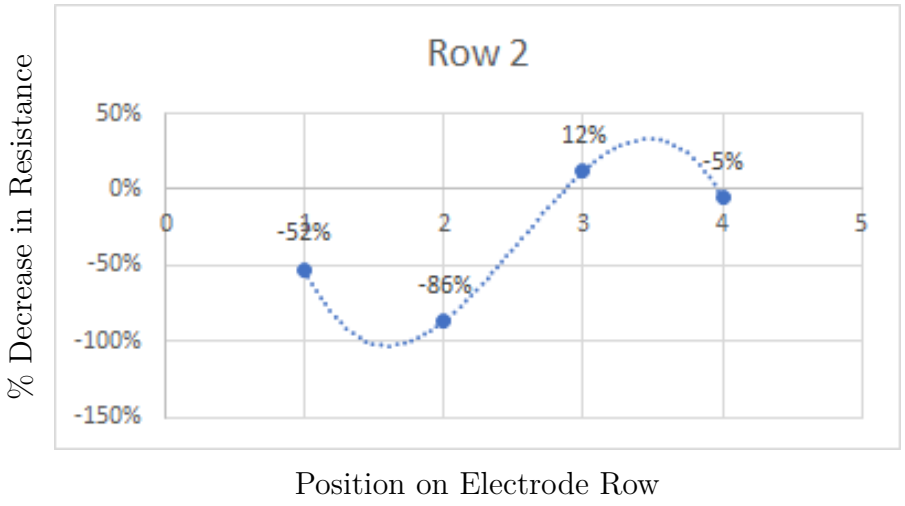

Figure 8.10: CD4 Pre and Post Proteins: Row 2. % Decrease in resistance across the electrode row.

Overall, the results from row 2 seem to correspond well to a 3rd order polynomial, much like some of the results pre and post antibody addition.

A plot of the % decrease in resistance corresponding to each electrode in row 2 can be seen in Figure 8.10.

8.3.3 Row 3

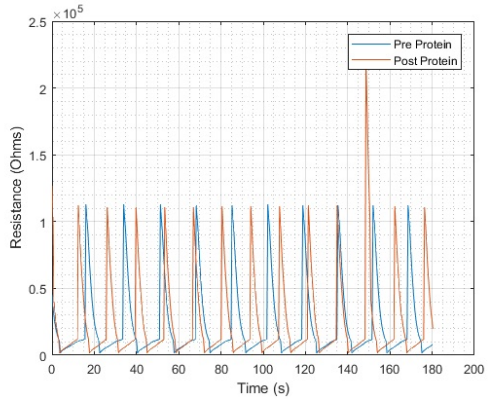

(a) CD4 Pre and Post Proteins: Test 8

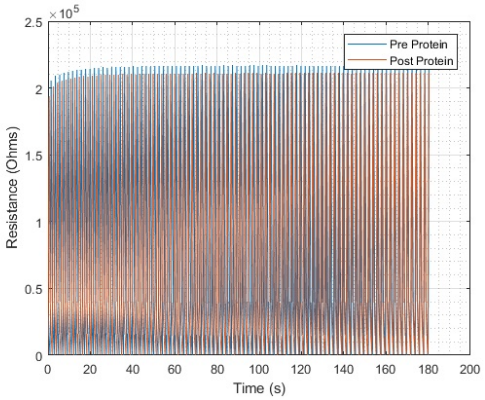

(b) CD4 Pre and Post Proteins: Test 9

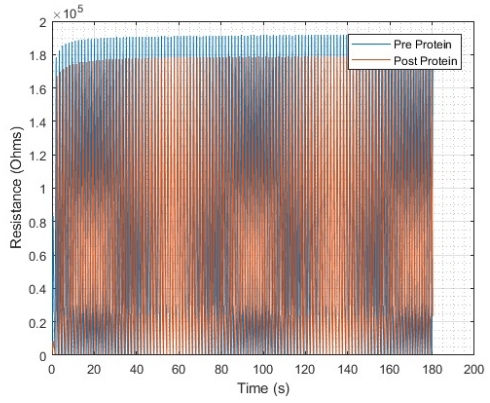

(c) CD4 Pre and Post Proteins: Test 10

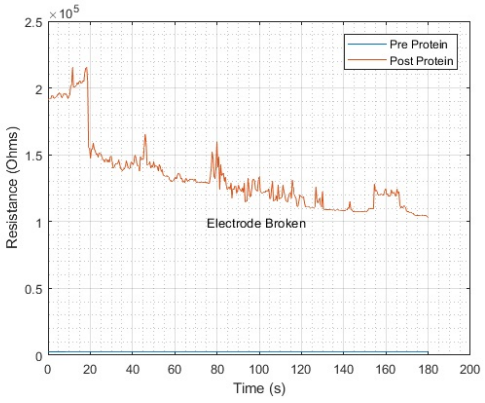

(d) CD4 Pre and Post Proteins: Test 11

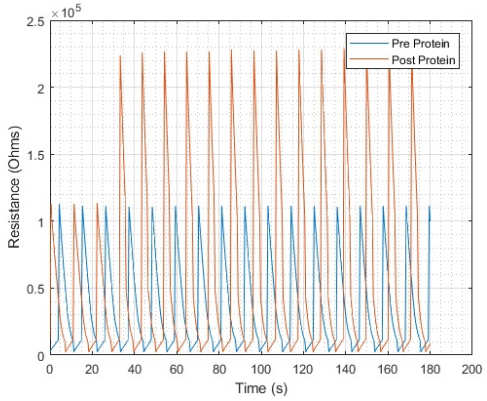

(e) CD4 Pre and Post Proteins: Test 12

Figure 8.11: Resistance over time of electrodes before and after the addition of CD4 proteins. Tests are arranged in order across one row of electrodes.

Test 8 found a periodic response, with a frequency of approximately 0.05 Hz, that increased in frequency after the addition of proteins. The amplitude of the signal decreased to an extent, however, an overall average increase in resistance of 10.93% was observed.

Test 9 found a periodic function with a frequency of approximately 0.5 Hz. After the addition of proteins, this function's frequency increased slightly while the amplitude decreased. Comparison of the integrals of the signals determined that there was an overall

decrease in resistance of approximately 1.64%. Test 10 saw a periodic function whose frequency (approximately 0.7 Hz) increased post protein addition. Similar to test 10, the function's amplitude decreased and integration found that there was an average decrease in resistance of 8.55%.

Test 11 found that the electrode had broken.

Test 12 found a periodic function that, like test 10, increased in frequency, in this case from approximately 0.0833 Hz. A significant increase in amplitude was noticed and the overall increase was approximately 109.09%.

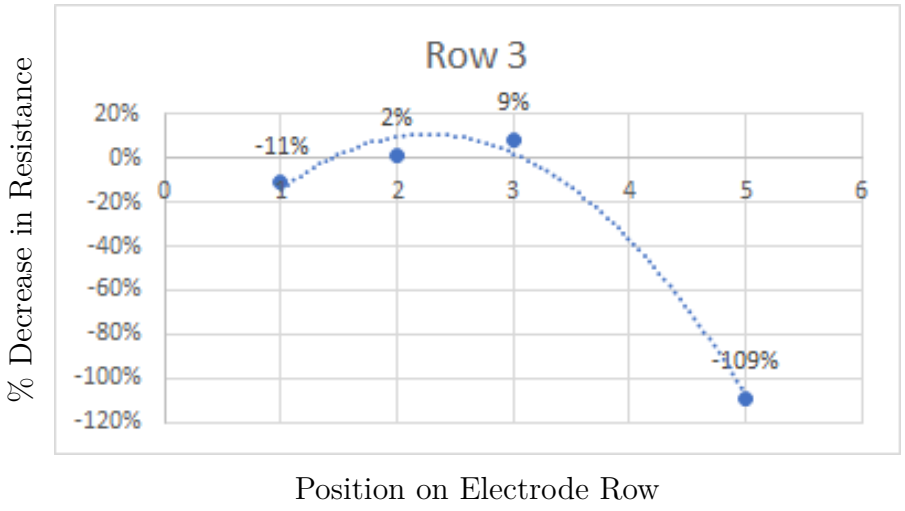

Figure 8.12: CD4 Pre and Post Proteins: Row 3. % Decrease in resistance across the electrode row.

The response from this row was, similar to row 1 (see section 8.5.1), parabolic in nature. The inflection point of the parabola here also lies where fibre density is largest.

A plot of the % decrease in resistance corresponding to each electrode in row 3 can be seen in Figure 8.12.

8.4 Discussion

The results obtained can, unfortunately, not be compared in terms of values as the values alone do not conform to a specific trend that could be used for quantification purposes. This is likely as a result of the varying nature of the electrodes themselves. It is thus imperative that, should this research be taken further, the electrode production procedure be optimised to produce far more reproducible results.

Nevertheless, two interesting things can be noted. The first is the periodic response observed. This response is clearly electrochemical in nature as the only external stimulus applied to the system is the low voltage at the probes of the electrodes. What is particularly interesting about this waveform is the fact that it is very similar to the action potential produced in neurons. Decreasing fibre density seems to correlate with increased periods for these waveforms. Binding events also seem to affect the frequency of these

responses, much like inhibitory and excitatory responses can affect the frequency of action potentials.

The second interesting observation concerns the general trend of the data sets. Such as they are, the responses from the row-by-row analysis seem to suggest a general response-curve that matches a specific pattern, namely that of a fourth-order polynomial. This polynomial typically sees the greatest change in one direction, be it increase or decrease in resistance, where the fibres are most dense and therefore provide a linear response. As the electrodes start to consist of lower fibre-density, the waveforms start to become periodic and the magnitude of the change starts to decay. As fibre density decreases, the periods of the waveforms also seem to increase. As this happens, the change eventually reaches an inflection point, after which the amount of change begins to increase in the other direction.

Chapter 9

Conclusion

In order to conclude this report, the initial aims, goals and objectives must be revisited, and the outcome of the research be compared to the aforementioned factors.

The aims and goals of the research were as follows:

1. produce intrinsically conductive nanofibres with a uniform diameter
2. produce sensors capable of producing a measurable change when exposed to CD4
3. plot the characteristic curves/trend lines and establish the relationship between increasing antibody concentrations and resistance.

The research objectives were:

i to determine the effect of a lower molecular-weight PEO on fibre production to investigate the effect of increasing amounts of PEO on the solution to investigate the effect of fibre alignment on mat conductivity

ii to adhere fibres directly to inter-digitated electrodes, thus forming resistive elements to design and produce resistive-sensing electronics

These electronics would need to mitigate noise

iii to analyse variance and establish trend-lines from the obtained data sets

In terms of producing intrinsically conductive nanofibres with a uniform diameter, this thesis was successful. As documented in this report (see Chapter 4), nanofibres of approximately 100 to 300 nm in diameter were consistently produced via the electrospinning method. The effect of using a lower molecular weight PEO was discussed, and the results of increasing amounts of PEO in the electrospinning solution was documented (see Chapter 5). Lastly, the effect of aligning fibres on mat conductivity was noted and discussed.

With respect to producing sensors capable of producing a measurable change when exposed to CD4, this thesis was largely successful. Fibres were successfully adhered directly to inter-digitated electrodes to form the necessary base resistive elements necessary for this thesis. Furthermore, the necessary functionalisation and immobilisation steps were carried out and proven to have taken place successfully. Additionally, the final electrodes'

resistance responded to the addition of the CD4 protein. Additional tests with lysozyme and anti-lysozyme antibodies yielded similar results. Resistive sensing electronics were designed, but not produced. The design implemented noise-cancellation techniques, however, it was not employed owing to the unexpected discovery of periodic responses from many of the electrodes. The electronics were designed under the assumption that a simple DC response would be observed, and were as such, not suited towards measuring these periodic signals.

Plotting the characteristic curves and or trend lines and establishing a relationship between increasing CD4 antibody concentrations and their reaction to protein stimulus was only partially successful. While the data was plotted and compared, no distinct trend emerged from the data, apart from the fact that the presence of proteins did indeed result in a change in base resistance. While no finite trend could be established, the data did suggest a polynomial trend corresponding to magnitude of change with respect to fibre density and periodic response frequency.

In this thesis, nanofibre-based sensors were produced that were sensitive to the presence of the desired antigen. While there is no definite trend obtainable from the data owing largely to base variances in the electrodes, the fact that there is indeed a response when the desired analyte is introduced to the system is promising. In terms of cost-effectivity, this thesis made use of a paper-substrate. The amount of materials used was very low, and, as a whole, the sensors were produced very cheaply. While there is room for further work to be done on this subject, this thesis has achieved its specified goals.

Chapter 10

Recomendations for Further Research

Most of the problems encountered in this research related to the lack of reproducibility between the different electrodes. A number of steps can be implemented to to address this problem in future research.

Firstly, use mechanical clamps to hold the electrode sheets down onto the rotating mandrel. To secure the electrode sheets, this thesis made use of double-sided tape. The tape could not withstand the cumulative effect of rotating at 15 000 rpm and would come loose after approximately 15 minutes of spinning. Consequently, spin time was limited to 15 minutes. A mechanical clamp would allow for a longer spin time, which, in turn would allow for a greater degree of fibre deposition on the electrode sheets. With sufficient spin time, after-rinsing, the electrodes should all have the same degree of fibre coverage.

A second suggestion is to affix the fluid-ejecting needle onto a linear actuator. Using a linear actuator to move the needle from one end of the mandrel to the other could result in even fibre thicknesses as the centre of the normal distribution that the ejected fibres follow would move along with the needle.

A third suggestion is to employ a multi-needle approach. Using multiple needles could serve to increase the amount of fibre deposition occurring at one time. If this were to be implemented, the effect on the electrostatic environment within the electrospinner would need to be considered as multiple charged needles would likely affect the distribution of the fibres.

Another recommendation for further research on this topic would be the use of PAMAM dendrimers. PAMAM dendrimers could be employed as an intermediary in the crosslinking stage of electrode development. These dendrimers would drastically increase the number of binding sites available for antibodies to bind to. This could help to ensure that there is a sufficient number of antibodies to bind to all conceivable available proteins. That being said, the spatial ramifications of using these dendrimers would need to be considered. The size of CD4+ cells could mean that binding to one dendrimer might prevent other cells from also binding.

Further research should also endeavour to make use of actual CD4+ cells. While this report used CD4 proteins for proof of concept, it is believed that the use of cells could have a much larger impact on overall resistance owing to the size difference between the CD4 proteins and the cells themselves.

Another topic that should be investigated is changing PVA concentrations and seeing what effect it has on conductivity both pre and post functionalisation with APTES.

Appendices

Appendix A

Solution Experiments

	A	B	C	D
1	Date	Actions	Findings/Discussion	Notes
2	2017/07/20	Mixed PEI and PEDOT:PSS	Dropped out of solution	
3			Cannot mix and spin together	
4				
5	2017/08/25	Test Sweep	Most stable at end parameters	
6		5%PVA in H2O (DI)		
7		15kV (start) - 20kV (end)		
8		10cm (start) - 8cm (end)		
9		2ml		
10		0.8ml/h (start) - 1.2ml/h (end)		
11		15G needle		
12				
13	2017/08/28	Test Sweep	Most stable at end parameters	
14		5%PVA in H2O (DI)		
15		15kV (start) - 12.54kV (end)		
16		5cm		
17		15G needle		
18		0.8ml/h (start) - 0.68ml/h (end)		
19				
20	2017/08/30	Test Sweep	Most stable at end parameters	
21		10% PVA in H2O (DI)		
22		15kV (start) - 23.5kV (end)		
23		10cm		
24		15G needle		
25		0.8ml/h (start) - 1.35ml/h (end)		
26				
27	2017/08/30	Test Sweep	Most stable at end parameters	
28		10% PVA in H2O (DI)		
29		15G needle		
30		15kV		
31		5cm		
32		0.8ml/h (start) - 1.2 ml/h (end)		
33				
34	2017/09/04	25% PEI in H2O (DI)	No nanofibers - fibers only in micrometer range	
35		(1ml water in 1 ml 50%PEI solution)		
36		15G needle		
37		5cm		
38		0.2ml/h		
39				
40	2017/09/04	12.5% PEI in H2O (DI)	No success	
41		(2ml water in 50%PEI solution)		
42		15G needle		
43		10kV		
44		5cm		
45		0.2ml/h		
46				
47	2017/09/30	PEDOT:PSS:PEO:DMF (Batch 1) 2.56:0.067:0.345 (APPROX)	Balance not yet found	
48		15G needle	Potential Problems:	
49		8.5kV - swept up to 20kV	imperfect mix ratio (scale not sensitive enough)	Scale used has divisions of 0.1g - also large degree of error
50		0.2ml/h swept up to 3ml/h	mixer heated causing evaporation	
51		10cm swept down to 8cm	PEO MW = 600 000 not 900 000	
52			15G needle not 21G	
53				
54	2017/10/20	1ml Batch 1 + 0.25ml DMF	Produced some nanofibers	
55		10cm		
56		8.5kV		

	A	B	C	D
1	Date	Actions	Findings/Discussion	Notes
57		0.8ml/h		
58				
59	2017/10/23	Batch 1	No success	
60		15G needle		
61		15kV		
62		0.8ml/h		
63		10cm		
64				
65		1.5g Batch 1 + 0.1g DMF	Fibers not depositing on SC	
66		15G needle	Formed "trees" growing off SC towards needle	Charged environment caused fibres to coallesce in branch-like structures
67		15kV		
68		0.8ml/h		
69				
70	2017/10/28	PEDOT:PSS:PEO:DMF (Batch 2) 2.56:0.067:0.345 (APPROX)	Formed trees	Scale used has divisions of 0.1g - also large degree of error
71		9kV	Sprays (some droplets form)	
72		0.1ml/h	no proper taylor cone	
73		15G needle	perhaps PEO too low?	
74		10cm	perhaps voltage too low?	
75				
76	2017/11/02	Batch 2	no trees	
77		20kV	fairly even deposition - some spray	
78		5.7ml/h	deposited onto surroundings too	
79		15G needle	cone sometimes unstable	
80		10cm		
81				
82	2017/11/09	Mix made at POLSCI: 2.56:0.067:0.345 (Accurate)	Found quite stable at	NOTES on POLSCI MIX:
83		Test Sweep	14kV	kept under agitation
84		5pm-7:30pm	1.3-1.5ml/h	sealed to prevent evaporation resulting in water loss
85		8.5kV (start)	trees	accurate owing to appropriately sensitive scale
86		0.2ml/h(start)		
87		21G needle		
88		10cm		
89				
90				
91	2017/11/15	POLSCI mix	No trees	
92		8.5kV	drops formed (wastage)	
93		0.2ml/h	maybe a higher deposition rate? Try increasing voltage	
94		10cm	rough surface formed	
95		21G	perhaps more PEO or DMF?	
96		3pm-6:30pm		
97				
98	2017/11/20	POLSCI mix	similar number of drops as before	
99		10cm	no trees	
100		21G		
101		0.2ml/h		
102		13:45 - 14:15		
103		0.2ml/h		
104		voltage from 8 -13kV		
105				
106	2017/11/20	POLSCI mix	fewer drops	
107		10cm	no trees	

	A	B	C	D
1	Date	Actions	Findings/Discussion	Notes
108		15G	rough surface	
109		14:15-14:45		
110		0.2ml/h		
111		11kV		
112				
113	2017/11/20	POLSCI mix	microfibers forming	
114		5cm		
115		15G		
116		15:00-15:20		
117		0.3ml/h		
118		8.5kV		
119				
120	2017/11/24	10cm	small trees formed that collapse	
121		90wt% POLSCI mix	increased dopant likely caused increased sensitivity to field	
122		10wt% DMF		
123		0.3ml/h		
124		10kV		
125		15G		
126		14:00-15:30		
127				
128				
129	2018/02/15	PEDOT:PSS:PVA:PEO: 98:1:1		
130		Too Viscous		
131				
132	2018/02/19	PEDOT:PSS:DMF:PEO: 2.56:0.067:0.345	trees	
133		RH 22%	no drops	
134		10cm	small amount of spraying	
135		22G needle		
136		0.2ml/h		
137		8.5kV		
138				
139				
140	2018/02/19	PEDOT:PSS:PVA:PEO: 99:0.5:0.5		
141		added 5wt% DMSO		
142		15kV		
143		0.2ml/h		
144		25G needle		
145		22% RH		
146		Spraying and spinning		
147				
148	2018/02/19	PEDOT:PSS:PEO:DMF: 2.56:0.075:0.345		
149		Too viscous		
150				
151	2018/02/20	PEDOT:PSS:PEO:DMF: 2.56:0.07:0.345		Primary Mix
152		15kV		
153		10cm		
154		30%RH		
155		trees		
156		0.1ml/h		
157		some drops form		
158		continuous		
159				
160				
161	2018/07/25	Primary Mix		Desirable nanofibres

	15kV		
	10cm		
	15000rpm		
	0.9ml/h		
	20%RH		
2018/11/05	PEDOT:PSS:DMF:PEO:PVA		Final Fibre Solution
	2.56:0.35:0.07:0.005		
	15kV		
	10cm		
	15000rpm		
	0.9ml/h		
	20%RH		

Appendix B

Circuit Diagrams

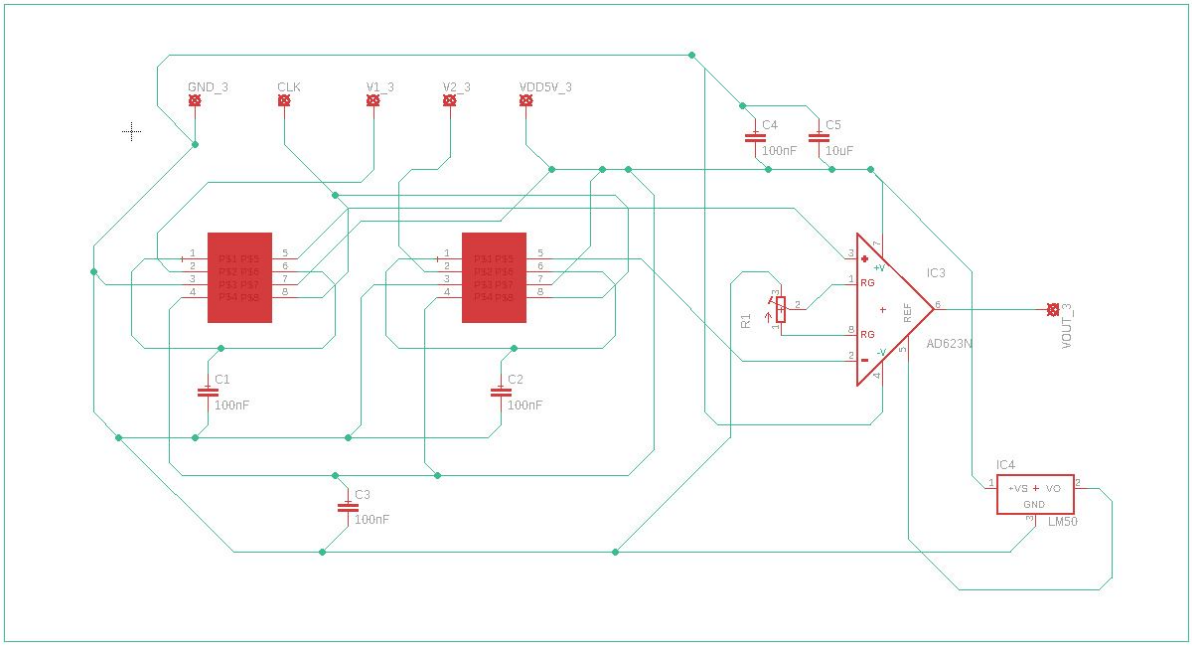

Figure B.1: Filtration and Amplification Sub-circuit

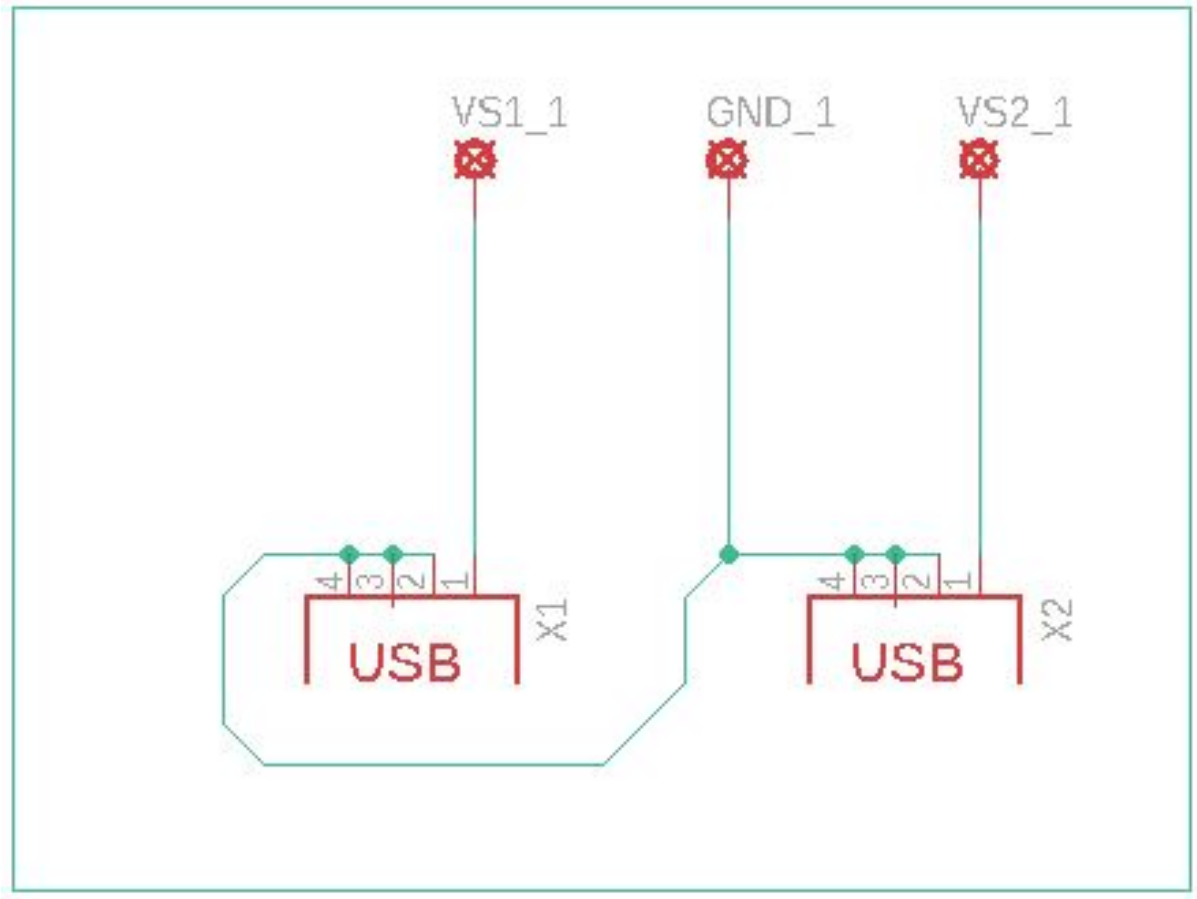

Figure B.2: Sensor Attachment Sub-Circuit

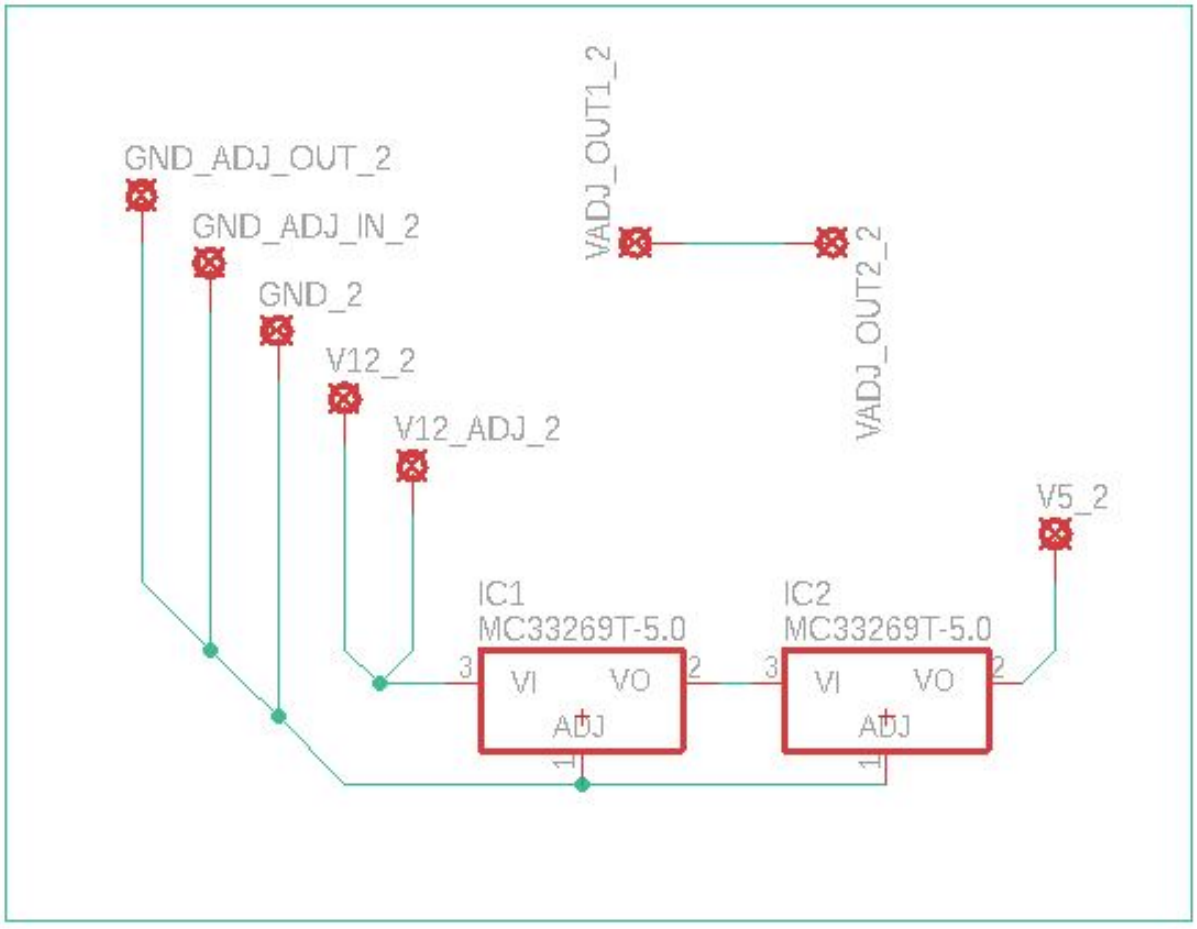

Figure B.3: Power and Voltage Supply Sub-circuit

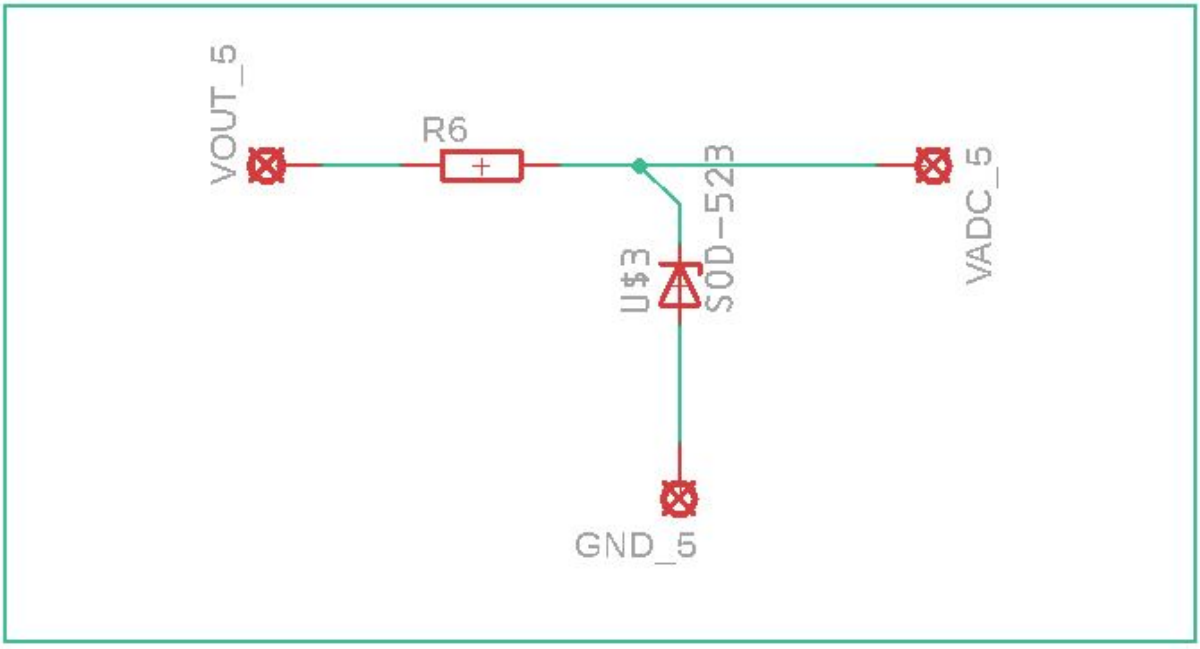

Figure B.4: Voltage Clamp Sub-circuit

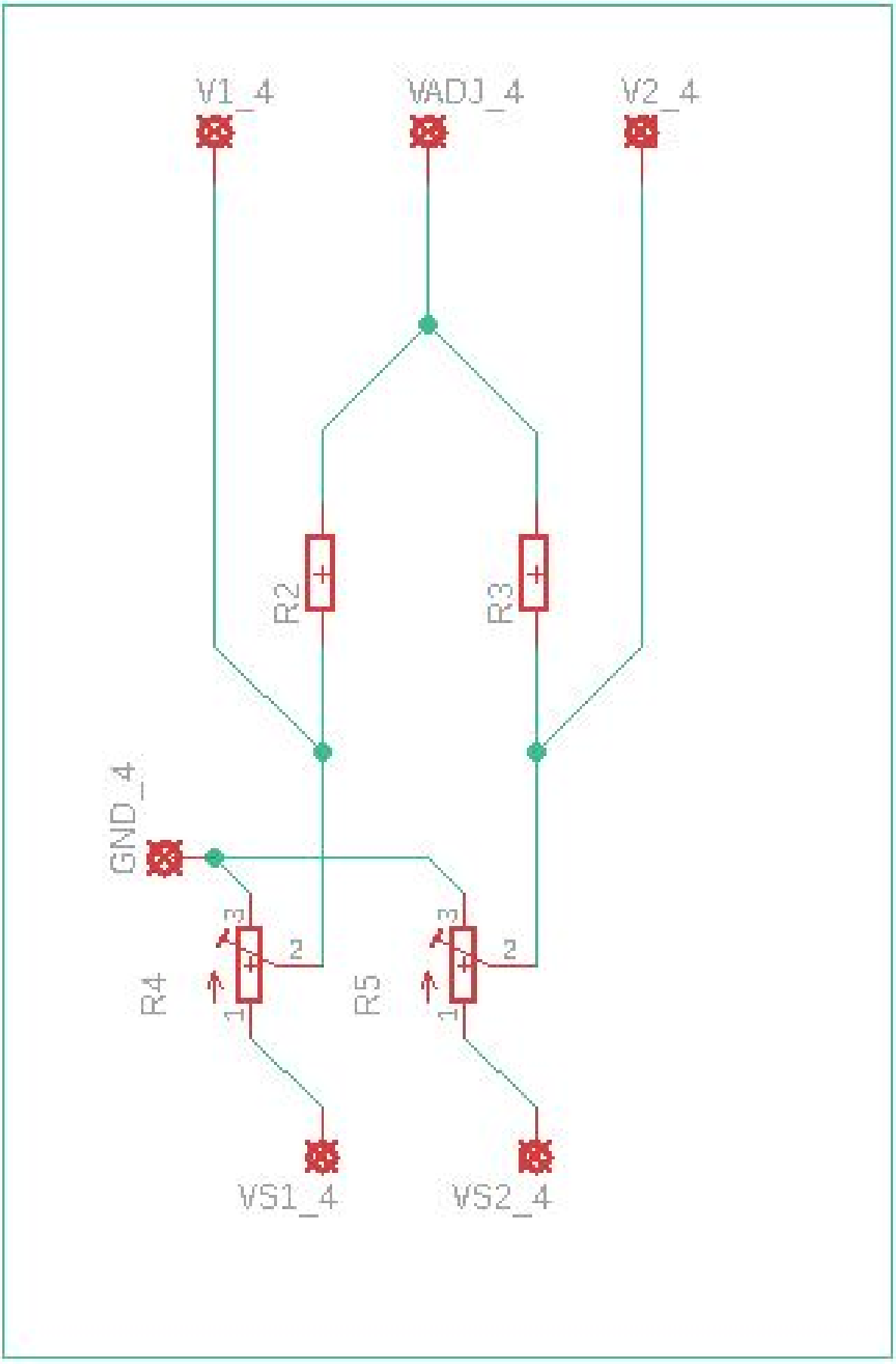

Figure B.5: Resistive Bridge Sub-circuit

Appendix C

Data Sheets

abcam

Product datasheet

Recombinant human CD4 protein ab167756

2 Images

Overview

Product name	Recombinant human CD4 protein
Protein length	Protein fragment

Description

Nature	Recombinant
Source	HEK 293 cells
Amino Acid Sequence	
Accession	P01730
Species	Human
Sequence	KKVVLGKKGDTVELTCTASQKKSIQFHWKNSNQIKILG NQGSFLTKGPSK LNDRADSRRSLWDQGNFPLIIKNLKIEDSDTYICEVEDQ KEEVQLLVFGL TANSDTHLLQGQSLTLTLESPPGSSPSVQCRSPRGKNI QGGKTLSVSQLE LQDSGTWTCTVLQNQKKVEFKIDIVVLAFQKASSIVYK KEGEQVEFSFPL AFTVEKLTGSGELWWQAERASSSKSWITFDLKNKEV SVKRVTQDPKLQMG KKLPLHLTLPQALPQYAGSGNLTLALEAKTGKLHQEVN LVVMRATQLQKN LTCEVWGPTSPKLMLSLKLENKEAKVSKREKAVWVL NPEAGMWQCLLSDS GQVLLESNIKVLPTW
Molecular weight	68 kDa including tags
Amino acids	26 to 390
Additional sequence information	Recombinant Human CD4 Protein fused with Fc fragment of human IgG1 at the C-terminus

Specifications

Our Abpromise guarantee covers the use of **ab167756** in the following tested applications.

The application notes include recommended starting dilutions; optimal dilutions/concentrations should be determined by the end user.

Biological activity	Measured by its ability to bind with HIV-1 gp120 in a functional ELISA.

Applications	Functional Studies SDS-PAGE ELISA
Endotoxin level	< 1.000 Eu/µg
Purity	> 98 % SDS-PAGE. ab167756 is lyophilized from 0.22 µm filtered solution.
Form	Lyophilised

Preparation and Storage

Stability and Storage	Shipped at 4°C. Store at +4°C short term (1-2 weeks). Upon delivery aliquot. Store at -20°C or -80°C. Avoid freeze / thaw cycle. pH: 7.00 Constituents: 5% Trehalose, 0.75% Glycine, 0.61% Tris This product is an active protein and may elicit a biological response in vivo, handle with caution.
Reconstitution	It is recommended to reconstitute the lyophilized protein in sterile deionized water. Solubilise for 30 to 60 minutes at room temperature with occasional gentle mixing. Carrier protein (0.1% HSA or BSA) is strongly recommended for further dilution and long term storage.

General Info

Function	Accessory protein for MHC class-II antigen/T-cell receptor interaction. May regulate T-cell activation. Induces the aggregation of lipid rafts.
Sequence similarities	Contains 3 Ig-like C2-type (immunoglobulin-like) domains. Contains 1 Ig-like V-type (immunoglobulin-like) domain.
Post-translational modifications	Palmitoylation and association with LCK contribute to the enrichment of CD4 in lipid rafts.
Cellular localization	Cell membrane. Localizes to lipid rafts. Removed from plasma membrane by HIV-1 Nef protein that increases clathrin-dependent endocytosis of this antigen to target it to lysosomal degradation. Cell surface expression is also down-modulated by HIV-1 Envelope polyprotein gp160 that interacts with, and sequesters CD4 in the endoplasmic reticulum.

Images

abcam

Product datasheet

Anti-CD4 antibody ab203034

★★★★☆ 2 Abreviews 1 References 6 Images

Overview

Product name	Anti-CD4 antibody
Description	Rabbit polyclonal to CD4
Host species	Rabbit
Tested applications	**Suitable for:** WB, IHC-P
Species reactivity	**Reacts with:** Rat, Human **Predicted to work with:** Pig ⚠
Immunogen	Synthetic peptide within Rat CD4 aa 420-457 conjugated to keyhole limpet haemocyanin. The exact sequence is proprietary. Sequence: RCRHQQRQAARMSQIKRLLSEKKTCQCSHRMQKSHN LI Database link: P05540 Run BLAST with Run BLAST with
Positive control	IHC-P: Human colon carcinoma, rat kidney, human kidney and rat lung tissues. WB: CD4 recombinant protein; Raji cell lysate.

Properties

Form	Liquid
Storage instructions	Shipped at 4°C. Store at +4°C short term (1-2 weeks). Upon delivery aliquot. Store at -20°C long term. Avoid freeze / thaw cycle.
Storage buffer	Preservative: 0.09% Sodium azide Constituents: 50% Glycerol, 1% BSA
Purity	Protein A purified
Clonality	Polyclonal
Isotype	IgG

Applications

Our Abpromise guarantee covers the use of **ab203034** in the following tested applications.

The application notes include recommended starting dilutions; optimal dilutions/concentrations should be determined by the end user.

Application	Abreviews	Notes
WB		1/100 - 1/1000. Predicted molecular weight: 51 kDa.
IHC-P		1/100 - 1/500. Perform heat mediated antigen retrieval with citrate buffer pH 6 before commencing with IHC staining protocol. When using a fluorescent probe the recommended dilution is 1/50 – 1/200.

Target

Function	Accessory protein for MHC class-II antigen/T-cell receptor interaction. May regulate T-cell activation. Induces the aggregation of lipid rafts.
Sequence similarities	Contains 3 Ig-like C2-type (immunoglobulin-like) domains. Contains 1 Ig-like V-type (immunoglobulin-like) domain.
Post-translational modifications	Palmitoylation and association with LCK contribute to the enrichment of CD4 in lipid rafts.
Cellular localization	Cell membrane. Localizes to lipid rafts. Removed from plasma membrane by HIV-1 Nef protein that increases clathrin-dependent endocytosis of this antigen to target it to lysosomal degradation. Cell surface expression is also down-modulated by HIV-1 Envelope polyprotein gp160 that interacts with, and sequesters CD4 in the endoplasmic reticulum.

Images

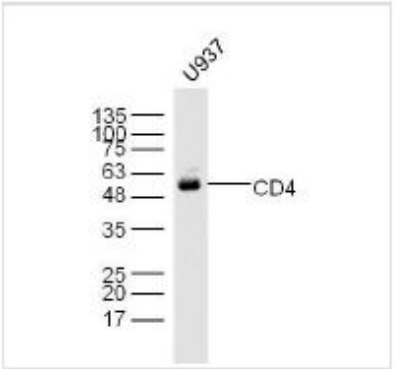

Western blot - Anti-CD4 antibody (ab203034)

Anti-CD4 antibody (ab203034) at 1/300 dilution + U937 Cell Lysate at 40 µg

Secondary

IRDye800CW Goat Anti-Rabbit IgG at 1/20000 dilution

Predicted band size: 51 kDa

Observed band size: 55 kDa

why is the actual band size different from the predicted?

Bibliography

[1] World Health Organisation, "Global Framework for Development & Stewardship to Combat Antimicrobial Resistance - Draft Roadmap", 2017.

[2] Pan American Health Organization, "Antimicrobial Resistance", PAHO, Tech. Rep. April, 2012, pp. 1–5.

[3] F. C. Tenover and J. E. McGowan, "Reasons for the emergence of antibiotic resistance", *The American Journal of the Medical Sciences*, vol. 311, no. 1, pp. 9–16, 1996, ISSN: 0002-9629. DOI: 10.1097/00000441-199601000-00003.

[4] R. Gaynes, "Antibiotic Resistance in ICUs: A Multifaceted Problem Requiring a Multifaceted Solution", *Infection Control and Hospital Epidemiology*, vol. 16, no. 6, pp. 328–330, 1995.

[5] J. M. Hamilton-Miller, "Antibiotic resistance from two perspectives: Man and microbe", *International Journal of Antimicrobial Agents*, vol. 23, no. 3, pp. 209–212, 2004, ISSN: 09248579. DOI: 10.1016/j.ijantimicag.2003.12.001.

[6] WHO. (2017). WHO | Global action plan on HIV drug resistance 2017 to 2021, [Online]. Available: http://www.who.int/hiv/pub/drugresistance/hivdr-action-plan-2017-2021/en/ (visited on 03/26/2018).

[7] W. C. Woodward. (1999). Can you explain AIDS and how it affects the immune system? How does HIV become AIDS? - Scientific American, [Online]. Available: https://www.scientificamerican.com/article/can-you-explain-aids-and/ (visited on 03/26/2018).

[8] D. R. Thévenot *et al.*, "Electrochemical biosensors: recommended definitions and classification", *Biosensors and Bioelectronics*, vol. 16, no. 1-2, pp. 121–131, Jan. 2001, ISSN: 0956-5663. DOI: 10.1016/S0956-5663(01)00115-4.

[9] J. Tang *et al.*, "CD4:CD8 lymphocyte ratio as a quantitative measure of immunologic health in HIV-1 infection: findings from an African cohort with prospective data.", *Frontiers in microbiology*, vol. 6, p. 670, 2015, ISSN: 1664-302X. DOI: 10.3389/fmicb.2015.00670.

[10] National Institute of Allergy and Infectious Diseases. (2018). Definition of Terms, Antimicrobial (Drug) Resistance | NIH: National Institute of Allergy and Infectious Diseases, [Online]. Available: https://www.niaid.nih.gov/research/antimicrobial-resistance-definitions (visited on 03/27/2018).

[11] Centers for Disease Control and Prevention. (2014). CDC Year in Review: Mission: Critical | CDC Online Newsroom | CDC, [Online]. Available: https://www.cdc.gov/media/releases/2014/p1215-2014-year-in-review.html.

[12] ——, (2016). What CDC is Doing: AR Solutions Initiative | Antibiotic/Antimicrobial Resistance | CDC, [Online]. Available: https://www.cdc.gov/drugresistance/solutions-initiative/index.html (visited on 03/28/2018).

[13] M. Lipsitch and M. H. Samore, "Antimicrobial Use and Antimicrobial Resistance: A Population Perspective", *Emerging Infectious Diseases @BULLET*, vol. 8, no. 4, 2002.

[14] A. Sageman, "Antibiotic Resistance Mechanisms, Problems, and Solutions",

[15] T. Saga and K. Yamaguchi, "History of Antimicrobial Agents and Resistant Bacteria", *JMAJ*, vol. 52, no. 522, pp. 103–108, 2009.

[16] A. Mack *et al.*, *Antibiotic resistance: implications for global health and novel intervention strategies: workshop summary*. National Academies Press, 2011.

[17] WHO. (2017). The world is running out of antibiotics, WHO report confirms, [Online]. Available: http://www.who.int/mediacentre/news/releases/2017/running-out-antibiotics/en/.

[18] S. A. Billstein, "How the Pharmaceutical Industry Brings an Antibiotic Drug to Market in the United States", *ANTIMICROBIAL AGENTS AND CHEMOTHERAPY*, pp. 2679–2682, 1994.

[19] A. Tran-Dien *et al.*, "Early transmissible ampicillin resistance in zoonotic Salmonella enterica serotype Typhimurium in the late 1950s: a retrospective, whole-genome sequencing study", *The Lancet Infectious Diseases*, vol. 18, no. 2, pp. 207–214, Feb. 2018, ISSN: 14733099. DOI: 10.1016/S1473-3099(17)30705-3.

[20] MedlinePlus. (2018). Immune response: MedlinePlus Medical Encyclopedia, [Online]. Available: https://medlineplus.gov/ency/article/000821.htm (visited on 04/01/2018).

[21] B. Alberts *et al.*, "Lymphocytes and the Cellular Basis of Adaptive Immunity", 2002.

[22] K. Mishra. (2018). Origin of Immune Cells, [Online]. Available: https://meromicrobiology.blogspot.com/2011/08/cellular-basis-of-immune-response_05.html (visited on 10/08/2018).

[23] H. Cantor and E. A. Boyse, "Regulation of cellular and humoral immune responses by T-cell subclasses", *Cold Spring Harbor Symposia on Quantitative Biology*, vol. 41, pp. 23–32, 1976.

[24] U.S. Department of Veterans Affairs. (2018). CD4 count (or T-cell test) - HIV/AIDS, [Online]. Available: https://www.hiv.va.gov/patient/diagnosis/labs-CD4-count.asp (visited on 04/02/2018).

[25] M. Brown and C. Wittwer, "Flow cytometry: Principles and clinical applications in hematology", *Clinical Chemistry*, vol. 46, no. 8, pp. 1221–1229, 2000, ISSN: 0009-9147. eprint: http://clinchem.aaccjnls.org/content/46/8/1221.full.pdf.

[26] Avert.org. (2016). HIV and AIDS in South Africa, [Online]. Available: https://www.avert.org/professionals/hiv-around-world/sub-saharan-africa/south-africa (visited on 03/26/2018).

[27] UNAIDS. (2018). South Africa | UNAIDS, [Online]. Available: http://www.unaids.org/en/regionscountries/countries/southafrica (visited on 03/26/2018).

[28] Merriam-Webster. (2018). Biosensor | Definition of Biosensor by Merriam-Webster, [Online]. Available: https://www.merriam-webster.com/dictionary/biosensor (visited on 04/05/2018).

[29] R. Vargas-Bernal *et al.*, "Evolution and Expectations of Enzymatic Biosensors for Pesticides", in *Pesticides - Advances in Chemical and Botanical Pesticides*, InTech, Jul. 2012. DOI: 10.5772/46227.

[30] B. A. E Mirsky and M. L. Anson, "A DESCRIPTION OF THE GLASS ELECTRODE AND ITS USE IN MEASURING HYDROGEN ION CONCENTRATION. 582 Glass Electrode", 2018.

[31] Science History Institute. (2018). Søren Sørensen | Science History Institute, [Online]. Available: https://www.sciencehistory.org/historical-profile/soren-sorensen (visited on 04/09/2018).

[32] N. Bhalla *et al.*, "Introduction to biosensors.", *Essays in biochemistry*, vol. 60, no. 1, pp. 1–8, 2016, ISSN: 1744-1358. DOI: 10.1042/EBC20150001.

[33] M. Mascini, "A Brief Story of Biosensor Technology", *Biotechnological Applications of Photosynthetic Proteins Biochips, Biosensors and Biodevices*, pp. 4–10, 2006. DOI: 10.1007/978-0-387-36672-2_2.

[34] W. R. Heineman and W. B. Jensen, "Leland C. Clark Jr. (1918 to 2005)", *Biosensors and Bioelectronics*, vol. 21, no. 8, pp. 1403–1404, Feb. 2006, ISSN: 0956-5663. DOI: 10.1016/J.BIOS.2005.12.005.

[35] D. J. Pasto *et al.*, "A Urea-Specific Enzyme Electrode", *Du Pont Teaching Fellow*, no. 2021, pp. 1968–1969, 1967.

[36] J. P. Chambers *et al.*, "Biosensor Recognition Elements", *Curr. Issues Mol. Biol*, vol. 10, pp. 1–12,

[37] British Society for Immunology. (). Kohler and Milstein's hybridoma technology (1975) | British Society for Immunology, [Online]. Available: https://www.immunology.org/kohler-and-milsteins-hybridoma-technology-1975 (visited on 04/21/2018).

[38] D. V. Lim *et al.*, "Current and developing technologies for monitoring agents of bioterrorism and biowarfare.", *Clinical microbiology reviews*, vol. 18, no. 4, pp. 583–607, Oct. 2005, ISSN: 0893-8512. DOI: 10.1128/CMR.18.4.583-607.2005.

[39] A. Koyun *et al.*, "Biosensors and Their Principles", in *A Roadmap of Biomedical Engineers and Milestones*, 2012, ch. 4.

[40] C. Viviers *et al.*, "The design and fabrication of an autophagic flux biosensor", 2017.

[41] N. Lawrenson *et al.*, "Design of an Electrochemically Reactive HIV DNA Biosensor by use of Hairpin DNA Probes on Carbon Nanofibers", 2017.

[42] T. Ondarcuhu and C. Joachim, "Drawing a single nanofibre over hundreds of microns Related content Combing a nanofibre in a nanojunction",

[43] J. Bajáková *et al.*, “”DRAWING”-THE PRODUCTION OF INDIVIDUAL NANOFIBERS BY EXPERIMENTAL METHOD”, vol. 21, no. 9, 2011.

[44] T. Garg *et al.*, “Biomaterials-based nanofiber scaffold: Targeted and controlled carrier for cell and drug delivery”, *Journal of drug targeting*, vol. 23, no. 3, pp. 202–221, 2015.

[45] N. Tucker *et al.*, “The History of the Science and Technology of Electrospinning from 1600 to 1995”, *Journal of Engineered Fibers and Fabrics*, vol. 7, 2012.

[46] W. Gilbert, *De Magnete*, P. Fleury Mottelay, Ed. New York: Dover Publications, Inc., 1958.

[47] A. Khalil *et al.*, “Electrospun metallic nanowires: Synthesis, characterization, and applications”, *Journal of Applied Physics*, vol. 114, no. 17, p. 171 301, 2013.

[48] M. Lewin and E. M. Pearce, Eds., *Handbook of Fiber Chemistry, Second Edition, Revised and Expanded - Google Books*, 2nd ed. New York: Marcel Dekker, Inc, 1998, pp. 725–727, ISBN: 0-8247-9471-0.

[49] L. P. Santos *et al.*, “Water with Excess Electric Charge”, *J. Phys. Chem. C*, vol. 115, pp. 11 226–11 232, 2011. DOI: 10.1021/jp202652q.

[50] C. V. Boys, “On the Production, Properties, and some suggested Uses of the Finest Threads”, in *Proceedings of the Physical Society of London*, 1887.

[51] J. F. Cooley. (1903). Electrical Method of Dispersing Fluids, [Online]. Available: https://patentimages.storage.googleapis.com/8c/f4/63/15357cd9322d3a/US745276.pdf.

[52] B. Alberts *et al.*, “The Shape and Structure of Proteins”, 2002.

[53] H.-H. Lin *et al.*, “Understanding the thermally induced phase separation process via a MaxwellStefan model”, 2016. DOI: 10.1016/j.memsci.2016.01.049.

[54] C. A. *et al.*, “Scaffolds for Tissue Engineering Via Thermally Induced Phase Separation”, in *Advances in Regenerative Medicine*, InTech, Nov. 2011. DOI: 10.5772/25476.

[55] W.-E. Teo *et al.*, “Technological advances in electrospinning of nanofibers.”, *Science and technology of advanced materials*, vol. 12, no. 1, p. 013 002, Feb. 2011, ISSN: 1468-6996. DOI: 10.1088/1468-6996/12/1/11660944.

[56] C. G. Zoski, *Handbook of electrochemistry*. Elsevier, 2006.

[57] (). The Nobel Prize in Chemistry 2000, [Online]. Available: https://www.nobelprize.org/prizes/chemistry/2000/summary/ (visited on 08/26/2018).

[58] G. Inzelt, *Conducting Polymers: A New Era in Electrochemistry*, ser. Monographs in Electrochemistry. Springer Berlin Heidelberg, 2012, ISBN: 9783642276217.

[59] A. Håkansson *et al.*, “Effect of (3-glycidyloxypropyl)trimethoxysilane (GOPS) on the electrical properties of PEDOT:PSS films”, *Journal of Polymer Science Part B: Polymer Physics*, vol. 55, no. 10, pp. 814–820, May 2017, ISSN: 08876266. DOI: 10.1002/polb.24331.

[60] I. Nuramdhani *et al.*, “Electrochemical impedance analysis of a PEDOT: PSS-based textile energy storage device”, *Materials*, vol. 11, no. 1, pp. 1–11, 2017, ISSN: 19961944. DOI: 10.3390/ma11010048.

[61] Packaging Knowledge. (2018). Antistatic Bags & Conductive Bags, [Online]. Available: http://www.packagingknowledge.com/Anti_Static_Bags.asp (visited on 11/29/2018).

[62] T. Cheng *et al.*, "High-performance free-standing PEDOT:PSS electrodes for flexible and transparent all-solid-state supercapacitors", *Journal of Materials Chemistry A*, vol. 4, no. 27, pp. 10 493–10 499, Jul. 2016, ISSN: 2050-7488. DOI: 10.1039/C6TA03537J.

[63] J. Nevrela *et al.*, "Secondary doping in poly(3,4-ethylenedioxythiophene):Poly(4-styrenesulfonate) thin films", *Journal of Polymer Science Part B: Polymer Physics*, vol. 53, no. 16, pp. 1139–1146, Aug. 2015, ISSN: 08876266. DOI: 10.1002/polb.23754.

[64] K. Sanglee *et al.*, "PEDOT:PSS Nanofilms Fabricated by a Nonconventional Coating Method for Uses as Transparent Conducting Electrodes in Flexible Electrochromic Devices", *Journal of Nanomaterials*, vol. 2017, pp. 1–8, Jan. 2017, ISSN: 1687-4110. DOI: 10.1155/2017/5176481.

[65] Mu Yang *et al.*, "Characterization of PEDOT:PSS as a biocompatible conductive material", in *10th IEEE International Conference on Nano/Micro Engineered and Molecular Systems*, IEEE, Apr. 2015, pp. 149–151, ISBN: 978-1-4673-6695-3. DOI: 10.1109/NEMS.2015.7147397.

[66] B. Bessaire *et al.*, "Synthesis of continuous conductive PEDOT: PSS nanofibers by electrospinning: A conformal coating for optoelectronics", *ACS Applied Materials and Interfaces*, vol. 9, no. 1, pp. 950–957, 2017, ISSN: 19448252. DOI: 10.1021/acsami.6b13453.

[67] K. K. Khanum *et al.*, "Fabrication of free-standing PEDOT : PSS nanofiber mats using electrospinning",

[68] TAMINCO N.V., "Dimethylformamide Technical Data Sheet", Tech. Rep., 2005.

[69] M. ElMahmoudy *et al.*, "Tailoring the Electrochemical and Mechanical Properties of PEDOT:PSS Films for Bioelectronics", *Macromolecular Materials and Engineering*, vol. 302, no. 5, 2017, ISSN: 14392054. DOI: 10.1002/mame.201600497.

[70] X. Strakosas, "Integration of proteins with organic electrochemical transistors for sensing applications", Tech. Rep., 2015.

[71] H. Miura *et al.*, "Conductive and sensing performance of pva and pedot/pss blended fiber", *MRS Online Proceedings Library Archive*, vol. 1499, 2013.

[72] D. M. Ştefănescu, "Wheatstone Bridge - The Basic Circuit for Strain Gauge Force Transducers", in *Handbook of Force Transducers*, Berlin, Heidelberg: Springer Berlin Heidelberg, 2011, pp. 347–360. DOI: 10.1007/978-3-642-18296-9_18.

[73] EEEGuide.com. (2018). Wheatstone Bridge Circuit, [Online]. Available: http://www.eeeguide.com/wheatstone-bridge-circuit/ (visited on 10/08/2018).

[74] K. Hoffman, *Applying the Wheatstone Bridge Circuit*, 3rd ed. Hottinger Baldwin Messtechnik, 1986.

[75] HDCabling. (2018). HD Cabling 3 Meter USB 3.0 Superspeed Extension Cable – USB Type A male to USB Type A female, [Online]. Available: https://www.hdcabling.co.za/3-meter-usb-30-superspeed-extension-cable-usb-type-a-male-to-usb-type-a-female-p-451.html (visited on 11/29/2018).

[76] Sigma-Aldrich. (2018). Polyethylenimine, linear, [Online]. Available: https://www.sigmaaldrich.com/catalog/product/ALDRICH/764604?lang=en&region=ZA&gclid=Cj0KCQiA1sriBRD-ARIsABYdwwFBSzVxtJsAfJ7EaRL-SobB8moLwD_RD1nTX9HsOx09qNRNOzP00fUaAljvEALw_wcB (visited on 10/08/2018).

[77] K. M. Kim *et al.*, "Work function optimization of vacuum free top-electrode by pedot: Pss/pei interaction for efficient semi-transparent perovskite solar cells", *Solar Energy Materials and Solar Cells*, vol. 176, pp. 435–440, 2018.

[78] P. D. Angelo *et al.*, "Conductivity of inkjet-printed pedot: Pss-swcnts on uncoated papers", *Nordic Pulp and Paper Research Journal*, vol. 27, no. 2, p. 486, 2012.

[79] Sigma-Aldrich. (2018). Polyethylenimine, linear, [Online]. Available: https://www.sigmaaldrich.com/catalog/substance/3aminopropyltriethoxysilane2213791930211?lang=en&region=ZA (visited on 10/08/2018).

[80] ThermoFisher Scientific. (2018). Chemistry of Crosslinking, [Online]. Available: https://www.thermofisher.com/za/en/home/life-science/protein-biology/protein-biology-learning-center/protein-biology-resource-library/pierce-protein-methods/chemistry-crosslinking.html (visited on 10/08/2018).

[81] Sigma-Aldrich. (2018). Glutaraldehyde solution, [Online]. Available: https://www.sigmaaldrich.com/catalog/substance/%20glutaraldehydesolution1001211130811?lang=en&region=ZA (visited on 10/08/2018).

[82] Centers for Disease Control and Prevention. (2008). Guideline for Disinfection and Sterilization in Healthcare Facilities (2008), [Online]. Available: https://www.cdc.gov/infectioncontrol/guidelines/disinfection/disinfection-methods/chemical.html (visited on 10/08/2018).

[83] World Health Organisation. (2013). WHO Model List of Essential Medicines), [Online]. Available: https://www.who.int/medicines/publications/essentialmedicines/18th_EML.pdf (visited on 10/08/2018).

[84] ThermoFisher Scientific. (2018). Protein Crosslinking Applications, [Online]. Available: https://www.thermofisher.com/za/en/home/life-science/protein-biology/protein-biology-learning-center/protein-biology-resource-library/pierce-protein-methods/crosslinking-applications.html (visited on 10/08/2018).

[85] W. Luttmann *et al.*, *Immunology*, ser. The Experimenter Series. Elsevier Science, 2006, ISBN: 9780080916675.

[86] Sigma-Aldrich. (2018). Suberic acid bis(3-sulfo-N-hydroxysuccinimide ester) sodium salt, [Online]. Available: `https://www.sigmaaldrich.com/catalog/product/sigma/s5799?lang=en&region=ZA` (visited on 10/08/2018).

[87] ThermoFisher Scientific. (2018). BS3 (bis(sulfosuccinimidyl)suberate), [Online]. Available: `https://www.thermofisher.com/order/catalog/product/21580` (visited on 10/08/2018).

[88] ——, (2018). Blocking Strategies for IHC), [Online]. Available: `https://www.thermofisher.com/za/en/home/life-science/protein-biology/protein-biology-learning-center/protein-biology-resource-library/pierce-protein-methods/blocking-strategies-ihc.html` (visited on 10/08/2018).

[89] Sigma-Aldrich. (2018). TWEEN® 20, [Online]. Available: `https://www.sigmaaldrich.com/catalog/product/sigma/s5799?lang=en&region=ZA` (visited on 10/08/2018).

[90] ThermoFisher Scientific. (2018). PBS, pH 7.4, [Online]. Available: `https://www.thermofisher.com/order/catalog/product/10010023` (visited on 10/08/2018).